Numerical study on the development of alternate bars in varying discharge conditions

Roline Montijn

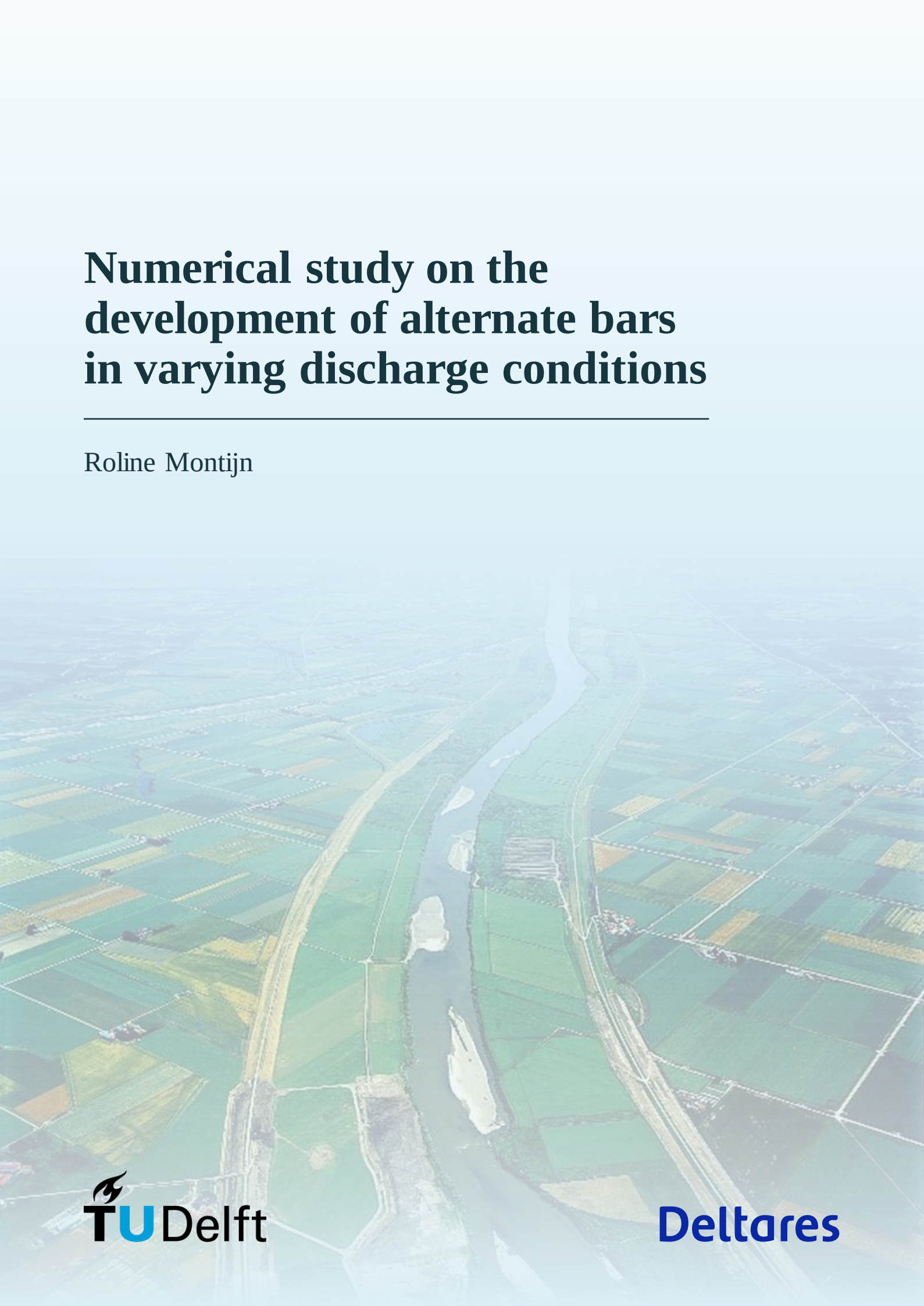

TU Delft

Deltares

Numerical study on the development of alternate bars in varying discharge conditions

---

Roline Montijn

In partial fulfilment of the requirements for the degree of

Master of Science
in Hydraulic Engineering

at Delft University of Technology.

To be defended on the 13th of April, 2021 at 15.30h.

Graduation committee

Dr. ir. A. Blom	Chair	Delft University of Technology
Dr. ir. R.J. Labeur		Delft University of Technology
Dr. R. Schielen		Delft University of Technology
Dr. ir. E. Mosselman	Daily supervisor	Deltares & Delft University of Technology
Dr. ir. C.J. Sloff	Daily supervisor	Deltares & Delft University of Technology

An electronic version of this thesis is available at http://repository.tudelft.nl/.

Cover image: Alternate bars in the Tokachi River, Japan. Flow is from top to bottom.
Source: Vincent Langlois.

Preface

Dear reader,

Thank you for showing your interest in my final thesis. I wrote this thesis to accomplish my master in Hydraulic Engineering, with a specialisation in River Engineering. I hope this thesis provides you with the information you are looking for or triggers your interest in the world of river bars.

My interest in river engineering was triggered by the courses in open channel flow and river dynamics. The first meeting with Kees provided the research setting I was looking for: an ongoing river restoration project to restore the natural river dynamics and nature development, as I was interested in river morphology and would like to contribute to nature development. The first four weeks were at Deltares, with Kees and Erik, to introduce me to the people and the working mentality of Deltares and the world of river bars. Due to the Covid-19 regulations, the conversation continued over Zoom, Skype or Teams. By introducing Astrid, Robert Jan and Ralph to my graduation committee, all my thesis aspects were covered, creating a fruitful working environment. I would like to thank you all for your help and guidance. Thank you, Kees and Erik, for your quick but elaborated replies, suggestions for the next steps, helping to process all the materials, and offering a listening ear. Thank you, Astrid, Robert Jan and Ralph, for your constructive feedback, encouragement to answer the 'why'-questions and suggestions to make my thesis, especially this report, a comprehensive story that I can now look back on nicely. Furthermore, I am grateful for the help I received from the people at Deltares, the Grensmaas and the University of Trento, Italy.

I would like to thank the Doezies for providing a great working place, for the distractions but also the motivation and the pleasure to graduate during these strange times. I am my parents and my sister, Myrthe, more than grateful for your endless support: looking forward to reuniting this summer. And last but not least, thank you, Floris, for all your help and support.

For all the future river engineers who are conducting their graduation research in the field of river bars, do not hesitate to contact me if you have questions or want to discuss your research. Looking forward to meeting you!

Roline Montijn
Rotterdam, April 2021

Executive summary

River bars are large-scale bedforms formed by the local deposition of sediments, the length of which scales with the channel width and the height with the water depth. They create suitable habitats for aquatic fauna and riparian vegetation, making them useful in river restoration projects. Understanding the dynamics of river bar development is required for a proper design of the restoration project and for developing a sustainable management scheme.
The channel half-width-to-depth ratio is the key controlling parameter for the formation of alternate bars. Existing stability analyses define a resonance point and critical width-to-depth ratio, marking the transition between the bar regimes. Seasonal variations in the river discharge and the propagation of flood waves make the half-width-to-depth ratio a time-dependent parameter, varying over periods of days to months. This research aims to create a better understanding of the development of alternate bars in varying discharge conditions. For that, insight into the timescale of development of the bars is necessary to link this with the timescales associated with natural discharge variability.

A straight river channel is modelled in Delft3D, with non-erodible banks to which a fixed perturbation is added, to trigger the formation of free bars and to which hybrid bars become fixed. In the first set of simulations, the upstream boundary condition is a constant discharge, with magnitudes between 50 and 1250 m^3/s, corresponding to a half-width-to-depth ratio between 77 and 8. The different types of alternate bars and the time to develop the bars are analysed from this constant-discharge analysis. The damping length and wavelength of the hybrid bars showed good agreement with the values determined from the theory of Struiksma et al. (1985). Free bars became suppressed when a hybrid bar pattern developed, showing that hybrid and free bars do not coexist locally. The resonance point is clearly obtained and assigned to a half-width-to-depth ratio of 37-38. Contrary to existing stability analyses, the critical half-width-to-depth ratio is marked by a gradual transition at half-width-to-depth ratios from 11 to 20 instead of a single value. In this transition, free bars develop with intervals of a few months.

A clear difference in the development of hybrid bars and free bars results in a shorter timescale of development for free bars than for hybrid bars, which is in line with laboratory experiments (Fujita and Muramoto 1985; Crosato et al. 2010). Also, in the mathematical derivations for describing the two types of bars, the distinction between an initial response (free bars, Colombini, Seminara, and Tubino (1987)) and a final stable bed (hybrid bars, Struiksma et al. (1985)) is considered. The numerical results show that free bars develop fastly when the bed becomes unstable, in the case of a relatively flat bed. The associated timescale shows little variation over the different simulations and stays around 20 days, which is in the same order of magnitude as the timescale related to seasonal variation. A pattern of hybrid bars develops in downstream direction, starting at the fixed perturbation. Based on the definition of the damping length by Struiksma et al. (1985), a theoretical expression is defined, which gives a good fit to the time at which a pattern of hybrid bars has developed.

The transition of alternate bars around resonant conditions is modelled using a steadily increasing and decreasing discharge. The distinction between the timescales of hybrid and free bars results in a different response of the bars to a varying discharge. The first response of the bed in the transition from subresonant to superresonant conditions is the adaptation of free bars towards the new bar regime. A pattern of hybrid bars follows, developing in downstream direction. The reversed transition is governed by a migration of the hybrid bar pattern, making room for the damped bar pattern. The difference in the transitions between rising and falling discharge in combination with a bed adaptation after a temporal in- or decreased discharge led to a type of hysteresis in the transition around the riverbed's resonance point, which was not earlier detected. Hysteresis is ascribed to the increased

bed stability when a hybrid bar pattern has developed, suppressing the formation of free bars in the transition from superresonant to subresonant conditions and to the time-lags associated with lower discharge conditions.

This thesis assesses the timescales of alternate bars and the transition around the resonance point. The numerical model is able to assess both free and hybrid bars and therefore gives valuable information in the difference of their development. The difference is linked to the (linear) theories describing the bars and applied for answering the research question, showing the development of free bars should be largely influenced by discharge variation due to seasonal variation. The varying discharge simulations provided insights into the response and transition of alternate bars around resonance conditions, leading to a type of hysteresis which was not detected earlier. Recommendations are made towards increasing the river geometry complexity and discharge variation and the assessment of the transition around critical conditions to verify analyses around critical conditions.

Contents

List of Figures

List of Tables

List of symbols

α	Direction of sediment transport	rad
α_1	Factor in the function describing the growth of the bar amplitude over time (Tubino 1991)	–
α_{1R}	Real part of the complex coefficient α_1 (Tubino 1991)	–
β	Half-width-to-depth ratio = $0.5\ B/h$	–
β_c	Critical half-width-to-depth ratio	–
Δ	Relative submerged sediment density	–
δ	Direction of bed shear stress	rad
ϵ	Parameter for the "distance" of the actual conditions from the critical state (Tubino 1991)	–
θ	Shields parameter	–
θ_{cr}	Critical Shields parameter	0.047 –
κ	Von Kármán constant	0.40 –
λ	Dimensionless longitudinal wavenumber = πB / L_P	–
λ_s	Streamwise adaptation length for perturbations in the cross-sectional river bed profile	m
λ_w	Streamwise adaptation length for perturbations in the transverse profile of depth-averaged streamwise flow velocity	m
ρ	Mass density of the fluid	$\mathrm{kg\,m^{-3}}$
$\tau_{bx,y}$	Bed shear stress in x or y direction	$\mathrm{N^2\,m^{-1}}$
Ω	Exponential growth rate of perturbations in the linear regime (Tubino 1991)	–
B	Width of river	–
b	Degree of nonlinearity in dependence of sediment transport capacity on flow velocity	–
C	Chézy coefficient	$\mathrm{m^{0.5}\,s^{-1}}$
c_f	Friction coefficient = g / C^2	–
D_{50}	Median grain size	m
$\overline{d_s}$	Roughness parameter = D_{50} / h_0	–
$f(\theta)$	Shape factor of grains	–
Fr	Froude number	–
g	Acceleration due to gravity	$9.8\ \mathrm{m\,s^{-2}}$

h	Water depth	m
i_b	Streamwise bed level slope	$-$
L_D	Damping length	m
L_P	Longitudinal bar wavelength	m
m	Bar mode in transverse direction	$-$
p	Porosity	$-$
Q_{start}	Discharge for the starting conditions	$\mathrm{m^3\,s^{-1}}$
Q_w	Total water discharge	$\mathrm{m^3\,s^{-1}}$
$q_{sx,y}$	Bed-load transport per unit width, excluding pores, in x or y direction	$\mathrm{m^2\,s^{-1}}$
q_w	Water discharge per unit width	$\mathrm{m^2\,s^{-1}}$
T^*	Factor for a dimensionless time (Tubino 1991)	$\mathrm{s^{-1}}$
T_{free}	Timescale of the development of free based. Determined in the numerical simulations	s
$T_{hybrid\ L_D}$	Timescale of hybrid bars towards a full pattern of hybrid bars has developed (Equation 2.8)	s
$T_{hybrid\ L_P}$	Timescale of hybrid bars towards the development of the first bar (Equation 2.9)	s
T_{start}	Simulation time of the starting conditions	s
T_{Taal}	Timescale based on Taal (1989)	s
T_{Tubino}	Timescale for the development of free bars based on Tubino (1991)	s
t	Time	s
$\hat{U}$	Ratio between the timescale of basic unsteadiness and the timescale of bar growth (obtained from linear analysis) (Tubino 1991)	$-$
u	Depth-averaged flow velocity in x direction	$\mathrm{m\,s^{-1}}$
v	Depth-averaged velocity in y direction	$\mathrm{m\,s^{-1}}$
x	Streamwise direction	$-$
x_p	Spatial lag	m
y	Lateral direction	$-$
z_b	Bed level	m

Chapter 1

Introduction

1.1 Context and problem definition

River bars are large-scale bedforms formed by the local deposition of sediments, the length of which scales with the channel width and the height with the water depth. From an ecological perspective, river bars create suitable habitats for aquatic fauna and riparian vegetation, contributing to habitat diversity. In Europe, human interventions in the past century have converted braided reaches into straight or meandering rivers (Singh et al. 2017), suppressing the formation of bars. Since the early 1980s, there has been an increasing awareness of the need to rehabilitate river ecosystems through restoration programmes (Buijse et al. 2002). An example of an ongoing Dutch river rehabilitation project is along the Grensmaas, which is a typical rain-fed river, on the border of The Netherlands and Belgium. Since 2001, river sections have been widened with the aim to restore the natural river dynamics, like the formation of river bars. The Grensmaas has responded to the local widening by the formation of mid-channel bars or local bank accretion. However, the predictability of the type and location of the bars is limited, and the response strongly differs per location [1]. This has led to the need for increased understanding of the dynamics of river bar development in typical rain-rivers like the Grensmaas, for a proper design of the restoration project and for developing a sustainable management scheme.

Alternate bars are formed in wide rivers and suppressed in relatively narrow rivers. The controlling parameter for the formation of bars is the ratio of the river width to water depth, represented by the half-width-to-depth ratio. The formation of bars can be explained by means of an instability mechanism; in relatively wide channels, an initially small perturbation generates topographic steering of the flow field that produces growth of the perturbation itself, which leads to the spontaneous development of periodic, alternate bars. Linear and weakly nonlinear stability analyses have defined a threshold value of the half-width-to-depth ratio, representing the lower limit at which alternate bars are expected to form. These studies use a constant discharge, for instance the 'bankfull discharge' or 'formative discharge' (Engelund and Skovgaard 1973; Parker 1976; Fredsøe 1978; Colombini, Seminara, and Tubino 1987). However, seasonal variations in the river discharge and the propagation of flood waves make the half-width-to-depth ratio a time-dependent parameter, varying over periods of days to months. Since the half-width-to-depth ratio is such an important parameter for the formation of alternate bars, it may be expected that these variations influence the behaviour of alternate bars. Particularly so because the timescale of the formation of cross-stream profiles like river bars is relatively short with respect to the timescales of the reach-scale or basin-scale processes.

Alternate bars are formed by the deposition and entrainment of sediments. As such, the rate of bar formation is governed by the amount of transported sediments. A power law governs the relationship between the sediment transport capacity of the river and the discharge. As a result of this, the bars may form during low-flow conditions with a large half-width-to-depth ratio. On the other hand, the sediment transport rates during low-flow conditions are marginal. This means that the channel bed

[1] Personal communication with Ron Agtersloot, hydraulic advisor of Consortium Grensmaas

needs a longer time to reach its final configuration (Crosato and Mosselman 2009). Thus, the formation of bars results from a competition between the timescale of discharge variability and the timescale of bar growth. The interplay between these two timescales on the development of free bars has been analysed in the literature.

Tubino (1991) and Hall (2004) theoretically analysed the effect of flow unsteadiness on free, migrating bars through a weakly nonlinear stability analysis. Tubino (1991) showed that the timescale of bar growth and the timescale of the basic flow are in nature often in the same order, and therefore "the bar amplitude proves to be strongly affected by the unsteady character of the flow". The variation of the flow, and therefore the variation of the shear stress on the mobile bed, is differently assessed by Tubino (1991) and Hall (2004), being always above the critical shear stress for sediment motion, or only during the flood, respectively. Both models are restricted to conditions close to the critical half-width-to-depth ratio, and the choice of closure relation strongly determines the accuracy of the results. To summarise, the effect of a variable discharge on bar evolution is still limited to theoretical analyses of free bars and prone to strong simplifications.

This thesis assesses the evolution of alternate bars in varying discharge conditions using a fully nonlinear numerical model, assessing the timescales of bar growth and the transition between bar regime due to a varying discharge. The results are coupled to existing analytical models and natural discharge variability.

1.2 Objective and research questions

Following the motivation and problem definition, the objective of this research is formulated as follows:

"To create a better understanding of the development of alternate bars in varying discharge conditions"

To do so, the following research questions are formulated:

1. What are the timescales related to the development of alternate bars with respect to natural discharge variability?
2. How is the transition from super- to subresonant conditions, and vice versa, due to a varying discharge?
3. How do alternate bars respond to a temporal in- or decreased discharge?

1.3 Methodology

A review of the literature and previous studies is performed to obtain a first understanding of the development of alternate bars in general and their development in varying discharge conditions. The forming mechanism of alternate bars can be described as a morphodynamic instability, and therefore a study on stability analyses provides insight into the two types of alternate bars (free and hybrid) and their characteristics. Further insight into their development is obtained from previously conducted laboratory experiments. A study towards available morphological timescales is conducted to link them with the timescales associated with bar development.

The thesis continues with a numerical study. A numerical model is used to determine the timescales

associated with the development of alternate bars and to analyse the bars' response to a varying discharge. The numerical model is a physics-based, fully nonlinear morphodynamic Delft3D model. The suitability of the numerical model is verified by comparing the numerical results with characteristics of the alternate bars and the theoretically obtained values for the damping and wavelengths of the hybrid bars at different constant-discharge magnitudes. The limitations of both the (linear) theories and the numerical model are assessed.

Afterwards, the timescales related to bar development are determined to answer the first research question. These timescales are compared with existing morphological timescales to assess their validity, and they are compared with timescales related to natural discharge variability. As the last two prove to be in the same order of magnitude, it is expected that the bars should be influenced by discharge variability, and therefore, it is still interesting to study the bars' response to varying discharge conditions. By modelling a steadily increasing and decreasing discharge at the upstream boundary, the development of alternate bars in varying discharge conditions is assessed, answering the last two research questions.

1.4 Thesis outline

First, the theoretical background and literature study are presented in Chapter 2. Section 2.1 ends with a comprehensive list of definitions of the extensively used terms in this thesis. Chapter 3 provides the model used in this thesis and the appropriate settings.

The results of the constant-discharge simulations are provided in Chapter 4 and Chapter 5. In Chapter 4, the characteristics of the different types of bars, developing in the different simulations, are analysed and interpreted in the theoretical background. In Chapter 5, the timescales of the different types of bars are determined. The results of the varying discharge simulations are provided in Chapter 6. Chapter 7 provides the discussion points related to this research. Chapter 8 provides the conclusion of this research by reflecting on the objective of this research and the research questions.

Chapter 2

Literature study

Objective

The objective of this chapter is to get insight into the type and characteristics of alternate bars developing in different discharge magnitudes. Findings of recent research in the field of bars in varying discharge conditions is provided.

Chapter outline

Section 2.1 gives information about the types of alternate bars which develop in different discharge magnitudes. Firstly, the bar types classification is provided, followed by the theories for determining the bar characteristics. These theories are used to verify the numerical model. Section 2.2 continues with information about the development over time of alternate bars and morphological timescales associated with bar development. Section 2.3 provides relevant studies about the development of alternate bars in varying discharge conditions.

2.1 Instability regime of the riverbed and its resonance point

Bar classification

The type of bars of interest for this research are hybrid and free bars, which form an alternating pattern of bars and pools in the river. The classification of bars introduced here is based on the forming mechanism and obtained from Duró, Crosato, and Tassi (2015). Free and hybrid bars are formed by a morphodynamic instability and, therefore, arise in the riverbed's instability regime. The main difference between free bars and hybrid bars lies in their migration behaviour. Free bars can be migrating or non-migrating. Non-migrating (free) bars are called 'resonant', a term introduced by Blondeaux and Seminara (1985). Free bars mostly migrate in downstream direction, but in superresonant conditions, the bars may migrate in upstream direction too (Zolezzi and Seminara 2001). Hybrid bars do not migrate as they are fixed to a stable and local perturbation, such as for example, a groyne.

The periodic pattern of both hybrid and free bars can be characterised using a system of bar modes (m) which is related to the number of bars in cross-stream direction. m = 1 corresponds to an alternating bar pattern formed at the channel's left and right bank. m = 2 indicates central bars. Higher bar modes correspond to braided rivers, with multiple bars in cross-stream direction. The observed bar mode is always an integer. A predictor of the bar mode for a river is provided by Crosato and Mosselman (2009), which is not an integer, but can be any real number. A particular application is that it predicts the river planform style: meandering is characterised by at most one bar per cross-section and braiding by at least two bars.

The third type of bars that are encountered in the river system are forced bars. Forced bars are local bars generated by sediment deposits due to a geometrical induced deformation of the water flow. Forced bars differ from hybrid, as forced bars can develop outside the riverbed's instability regime and are therefore non-periodic. An example of a forced bar is a point bar in a river bend. An overview of the described bar types and their characteristics is shown in Figure 2.1.

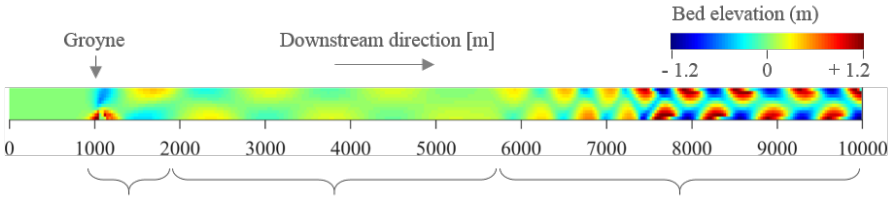

	Forced bars	Hybrid bars	Free bars
Periodic?	No	Yes	Yes
Migrating?	No	No	Yes, except in resonance conditions

FIGURE 2.1: Bar classification and characteristics applied to a simulation (U150) from the numerical analysis. The model shows a perfectly straight river with hybrid bars attached to the fixed perturbation at x = 1100 m and free, migrating bars at the end of the domain.

Instability regime of the riverbed

The key controlling parameter for the formation of free alternate bars is the half-width-to-depth ratio β. The critical half-width-to-depth ratio β_c is the lower limit for which free bars are expected to form,

which is the lower limit of the riverbed's instability regime. The bed instability can be explained in physical terms by the topographically induced steering of the flow field. Topographic steering of the flow refers to the redistribution of the flow around a locally increased bed level. This redistribution, and therefore redistributed sediment flux, produces erosion at the upstream side of the bed feature, and deposition on the downstream side: a perturbation that migrates downstream. The growth or decay of the bed feature depends on the location of the transition from erosion to deposition along the bed feature relative to the top of the bed feature. If the transition is just downstream of the top, the bed feature will decrease in height. When the transition moves far enough downstream, sedimentation will shift towards the upperside of the next bed perturbation, increasing the bed perturbation. The redistribution of the flow increases for increasing width(-to-depth ratio), increasing the inertial lag, shifting towards an unstable bed.

Resonance point

The instability regime of the riverbed is split into two subregimes, delineated by the resonance point. The characteristics of alternate bars vary for the two subregimes. During resonant conditions, the celerity of free bars goes to zero. For hybrid bars, resonance occurs when the damping length goes to infinity, which means a constant amplitude in downstream direction. Sub- and superresonant conditions refer to half-width-to-depth ratios below and above the resonance point, respectively. The hybrid and free bars' characteristics in sub- or superresonant conditions are elaborated in the subsequent sections.

Research approaches

Values to determine the resonance point and critical half-width-to-depth ratio are based on linear analyses. Two approaches have been defined and are now commonly referred to as the Genoa school and the Delft school, based on the terminology of Parker and Johannesson (1989). The approaches have a slightly different focus. The Genoa school assumes an infinitely long straight river and analyses the development of free bars. The Delft approach takes a fixed, local perturbation and has defined values for damping lengths and wavelengths for hybrid bars fixed to this perturbation. The linear analyses in both methods provide expressions for resonant conditions. The critical half-width-to-depth ratio holds especially for free bars (Genoa approach), as hybrid bars can occur at half-width-to-depth ratios above and below the critical half-width-to-depth ratio (Meer et al. 2011). An overview of the bar regimes within the instability regime of the riverbed, their characteristics and the accompanied research approach is shown in Table 2.1.

TABLE 2.1: Regimes within the instability regime of the riverbed.

	Bar type	Hybrid bars	Free bars	
	Approach	Delft school	Genoa school	
	Condition	Fixed, local perturbation	Perfectly straight river	
	Characteristic	Steady	Migrating	
Regime	Subresonant	Amplitude damped in downstr. direction	Downstream migrating	$\beta\uparrow$
	Resonant	No amplitude variation	Zero celerity	
	Superresonant	Amplitude growing in downstr. direction	Upstream migrating	$\downarrow$

Theory of hybrid bars

Hybrid bars arise in the instability regime of the riverbed from a fixed local perturbation and are non-migrating. Struiksma et al. (1985) derived an expression for the left bank water depth perturbation H at a distance x from the upstream boundary (Equation 2.1), based on a linearized model from the basic depth-averaged equations for water flow and sediment transport. The expression includes λ_w and λ_s, the streamwise adaptation length for water and sediment, respectively, representing first-order relaxation equations for flow and bed topography (Equation 2.3). Combination results in a single second-order equation, which may exhibit an oscillatory behaviour in downstream direction. For the derivation of the expression, the reader is referred to the work of Struiksma et al. (1985).

$$H(x) = H(0) \exp\left(-\frac{x}{L_D}\right) \sin\left(\frac{2\pi}{L_P}(x + x_P)\right) \tag{2.1}$$

with

$H(x)$	=	Left bank water depth perturbation at a distance x from the upstream boundary	m
$H(0)$	=	Left bank water depth perturbation at the upstream end	m
$2\pi/L_p$	=	Streamwise wavenumber	m^{-1}
$1/L_D$	=	Damping coefficient	m^{-1}
x_p	=	Spatial lag	m

The damping length L_D and wavelength L_P can be determined with Equation 2.2.

$$\begin{aligned} \frac{2\pi}{L_P} &= \frac{1}{2\lambda_w}\left((b+1)\frac{\lambda_w}{\lambda_s} - \left(\frac{\lambda_w}{\lambda_s}\right)^2 - \frac{(b-3)^2}{4}\right)^{1/2} \\ \frac{1}{L_D} &= \frac{1}{2\lambda_w}\left(\frac{\lambda_w}{\lambda_s} - \frac{(b-3)}{2}\right) \end{aligned} \tag{2.2}$$

with

$$\lambda_w = \frac{h}{2c_f} \quad , \quad \lambda_s = \frac{1}{(m\pi)^2} h \left(\frac{B}{h}\right)^2 f(\theta) \quad \text{and} \tag{2.3}$$

b	=	Degree of nonlinearity in dependence of sediment transport capacity on flow velocity	-
λ_w	=	Streamwise adaptation length for perturbations in the transverse profile of depth-averaged streamwise flow velocity	m
λ_s	=	Streamwise adaptation length for perturbations in the cross-sectional bed profile	m
h	=	Water depth	m
c_f	=	Friction coefficient	-
m	=	Bar mode in transverse direction	-
B	=	Width of river	m
$f(\theta)$	=	Shape factor of grains	-
θ	=	Shields parameter	-

The solution of Equation 2.1 has three regimes. The ratio λ_s over λ_w arises as the key parameter, with the width-to-depth ratio as dominant contributor, for this second-order system. Here, the results are provided in terms of L_D and L_P. For $L_D > 0$, the solution is stable: the bar amplitude is damped in downstream direction. This, in combination with $L_p \to \infty$, leads to an amplitude which is over-damped, suppressing the formation of hybrid bars, corresponding to a stable riverbed. Otherwise, the

amplitude is underdamped, still showing a periodic behaviour (Figure 2.2a), corresponing to subresonant conditions.

The solution of L_D also allows negative values. This superresonant regime corresponds to bars that grow spatially downstream (Figure 2.2b). Originally, this regime was linked to incipient braiding (Struiksma and Klaassen 1988). A weakly nonlinear analysis by Seminara and Tubino (1992) showed that the amplitude will not grow beyond a finite amplitude due to nonlinear effects. The resonance point for hybrid bars is the point where $1/L_D = 0$, yielding a constant bar amplitude over the domain.

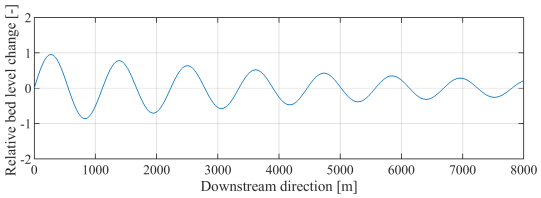

(a) Hybrid bars in subresonant conditions. The amplitude is damped in downstream direction.

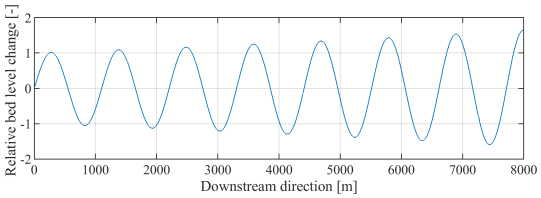

(b) Hybrid bars in superresonant conditions. The amplitude grows in downstream direction.

FIGURE 2.2: Representation of hybrid bars based on the theory of Struiksma et al. (1985) in super- en subresonant conditions.

Theory of free bars

Free bars arise from an instability mechanism. The formative conditions can be assessed by means of a stability analysis of the linearized flow and sediment formulations. Within the Genoa school, this linearized stability analysis was done by Colombini, Seminara, and Tubino (1987), based on the work of Blondeaux and Seminara (1985). A clear presentation of their results is provided with the neutral stability curve (Figure 2.3a). The horizontal axis shows the non-dimensional wavenumber λ; the vertical axis shows the half-width-to-depth ratio β. The curve represents the solution for a zero growth rate, dividing a region where bars cannot develop from a region where bars can. The lower limit of β where bars still can develop is defined as the critical value.

Adami, Bertoldi, and Zolezzi (2014) applied the theory of Colombini, Seminara, and Tubino (1987) to the Alpine Rhine Reach between Switzerland, Austria and Liechtenstein, which is a long channelized reach with almost uniform channel width and slope. Their neutral stability curve is shown in Figure 2.3b. Four regions are present, named with roman numerals. In region I and IV, bars are damped (negative growth rate), while in region II and III, bars can develop. The intersection of the curves of zero growth rate and zero angular frequency denotes the resonant conditions. Experimental studies of Zolezzi et al. (2005) show that the model provides reasonable predictions for the wavelengths and β associated with resonance.

To describe the magnitude of the bar amplitude, nonlinear effects have to be taken into account. A weakly nonlinear stability analysis investigates the region near the critical value of stability, which was also done by Colombini, Seminara, and Tubino (1987) and led to a relationship for the maximum height and the maximum scour depth of bars. To investigate the evolution of perturbations in this region, different timescales have been proposed and were referred to as a 'slow' and a 'fast' timescale. Fukuoka (1989) also conducted a weakly nonlinear stability analysis by analysing the perturbation on two different timescales: one timescale in the range of the growth of bars and one timescale in the range of the typical period of the waves. This two-time-scale analysis is a so-called Landau equation, for which the wavenumber is fixed, eliminating other wavenumbers in the area of

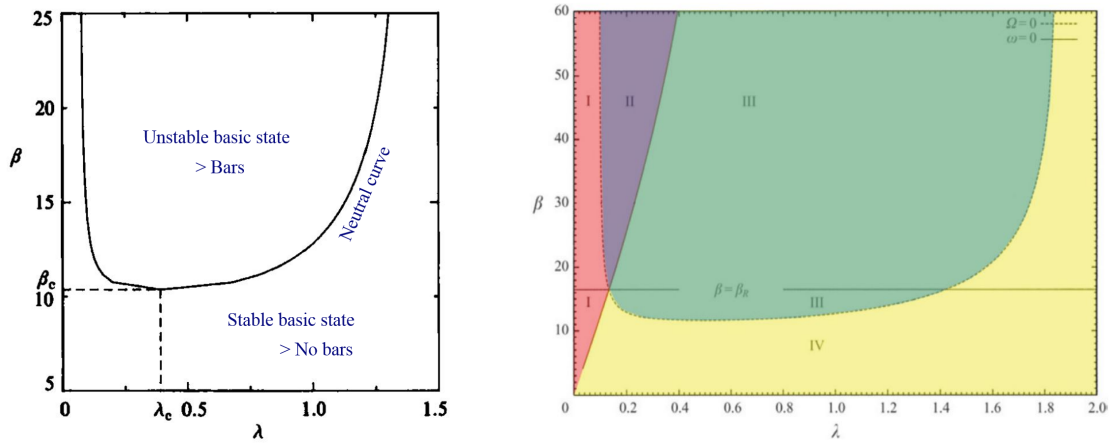

(a) Neutral stability curve for $\theta = 0.3$ and $d_s = 0.01$.
From Colombini, Seminara, and Tubino (1987).

(b) Neutral stability curve from Colombini, Seminara, and Tubino (1987) applied to Alpine Rhine River reach by Adami, Bertoldi, and Zolezzi (2014)

FIGURE 2.3: Neutral stability curves for alternate-bar formation.

the criticial wavenumber. This analysis only described the temporal evolution. An extension of the Landau equation, being the Ginzburg-Landau equation, describes the spatial and temporal evolution and is proposed by Schielen, Doelman, and Swart (1993), to determine the stability of general perturbations. It is demonstrated that the periodic alternate bar patterns, obtained by Colombini, Seminara, and Tubino (1987), can be unstable in the case of a dune-covered bed and results in a quasi-periodic bar pattern.

Upstream influence in superresonant conditions

Theoretical findings based on a linearized analysis have discovered an upstream influence in superresonant conditions (Zolezzi and Seminara 2001). A physical explanation of the upstream influence was sought in the upstream migration of free bars, at least in a linear context. Laboratory experiments in superresonant conditions show an upstream and a downstream influence (Zolezzi et al. 2005). The downstream influence in superresonant conditions is in line with an analysis of characteristics, showing a positive (downstream direction) of the celerity of (infinitesimally) small perturbations (Mosselman, Tubino, and Zolezzi 2006).

Numerical simulations by Meer et al. (2011) analyse the development of alternate bars in both sub- and superresonant conditions. The upstream overdeepenings (the development of hybrid bars in upstream direction) " developed from free bars that migrated in downstream direction rather than the upstream direction expected for superresonant conditions". They explain this by the presence of higher-mode free bars, as they were still in the subresonant regime. Furthermore, they highlight that the theoretically predicted upstream migration of free bars is only applicable when their amplitude is small, "as the upstream-migrating bars have a much smaller temporal growth rate than their downstream-migrating counterparts". Verbruggen (2012) advanced the modelling work of Meer et al. (2011) to assess to what extent the numerical results agree with linear theory and experimental observations. The upstream development was only observed if no perturbation was applied in the upstream boundary. A downstream development dominated with an upstream perturbation. Only very small-amplitude bars did migrate upstream. Verbruggen (2012) ascribes the downstream migration to nonlinear effects.

Conclusion and limitations

The linear bar theories of Struiksma et al. (1985), Blondeaux and Seminara (1985) and Colombini, Seminara, and Tubino (1987) have provided useful insight in the characteristics of bars developing in the different regimes, delineated by the resonance point and the critical half-width-to-depth ratio. However, limitations are due to the neglected nonlinear effects and that they are only valid for the incipient state, or for weakly nonlinear analyses only valid near critical conditions. The advantage of numerical studies lies in their full nonlinearity, allowing the simulation of bar development beyond their incipient state and far from critical conditions. Therefore, this research will rely on a numerical model. The presented theories have provided the underlying physics and are therefore necessary to interpret the results of the numerical model.

In this section, several definitions have been used. As these definitions will frequently reappear in the remainder of this thesis, a brief overview is created below for the sake of clarity.

Half-width-to-depth ratio Controlling parameter for the formation of periodic bars. Depending on the research approach, either the ratio between the half width and depth is used, or between the full width and depth. In this research, values for the half width are used.

Stable riverbed On a stable riverbed, neither free nor hybrid bars develop.

Critical half-width-to-depth ratio Marks the transition between a stable and an unstable riverbed. In other words: this is the lower limit in terms of half-width-to-depth ratios of the instability regime of the riverbed.

Forced bars River bars, solely depending on the local river geometry. They can develop both on stable and on unstable riverbeds. Not periodic.

Free bars Migrating bars, except at the resonance condition. They develop inside the instability regime of a perfectly straight river. Periodic.

Hybrid bars A pattern of bars which is fixed to a local perturbation (for instance a groyne), developing inside the instability regime of the riverbed. Periodic.

Instability regime of the riverbed Periodic bars (free or hybrid, depending on the river geometry) develop on an unstable riverbed. The instability regime of the riverbed consists of two 'subregimes': subresonant and superresonant, delineated by the resonance point of the river.

Resonance point Refers to conditions (a width-to-depth ratio) where the celerity of the free bars goes to zero, and the amplitude of hybrid bars is constant in downstream direction.

Subresonant Conditions below the resonance point and above the critical value in terms of half-width-to-depth ratio. In subresonant conditions, free bars migrate downstream, and the amplitude of the hybrid bars is damped in downstream direction.

Superresonant Conditions above the resonance point in terms of half-width-to-depth ratio. In superresonant conditions, free bars migrate upstream, and the amplitude of the hybrid bars grows in downstream direction.

2.2 Time dependency of alternate bars

Section 2.1 has provided insight into the type of river bars developing in the different bar regimes. To study alternate bars in varying discharge conditions, insight into the timescales of the development of the different types of bars is necessary. Laboratory experiments have given valuable information in this development. Furthermore, some morphological timescales are introduced in this section. These are assessed on their usability for the timescale of the development of alternate bars from the numerical simulations. These timescales are either a physics-based derivation (timescale of Taal (1989) and Tubino (1991)) or a combination of relevant parameters to obtain the right dimensions for time. Finally, a new timescale concerning the development of hybrid bars is introduced, which is also a combination of relevant parameters, with a length scale obtained from the theory of hybrid bars.

Development of alternate bars

Laboratory experiments by Fujita and Muramoto (1985) showed that the bar development process can be divided into three phases. In the first phase, the bar edge has become clear, and the wavelength has developed. In this phase, the increase in wavelength is rapid. Interestingly, this process differs from linear stability analyses (referring to the analysis of Fredsøe (1978)), which assume a constant wavelength. In the second phase, the bars increase in height. The final stage is the equilibrium state of the bar geometry. The process of bar elongation (phase 1) is again highlighted in the numerical experiments of Nelson (1990). He relates the mismatch of bar elongation between the laboratory and numerical experiment and the linear stability analyses to the nonlinearity of the equations governing the flow and sediment transport and due to the production of helical secondary flows due to streamline curvature. Linear analysis of Fredsøe (1978) only show agreement with the initial wavelength, which is 60%-70% of the final wavelength.

Long-duration flume experiments of a straight mobile-bed flume were conducted both with and without the presence of external forcing (transverse plate), with a constant discharge, for a period of 10 weeks long (Crosato et al. 2010) in non-resonant conditions. In the test with external forcing, steady alternate (hybrid) bars started to develop just after the start of the experiment. Free, migrating bars developed in the second half of the flume, and this area gradually reduced in size due to the gradual dominance of hybrid bars, moving downstream. In the test without an external forcing, free bars started to form along most of the flume length. Interestingly, after three weeks, a pattern of non-migrating bars developed, even though the absence of external forcing or resonant conditions. The experiments demonstrate the difference in growth rates between hybrid and free bars, as the former is much smaller, and therefore, hybrid bars appear at a later stage. Crosato and Desta (2009) also obtained this result from numerical experiments.

Morphological timescales

First of all, the time needed for cross-stream profiles, like river bars, to reach their equilibrium state is generally much shorter than the time required for the downstream slope to establish because the sediment that needs to be replaced to establish this equilibrium profile is transported over a much shorter distance (order of magnitude of the channel width) (Vriend et al. 2011). Three morphological timescales which are linked to bar development or morphological changes are evaluated.

Timescale for bed deformation by Taal (1989)
Taal (1989) defined a timescale in which bed deformations adapt to changing flow conditions. The timescale is based on a quasi-steady, linearized 2D flow model and uses a time-dependent sediment

motion model. The two length scales in the numerator are the streamwise adaptation length of perturbations in the river bed profile and the water depth. The timescale is defined as:

$$T_{Taal} = \frac{\lambda_s h}{q_s} \tag{2.4}$$

with

λ_s	=	Streamwise adaptation length for perturbations in the cross-sectional bed profile (see Equation 2.3)	m
h	=	Water depth	m
q_s	=	Bed-load transport per unit width, excluding pores	$\mathrm{m^2\,s^{-1}}$

Morphological timescale by Schielen, Doelman, and Swart (1993)
In the steps towards a linearized flow model for the analysis of free bars, Schielen, Doelman, and Swart (1993) made the time-variable dimensionless by introducing a morphological timescale T_{morph} with in the numerator the water depth and river width:

$$T_{morph} = \frac{Bh}{q_s} \tag{2.5}$$

with

B	=	Width of river	m

Timescale of bar growth by Tubino (1991)
Tubino (1991) defined the timescale of bar growth, which is the inverse of the linear growth rate of the bar amplitude based on a linear stability analysis for the development of free bars. The study of Carlin, Redolfi, and Tubino (2020) on the effect of flow unsteadiness on the long-term evolution of alternate bars applies this timescale to determine the amplitude evolution. To determine the timescale, a few steps should be taken [1]. The steps toward T_{Tubino} for the river model used in this research are given in Appendix C.

1. Determine critical half-width-to-depth ratio, based on Figure 2.4 (left).
2. Determine α_{1R}, based on Figure 2.4 (right).
3. Follow Equations 2.6.

$$\epsilon = \frac{\beta - \beta_c}{\beta_c} \quad ; \quad \Omega = \alpha_{1R} * \epsilon \quad ; \quad T^* = \frac{\frac{1}{2}B}{u} \quad ; \quad T_{Tubino} = \frac{T^*}{\Omega} \tag{2.6}$$

with

ϵ	=	Parameter for the 'distance' of the actual conditions from the critical state	-
β_c	=	Critical half-width-to-depth ratio	-
Ω	=	Exponential growth rate of perturbations in the linear regime	-

[1] Approved by personal communication with Carlin (Carlin, Redolfi, and Tubino 2020)

α_{1R}	=	Real part of the complex coefficient α_1, which is a factor in the function describing the growth of the bar amplitude over time. Dependent on θ and $\overline{d_s}$. See Figure 2.4 (left)	-
T^*	=	Factor for a dimensionless time	s^{-1}
B	=	Width of river	m
u	=	Depth-averaged flow velocity	$\mathrm{m\,s}^{-1}$

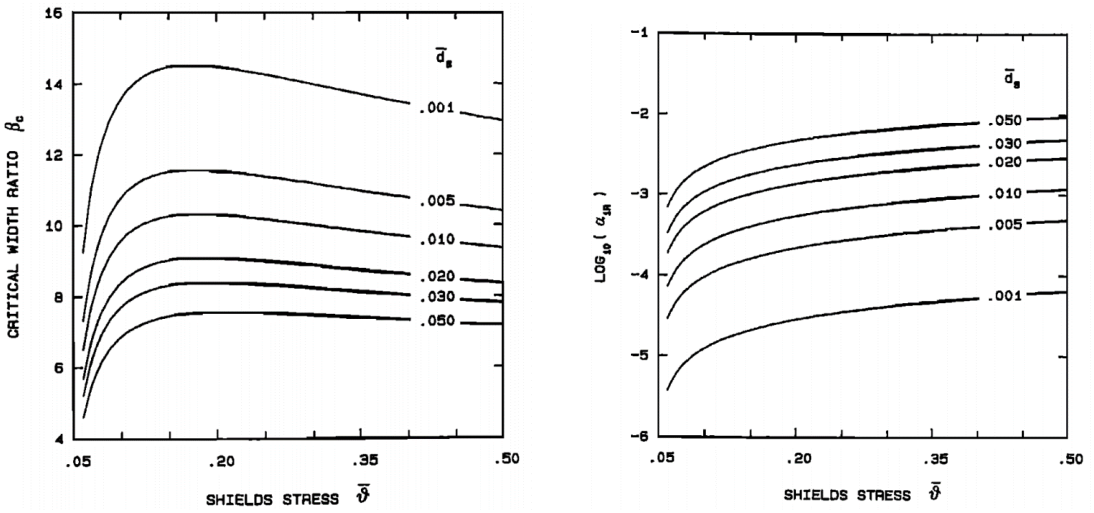

FIGURE 2.4: Figures from Tubino (1991) to determine T_{Tubino}.

A new timescale for the development of hybrid bars

Two new timescales for the development of hybrid bars are proposed to quantify the time hybrid bars need to develop towards their final topography. The development of hybrid bars starts at the fixed perturbation, developing in downstream direction. The water depth and a characteristic length are used, being the length of the complete pattern of hybrid bars or one bar's wavelength, resulting in two distinct timescales. When the two length scales are divided by the sediment transport rate ($[\mathrm{m}^2\,\mathrm{s}^{-1}]$), it yields a timescale ([s]).

To determine the length of the pattern of hybrid bars, the theory of Struiksma et al. (1985) is used. The limit to the envelope of the periodicity is set at 1 % of the initial perturbation, and the length towards this limit is referred to as L_{hybrid} (see Figure 2.5). This leads to the following formulation:

$$\exp\left(-\frac{L_{hybrid}}{L_D}\right) = 0.01 \quad \rightarrow \quad L_{hybrid} = -L_D \ln 0.01 \tag{2.7}$$

$$T_{hybrid,\,L_D} = \frac{L_{hybrid} h}{q_s} \tag{2.8}$$

L_{hybrid}	=	Length of the pattern of hybrid bars	m
L_D	=	Damping length of hybrid bars (See Equation 2.2)	m

In superresonant conditions, the length of the pattern of bars goes to infinity. Therefore, the timescale for the development of the first bar (one wavelength) is applicable:

$$T_{hybrid,\ L_P} = \frac{L_P h}{q_s} \tag{2.9}$$

L_P = Wavelength of hybrid bars (See Equation 2.2) m

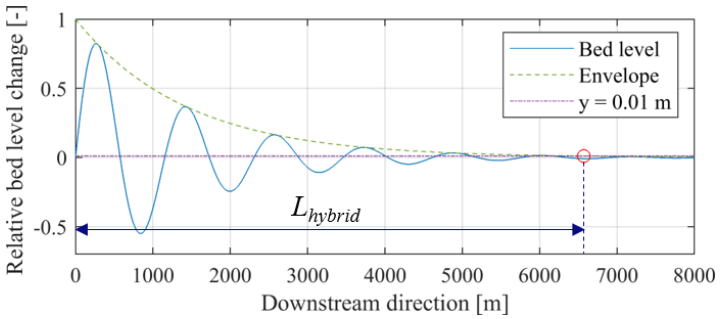

FIGURE 2.5: Example: L_{hybrid} for Q = 150 m^3/s. Bed levels and envelope with use of the theory of hybrid bars (Struiksma et al. 1985)

2.3 Alternate bars in varying discharge conditions

Discharge variability in natural rivers

The combined effects of climate, topography, lithology, soil properties, vegetation cover and land use determine the runoff and sediment yield and consequently river dynamic processes (Bai and Wang 2014). A typical 'rainfed river' shows more variation in the average discharge hydrograph than a 'glacier river'. The limited variation of the hydrograph of the glacier river is due to the temporal storage of precipitation in the form of snow, which is discharged with a delay in the springtime. Discharge measured in the Grensmaas from 1997 until 2016, measured at Borgharen Dorp, is plotted in Figure 2.6a. The large yearly variation shows the typical hydrograph of a rainfed river. The range of discharge forms the basis for the numerical model used in this thesis.

Figure 2.6b presents the average daily discharge, calculated over 20 years, showing the seasonal variation in discharge. A representative slope (450 m^3/s per 90 days) is added. The figure shows a typical 'rain river' hydrograph, with a decrease of discharge during the summer season.

Flood waves are temporary increases and decreases of water discharge and water level due to enlarged runoff in the catchment area or snowmelt, which travel downstream. Figure 2.6c presents the discharge during one flood. A representative slope of 450 m^3/s over 7 days is added. An interesting feature of the flood wave's hydrograph is the changing slope in the rising and falling stage of the flood wave. A steeper increase of discharge can be observed in the rise of the flood. In the fall of the flood, a more gradual decrease of discharge follows. The free surface slope's difference happens because of the increased propagation speed of the highest surface elevation. The steeper increase of discharge in the rise of the flood enhances the flow rate and eventually leads to the flood wave's flattening when it travels downstream. Furthermore, it means that the discharge is greater when the surface elevation rises than when it falls, which is a type of hysteresis.

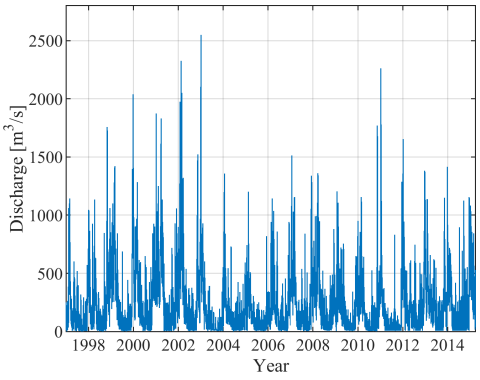

(a) Discharge measured at Borgharen Dorp (from https://waterinfo.rws.nl/).

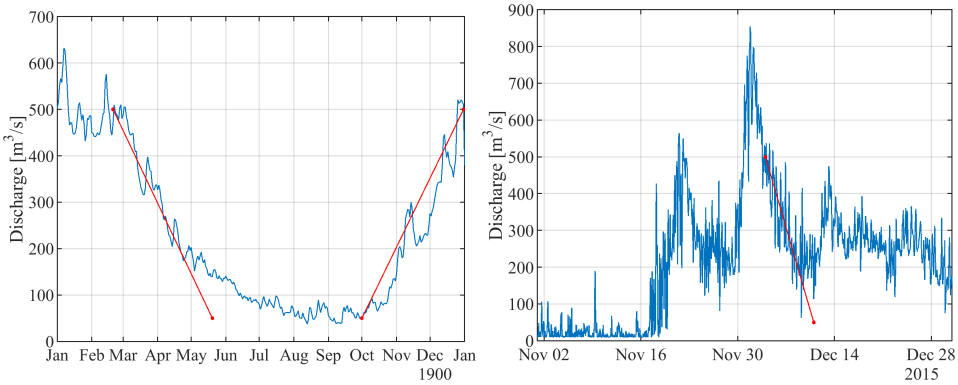

(b) Average discharge over 20 year. Slope of 450 m^3/s over 3 months.

(c) Flood wave. Slope of 450 m^3/s over 7 days.

FIGURE 2.6: Discharge data of the Grensmaas.

Influence of flow unsteadiness on bar formation

The first steps to analyse the effects of flow unsteadiness on bar formation have been made by Tubino (1991). His theory was applied for flood propagation and assumed that the steady flow is below the critical flow to set the sediment into motion, and thus the flood waves determine the bed topography. Tubino (1991) defined a quantity $\hat{U}$, representing the ratio between the timescale of basic unsteadiness and the timescale of bar growth (obtained from the linear analysis), which is the appropriate parameter that controls the influence of flow unsteadiness on bar development. If the timescale of basic unsteadiness and the timescale of bar growth are in the same order, $\hat{U}$ is around 1, flow unsteadiness affects bar development. In experiments to verify his theory, the interaction between bar development and flow unsteadiness appears to emerge in the range of values of $\hat{U}$ close to unity, as predicted by the theory. Hall (2004) analysed the effect of flow unsteadiness on alternate bars by simulating a time-periodic flow field. The unsteadiness is simulated through an oscillatory wave around a mean value. It was assumed that the flow rate never falls below the level at which no sediment transport occurs. Using a weakly nonlinear stability analysis, Hall (2004) shows that the critical wavenumber increases with the magnitude of variation of the flow field, meaning that flow unsteadiness produces bars with smaller wavelength at the critical half-width-to-depth ratio. Furthermore, it is argued that the interaction of discharge variations and migrating alternate bars produces a non-migrating sinusoidal structure of the bed. However, Crosato et al. (2011) argued that this is because discharge variations can be seen as an external forcing and could therefore explain the non-migrating bed structure.

A laboratory investigation of the height of bars formed under different discharges was conducted by Redolfi et al. (2020). The laboratory experiments were compared to the theoretically predicted bar height of Colombini, Seminara, and Tubino (1987). Although this weakly nonlinear theory is formally valid near the critical conditions, comparisons with experimental data suggest its applicability within a wider range of conditions (Lanzoni 2000). However, during extremely low discharge, the theory predicts an equilibrium elevation exceeding the water surface, which makes it no longer meaningful. Therefore, Redolfi et al. (2020) used the fully-wet threshold to predict the bar elevation: under these conditions, the maximum bar elevation is set equal to the water surface elevation. The largest bedforms tend to develop under moderate flow conditions, where discharge is high enough to mobilise the bed material and at the same time is sufficiently low with respect to the critical half-width-to-depth ratio for bar formation.

Comparable laboratory experiments by Visconti, Camporeale, and Ridolfi (2010) simulate the role of discharge variability in channel morphodynamics. The variable discharge is modelled using a stepwise hydrograph, where both conditions are significantly above the threshold of motion of the bed material. The experiments in varying discharge conditions are compared to experiments in steady discharge conditions, showing that discharge variability exhibits an acceleration in the formation of alternate bars compared to those with a steady flow, thus the final configuration is developed in less time than during steady flow conditions. They relate this to a phenomenon that they call 'triggering', a process in the transition from high to low discharges. When the discharge decreases, the curvature of the flow on the bars increases, which makes the flow able to start localized erosion. They also highlight the importance of low, while able to move sediments, discharges, playing a key role in the morphodynamics of channels, and recommend that discharge variability should be taken into account in the design of a stable straight channel, if alternate bars are expected.

Hysteresis

Hysteresis has been described in a hydrodynamic form during the passing of flood waves in the beginning of this section. Also in morphological features, a manifestation of hysteresis is observed. The transition of dune forms in rising and falling discharge stages is captured in a hysteresis loop, shown in Figure 6.6. Based on physical observations, the lag in the stage-discharge relationship is caused by bed resistance change induced by bedforms. As a result of this, the flow depth is different in rising and falling stages for similar discharges, resulting in a loop known as a hysteresis curve. Shimizu et al. (2009) performed a numerical analysis of this transition and successfully simulated the dune-flat bed transition and the associated hysteresis of the stage-discharge relationship by incorporating the variation of the form drag produced by the temporal growth or decay of bedforms under unsteady flow conditions.

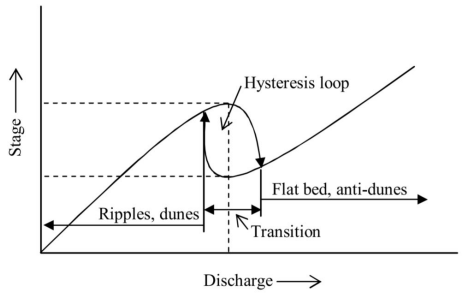

FIGURE 2.7: Hysteresis from stage-discharge curve (Shimizu et al. 2009).

Chapter 3

Numerical model and set-up

Objective

This chapter aims to provide a suitable numerical model for describing alternate bar formation such that it can be used for determining the timescales of development of free and hybrid bars and assessing alternate bars in varying discharge conditions later in this thesis.

Chapter outline

A short introduction of Delft3D is provided in Section 3.1. The set-up and the relevant parameters are discussed in Section 3.2. Two types of simulations are done; an overview of the simulations is provided in Section 3.3. The next chapters will present the results. Section 3.4 describes how to interpret the results.

3.1 Delft3D

The numerical modelling is carried out using Delft3D 4.04 Suite (version 4.04.02). Deltares has developed Delft3D to compute the hydrodynamics, water quality and morphological development on a computational domain. It is a fully nonlinear physics-based numerical model, based on the Reynolds equations for shallow flow (Lesser et al. 2004). The hydrodynamic part of the model is based on the 3D Reynolds-averaged Navier-Stokes equations for incompressible fluid and water (Boussinesq approach). A morphodynamic module is included to account for sediment transport and bed level changes.

An overview of the model parameters is shown in Table 3.1.

3.2 Model set-up

Domain
The model domain for this research is a straight river reach with a length of 10 km and a width is 90 m. An overview of the described computational domain is shown in Figure 3.1. A fixed perturbation by means of a groyne with a length of 18 m is applied for two reasons. Firstly, the groyne fixes the location where river bars develop and therefore ensures that the Delft school model is applicable to the obtained results, so the model triggers the formation of hybrid bars. Secondly, a groyne improves the similarity between the model and real rivers that are not perfectly straight. Since the rest of the domain is a perfectly straight channel where free bars can develop, the theory of Colombini, Seminara, and Tubino (1987) can be applied as well. Altogether, the choice of this model domain facilitates a comparison of the numerical model with two existing theoretical models for the formation of both hybrid as free bars.

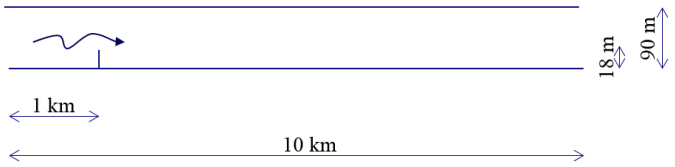

FIGURE 3.1: Modelled area.

Perturbation of the river
A fixed perturbation by means of a groyne is applied, which obstructs 20% of the channel width. A numerical study by Duró, Crosato, and Tassi (2015) showed that different groyne lengths generate a series of bars having the same characteristics (wavelengths, height, etc.) but starting at different distances from the groyne. In their study, the level of channel obstruction varied from 6.25 to 50 % of the channel width. Increasing the forcing, which is equivalent to an increased level of channel obstruction, decreases the spatial lag between the groyne and the first developed bar. Concerning the influence of groyne length on the temporal characteristics of bar formation, it was observed that the final equilibrium state is reached faster for larger groynes. A similar result was obtained from laboratory experiments with and without a groyne as upstream perturbation (Crosato et al. 2011). Therefore, in this research, the groyne length has been fixed at the 'average' of the forcings used by Duró, Crosato, and Tassi (2015). By doing so, the complexity of the numerical simulations is reduced, while the

impact on the reliability of the results is limited considering the marginal dependency of bar characteristics on the groyne length.

Boundary conditions
We impose two hydrodynamic boundary conditions, one upstream and one at the downstream end. The upstream hydrodynamic boundary condition is the imposed constant or varying (see Section 3.3) discharge. The downstream condition is modelled by means of a discharge rating curve. To determine the rating curve the uniform flow equations, based on the normal flow equations, which are a strong simplification of the 1D Shallow Water Equations (SWE), are applied. The upstream morphodynamic boundary condition is an equilibrium sediment transport rate, which prevents the bed level from changing at this boundary. The banks have been modelled as a closed wall with free-slip conditions (no tangential stress along the closed boundary).

Spatial discretisation
In general, the choice for the grid-related decisions is made by considering the trade-off between result accuracy and computation time. In this research, rectangular grid elements in a Cartesian coordinate system have been used. The grid covers a region of 27 m in the longitudinal direction and 9 m in the transversal direction. This means that the river model has 370 grid cells in the longitudinal direction and 10 in the transverse direction. The transverse wavelength of alternate bars is twice the river width. This means that half of a wavelength is represented by 10 grid cells. In general, a wavelength has to be represented by at least 20 grid points to be accurate, which is in line with the spatial grid used.

Simulation duration and time discretisation
For the constant-discharge simulations (see Section 3.3), the simulation duration is 12 months. This duration is long enough for the development of hybrid bars, which develop on a longer timescale crosatoetal2011. The two simulations with the highest discharge are stopped earlier, as the final situation was already developed after 4 months. The other sets of simulations are a temporal extension of the constant-discharge simulations, with a duration between the 40 and 800 days. The computational time-step is 30 seconds.

Sediments transport relation
The sediment transport in the Grensmaas is bed-load dominated (Wilkens and Lambeek 1997), and therefore the sediment transport relation for bed-load by Meyer-Peter and Müller (1948) is used (Equation 3.1).

$$q_s = 8\alpha D_{50}\sqrt{\Delta g D_{50}}\,(\mu\theta - \theta_{cr})^{\frac{3}{2}} \tag{3.1}$$

with

α	=	Calibration coefficient	-
D_{50}	=	Median grain size	m
θ	=	Shields parameter	-
θ_{cr}	=	Critical Shields parameter	-
μ	=	Ripple coefficient	-

The calibration coefficient α and the ripple factor μ are set equal to 1.

Sediments
The sediment size in the Grensmaas is larger than the sediment size used in the numerical model. This relatively small sediment size of 2 mm has been used for two reasons. Firstly, smaller sediment sizes enable simulations of morphological changes in the total discharge regime in the Grensmaas (50

- 1250 m^3/s). Secondly, during low discharges, corresponding to small Shields parameters, the degree of nonlinearity goes to infinity, limiting the validity of the sediment transport relation. Therefore, to model a flow regime from incipient motion to extreme mobility asks for applying different formulas during the computations (Singh et al. 2017). This is excluded by taking a relatively small sediment size, where the total discharge regime leads to Shields parameters above the critical value for the incipient motion.

Turbulence
The hydrodynamic grid is too coarse to solve the fluctuations on the turbulent scale. Therefore, the basic equations of Delft3D are Reynolds-averaged, introducing so-called Reynolds-stresses. The eddy viscosity, relating the turbulence stresses to the mean flow, is introduced to close the problem. The value depends on the flow and the grid size (proportional to a length scale and a velocity scale) used in the simulation. The length and velocity scales of this research are in the same order of magnitude as the numerical study of Duró, Crosato, and Tassi (2015). Therefore, the same value is used, being 0.1 m^2/s. The effect of the horizontal eddy viscosity on alternate-bar characteristics is investigated by Verbruggen (2012) and finds that the eddy viscosity affects the timescale of alternate-bar formation and not so much on the spatial properties. A physical explanation is provided. The horizontal eddy viscosity has a damping effect on hydrodynamic perturbations (more damping for greater value). The bed-load transport is proportional to a certain power. Therefore, the bed-load transport variation is larger for a lower eddy viscosity value, resulting in a faster formation.

This research uses the 2D depth-averaged version of Delft3D, with an appropriate parameterisation of two 3D effects: bed slope effect and secondary flow.

Secondary flow
Due to the development of alternate bars, the streamlines become curved. Secondary flow develops in curved streamlines, affecting the direction of the sediment transport. Delft3D determines the amount of secondary flow by calculating the centrifugal force in curved streamlines; the calibration factor, Espir, is set equal to 1. The parameter Betac specifies to which extent the shear stresses due to secondary flow are included in the momentum equations; this parameter is set equal to 0.5.

Bed slope effect
The formulation of Koch and Flokstra (1980), extended by Talmon, Struiksma, and Mierlo (1995), is used to take the effect on the transverse bed slope on the direction of the sediment transport into account. The direction of the bedload is adjusted according to the following formulation.

$$\tan(\varphi_s) = \frac{\sin(\varphi_\tau) + \frac{1}{f(\theta)}\frac{\partial z_b}{\partial y}}{\cos(\varphi_\tau) + \frac{1}{f(\theta)}\frac{\partial z_b}{\partial x}}, \tag{3.2}$$

with

φ_τ	=	Original direction of the sediment transport	rad
φ_s	=	Final direction of the sediment transport	rad
z_b	=	Bed level	m

$f(\theta)$ is a non-dimensional parameter weighing the effect of gravity on the motion of sediment particles on transverse bed slopes. The empirical relation of Talmon, Struiksma, and Mierlo (1995) (Equation 3.3) with a calibration factor E of 1 is used in this research.

$$f(\theta) = \frac{0.85}{E}\sqrt{\theta} \tag{3.3}$$

TABLE 3.1: Characteristics, values and justification of the parameters used in the model.

Parameter	Value	Unit	Remarks
Spatial scale			
Modelled area	9990 x 90	m^2	
Grid	370 x 10	cells	
Cell area	27 x 9	m^2	
Thin dam	18	m	20% of cross section
Temporal scale			
Period	4 - 12	months	
Time step	0.5	min	
Bed configuration			
Bed slope	$5{\cdot}10^{-4}$	m/m	From Duizendstra (1999)
Bed roughness	45	$m^{1/2}/s$	From Sharef (2006)
Median grain size	2	mm	
Turbulence			
Horizontal eddy viscosity	0.1	m^2/s	From Duró, Crosato, and Tassi (2015)

3.3 Simulation overview

Constant-discharge simulation

An overview of the simulation configurations is presented in Table 3.2. The varying input is the discharge magnitude, which is a constant value over time, ranging from 50 to 1250 m^3/s for the total simulations duration. The simulation ID is based on Q for discharge, followed by the imposed discharge.

Firstly, the final state of the simulation is analysed in Chapter 4. The hybrid bars are assessed on their damping lengths and wavelengths and compared to theoretically obtained values. These theoretically obtained values for damping length and wavelength are based on the theory of hybrid bars (Struiksma et al. 1985) and have been added to the table. Based on the damping lengths and wavelength, the theoretically predicted bar regime is determined and added in the last column. A qualitative description of the free bars is compared to the theory of free bars (Colombini, Seminara, and Tubino 1987).

Varying-discharge simulations: in- or decreasing discharge.

The upstream hydrodynamic boundary is modelled using a steadily increasing or decreasing discharge to study the river bars' response to a varying discharge. The starting points of the increasing-discharge simulations are the fully developed bed levels from simulation Q100, and for the decreasing-discharge simulations, the fully developed bed levels from simulation Q150. In this way, the transition from a superresonant to a subresonant regime, and vice versa, is modelled, which marks a clear transition for hybrid and free bars. Values of the timescales of development of free bars and hybrid bars around Q

TABLE 3.2: Overview simulations - Constant discharge.

#	Q [$m^3 s^{-1}$]	d_e [m]	β	L_P [10^3 m]	L_D [10^3 m]	Regime
Q50	50	0.67	66.9	-	- 0.13	Superresonant
Q100	100	1.07	42.1	1.08	- 1.14	Superresonant
Q125	125	1.24	36.3	1.11	10.6	Subresonant
Q150	150	1.40	32.1	1.15	1.43	Subresonant
Q200	200	1.70	26.5	1.25	0.70	Subresonant
Q250	250	1.97	22.9	1.34	0.53	Subresonant
Q300	300	2.22	20.3	1.44	0.45	Subresonant
Q400	400	2.69	16.7	1.64	0.38	Subresonant
Q500	500	3.12	14.4	1.88	0.33	Subresonant
Q750	750	4.09	11.0	2.86	0.28	Subresonant
Q1000	1000	4.96	9.1	-	0.25	Stable
Q1250	1250	5.75	7.8	-	0.23	Stable

= 125 m^3/s are used for the time intervals for the discharge variation. This results in six simulations which have been described in detail in Table 3.3. The simulation ID is based on Fastly, Medium and Slowly increasing (+) or decreasing (–) discharge.

TABLE 3.3: Overview simulations - In- or decreasing discharge.

	Starting conditions		Upstream boundary conditions	
#	Q_{start} [$m^3 s^{-1}$]	T_{start} [days]	ΔQ [$m^3 s^{-1}$]	ΔT [days]
S+	100	365	+ 50	400
S–	150	365	– 50	400
M+	100	365	+ 50	100
M–	150	365	– 50	100
F+	100	365	+ 50	40
F–	150	365	– 50	40

Varying-discharge simulations: temporal in- or decreasing discharge.

The last set of simulations is a temporal extension of the in- or decreasing discharge simulations. The increasing discharge simulations are extended with a decreasing discharge boundary condition; this set is referred to as 'a temporal increased discharge'. The decreasing discharge simulations are extended with an increasing discharge boundary condition; this set is referred to as 'a temporal decreased discharge'. The rate of increasing is the same as the rate of decreasing. This leads to the following six simulations, shown in Table 3.4. The simulation ID is extended with a T, referring to the Temporal increased or decreased discharge.

TABLE 3.4: Overview simulations - Temporal in- or decreasing discharge.

	Starting conditions	Upstream boundary conditions	
#	End of simulation	ΔQ [$\mathrm{m^3\,s^{-1}}$]	ΔT [days]
ST+	S+	– 50	400
ST-	S–	+ 50	400
MT-	M+	– 50	100
MT+	M–	+ 50	100
FT+	S+	– 50	40
FT-	S–	+ 50	40

3.4 Interpretation of the results

River bars develop as changes in bed elevation, and therefore the cumulative sedimentation or erosion of the bed as output from the numerical simulations is analysed. This corresponds to the change in bed level with respect to the initial (flat) bed. The results are provided by colour plots which represent the bed level over the full channel or the bed elevation along the left bank is projected. This is the cross-section of the colour plot along the left bank, as shown in Figure 3.2.

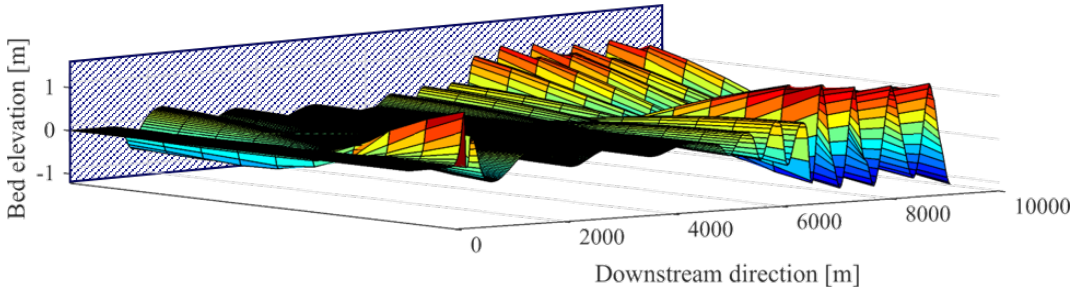

FIGURE 3.2: Visualization of bed elevation Q150 at t = 12 months. Bed elevation along left bank represents the cross-section of the dashed square with the contour plot.

Chapter 4

Instability regime of the riverbed and its resonance point

Objective

The objective of this chapter is to asses the suitability of the numerical model for describing aternate bar formation such that it can be used for determining the timescales of development of the bars and assessing alternate bars in varying discharge conditions later in this thesis. This is done by comparing the obtained insights for the variety of bar regimes from the literature study with the numerical results of the constant-discharge simulations.

Chapter outline

Section 4.1 provides the results of the numerical constant-discharge simulations. The alternate bars are assessed on their characteristics, being hybrid or free (migrating or not), their wavelength, damping length and amplitude. These results are compared with theoretical findings in Section 4.2. An overview of the bar regimes with the bar characteristics and regime limits is given in Section 4.3.

4.1 Results

This section provides the results of the constant-discharge simulations.

Bar regimes

The simulation results are discussed separately for each of the bar regimes from Table 2.1, being superresonant, subresonant and stable bed conditions. The bar characteristics per bar regime based on the literature study are recognised by the words in italic font. A ✓ follows if this is in line with the simulation results, or ✗ if this is not in line with the simulation results.

Forced bar
The forced bar is present in all simulations. Figure 2.1 shows that the erosion pit at the location of the groyne, and the sedimentation after the flow contraction, is the forced bar. When the bed level along the left bank is plotted, this means that the first wave (trough and crest) represents the forced bar.

Q50, Q100	Superresonant conditions

Hybrid bars: Amplitude growing in downstream direction. ✓
A pattern of hybrid bars, with an amplitude growing in downstream direction, can be observed in simulation Q50 and Q100 (see Figure 4.1), corresponding to superresonant conditions. A further increasing bar height in downstream direction is limited to the water depth. Therefore, the bar pattern becomes irregular for Q50 over the full domain and for Q100 from 5000 m untill the end of the domain.

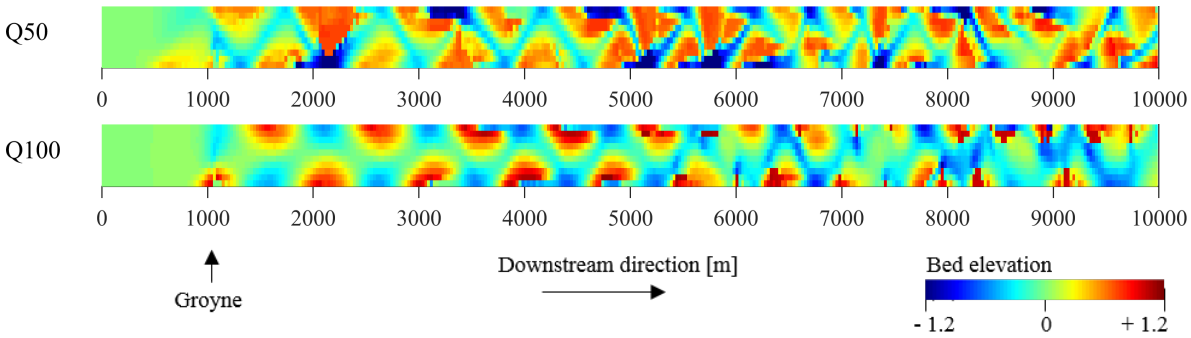

FIGURE 4.1: Bed elevation of simulation Q50 and Q100, which shows the development of alternate bars in superresonant conditions.

Free bars: Migrating in upstream direction. ✗
Free bars develop only as initial response and migrate in downstream direction. The final bed topography consists of a pattern of hybrid bars, suppressing the formation of free bars. Linear theory expects upstream migrating bars, which are not in the simulation results. The model domain has been adapted to analyse the free bars in superresonant conditions by an extension of 30 km and removal of the fixed perturbation, to limit the influence of boundary conditions. A fixed bed level is applied as upstream boundary condition, which is still a stationary perturbation for a unstable bed. As explained by Meer et al. (2011), higher-mode free bars developed, migrating in downstream direction. Downstream migrating free bars dominate the final bed topography.

The initial development of free bars is depicted in Figure 4.2. Two celerities can be deduced from Figure 4.2. Firstly, the celerity of the free bars, which is 1.8 m/day for Q50 and 3.5 m/day for Q100. Bar elongation is separated from the celerity of the bars, which is around 220% for Q50 and 130% for Q100 in the depicted month. Secondly, the celerity of the bed instability, leading to the development of new free, migrating bars, which is for both simulations around the 90 m/day!

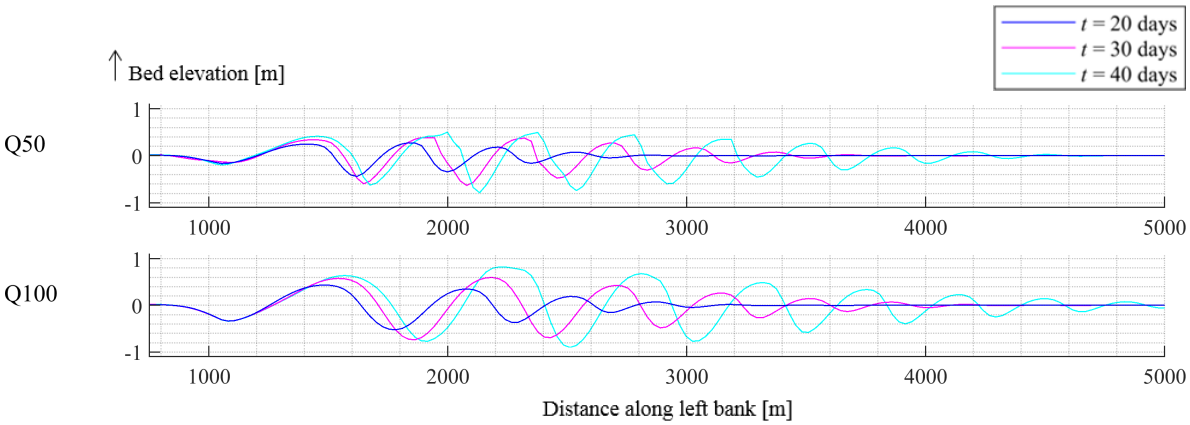

FIGURE 4.2: Development of migrating bars after 20, 30 and 40 days of simulations in superresonant conditions.

Q125-Q250	Subresonant conditions

Hybrid bars: Amplitude damped in downstream direction. ✓
See Figure 4.3. In simulation Q125 - Q250, a formation of hybrid bars damped in streamwise direction can be observed, which corresponds to subresonant conditions. The hybrid bars are damped more strongly in the simulations with a higher imposed discharge.

Free bars: Migrating in downstream direction. ✓
Between 6000 m and the end of the domain, free bars are migrating downstream while new migrating bars continuously develop at the lee side of the most downstream hybrid bars. The amplitude of the migrating bars decreases with increasing discharge. The celerity of the migrating bars increases for increasing discharge, with 7 m/day for Q125 up to 20 m/day for Q250.

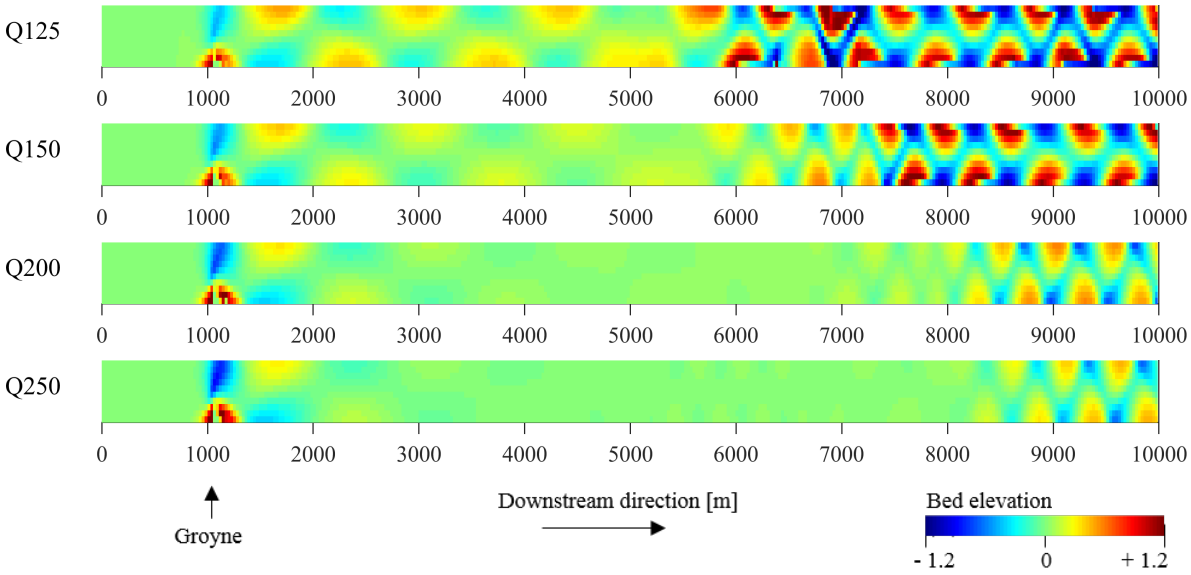

FIGURE 4.3: Bed elevation of simulation Q125 - Q250, which shows the development of alternate bars in subresonant conditions.

Q1000, Q1250 Stable bed conditions

Absence of both free as hybrid bars. ✓

Q1000 and Q1250 are in the stable bed regime, since no migrating bars develop in the domain. The forced bar is overdamped, so no hybrid bars are present in the domain. A sedimentation wave travels through the domain, starting at the erosion pit at the groyne. The final bed topography is shown in Figure 4.4, showing a forced bar around the groyne and a flat bed in the rest of the domain.

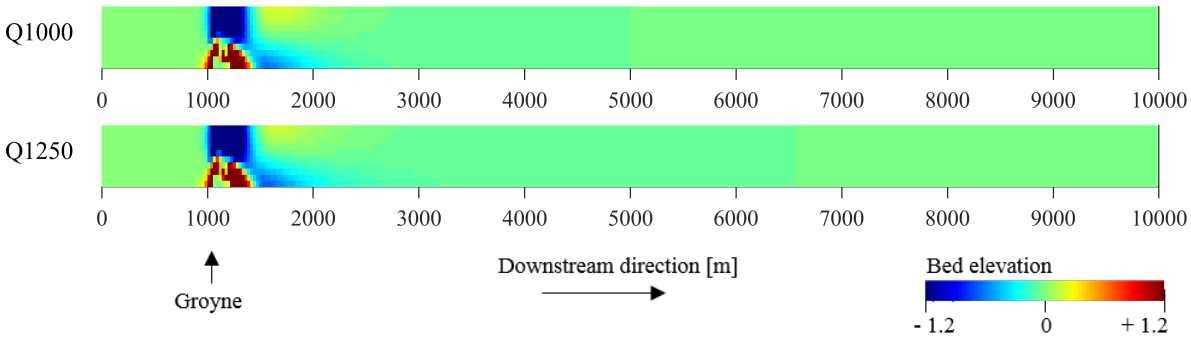

FIGURE 4.4: Bed elevation of simulation Q1000 and Q1250, which are in stable riverbed conditions.

Limits between bar regimes

The bar regimes are delineated by the resonance point and the critical half-width-to-depth ratio. Even though these limits do not resemble with one simulation, the following results can be obtained based on the numerical simulations.

Resonance point
The resonance point is characterized by a pattern of hybrid bars with a constant amplitude in downstream direction and the celerity of free bars goes to zero. A clear transition between an amplitude of the hybrid bars which is damped or growing in downstream direction can be observed between simulation Q100 and Q150, with a half-width-to-depth ratio of 42.1 and 36.3 respectively. This is shown in Figure 4.5. Therefore, the resonance point would be, based on the model, between a half-width-to-depth ratio of 42.1 and 36.3.

In both simulations, free, migrating bars develop as initial response, migrating in downstream direction. This is contradictory to the (linear) theory which expects free bars with zero celerity. Even though a pattern of steady bars resembles 'free bars with zero celerity', they can be distinguished based on their wavelength (wavelength of hybrid bars is around two times longer) and based on their shape, as free bars present a clear migration front and tend to be triangular. In simulations Q100 and Q125, the amplitude of the bars is either growing or damped in streamwise direction, so these bars are not free bars with zero celerity, but hybrid bars. Based on these simulations, free bars seem to be suppressed when a pattern of hybrid bars has developed.

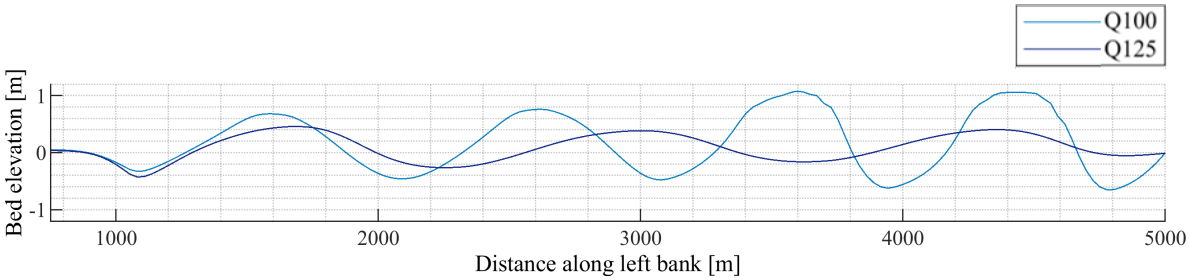

FIGURE 4.5: Bed elevation along the left bank of the river. Amplitude of the hybrid bars in Q100 grows in downstream direction, corresponding to superresonant conditions. Amplitude of the hybrid bars in Q125 is damped in downstream direction, corresponding to subresonant conditions.

Critical half-width-to-depth
The critical half-width-to-depth ratio marks the transition between a stable and an unstable riverbed. In terms of bars, it delineates the absence and presence of free, migrating bars and hybrid bars. Based on the absence or presence of free, migrating bars, the critical half-width-to-depth ratio is between 11.0 and 9.1 (simulations Q750 and Q1000), as no free bars develop in simulations Q1000 and Q1250. The presence or absence of hybrid bars is harder to observe, as the amplitude of the hybrid bars is very small, but would be between 16.7 and 14.4 (simulation Q400 and Q500).

One should take into consideration the 'occasional development' or 'only initial development' of free bars, suggesting a more gradual transition, instead of a single value for the critical half-width-to-depth ratio. In simulation Q750, a group of migrating bars (~ 5) with a small amplitude (< 0.1 m) develops from the local perturbation, migrating downstream. After migrating through the domain, a flat bed remains. Simulations Q300 - Q500 resemble this, however new bars develop with intervals of a few months from a flat bed, with shorter intervals for lower discharge simulations.

4.2 Theoretical interpretation

In this section, the results from the numerical simulations are interpreted based on the theoretical background, provided in Section 2.1.

Theory of hybrid bars

Characteristics of the hybrid bars which are provided by the theory of hybrid bars (Struiksma et al. 1985) are the damping lengths and wavelength. They are first determined based on the numerical simulations, and thereafter compared with theoretically obtained values.

Damping lengths
The sign of the damping lengths can be determined from the numerical simulations. Simulation Q50 and Q100 show a 'negative damping length' (amplitude growing in downstream direction); simulation Q150 and higher show a positive damping length. Overall, it can be derived that the bars are damped stronger with increasing discharge (shorter damping lengths).

Wavelenghts
The wavelengths of the hybrid bars are determined for simulations Q50 - Q400 when the pattern of hybrid bars is fully developed. For simulation Q500 and higher, the bars are damped so strong in downward direction that the number of bars goes to 1 and therefore it is hard to assign a wavelength to the bar. The wavelength is determined for the first bar (after the forced bar), and for clear visualisation, between two wave troughs, demonstrated in Appendix C. The results are shown as red circles in Figure 4.6.

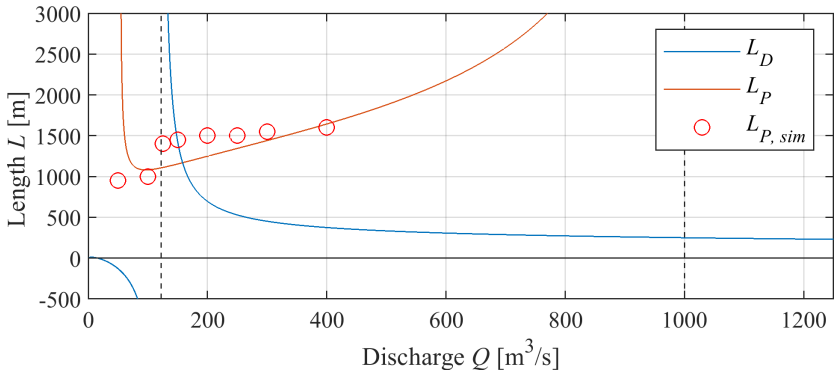

FIGURE 4.6: Damping length and wavelength for hybrid bars, from the numerical simulations (circles) and the theory of Struiksma et al. (1985) (lines)

Theoretical results
Figure 4.6 shows the damping length and wavelength for the river model, based on the theory of Struiksma et al. (1985) (see Section 2.1 and Equation 2.2). The asymptote at Q = 122 m^3/s corresponds to the resonance point, which is at a half-width-to-depth ratio of 37. The theory predicts unstable bars (growing in downstream direction) for Q < 122 m^3/s and hybrid bars which are damped in downstream direction for Q > 122 m^3/s. The asymptote at Q = 1000 m^3/s corresponds to the critical half-width-to-depth ratio, which is at a half-width-to-depth ratio of 9.1. The hybrid bars are expected to be overdamped in conditions when Q > 1000 m^3/s.

Theoretical interpretation
Applying the theory of hybrid bars to the simulations, hybrid bars growing in downstream direction

are expected in simulation Q50 and Q100 and hybrid bars which are damped in downstream direction for simulation Q125 and higher. This is in agreement with the simulations (see Figure 4.1 and Figure 4.3). Furthermore, the predicted stable regime for $Q > 1000$ m^3/s corresponds to the simulations. The wavelengths of the hybrid bars from the simulations are shown in Figure 4.6, which shows a reasonable fit to the theoretically obtained values.

Theory of free bars

The theory of free bars (Colombini, Seminara, and Tubino 1987) is not applied to the river model. However, the theory is applied to the laboratory experiments by Redolfi et al. (2020). These results are compared to the numerical output.

Figure 4.7a shows the bar height as function of discharge, applied to the settings of the laboratory experiments. The 'fully-wet limited' bar height represents the depth-limited values for bar height in simulations Q50 and Q100. The 'equilibrium' bar height shows the same shape as on the chart for the finite amplitudes of the migrating bars (Figure 4.7b).

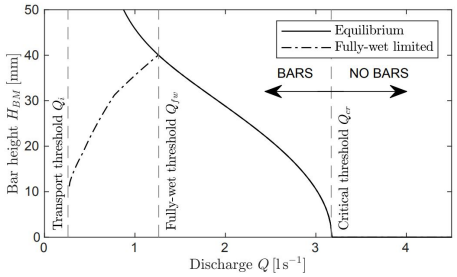

(a) Bar height as function of discharge, according to the theory of Colombini, Seminara, and Tubino (1987).

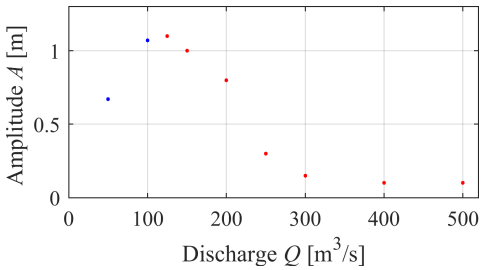

(b) Finite amplitude of migrating bars. Blue dots represents the amplitude of simulations Q50 and Q100, which are depth limited.

FIGURE 4.7: Amplitude of free bars from numerical analysis and laboratory experiments by Redolfi et al. (2020).

In the laboratory experiments the formation of diagonal bars is discussed, which developed during high flows. Comparing the shape of the migrating bars developing in low-flow conditions (Q200, Figure 4.8 left) with the shape of migrating bars in high-flow conditions (Q750, Figure 4.8 right), the through of the wavy pattern of bars in low-flow conditions (the blue triangles) are more diagonally orientated than the half cylindrical shape bars in Q750. This is in contradiction to the laboratory experiments. The laboratory experiments also highlight that "the transition from alternate-bar morphology to plane-bed configuration that is expected when discharge exceeds the critical threshold is not sharp" (Redolfi et al. 2020), which is in line with the 'occasional development' in Q300-Q750.

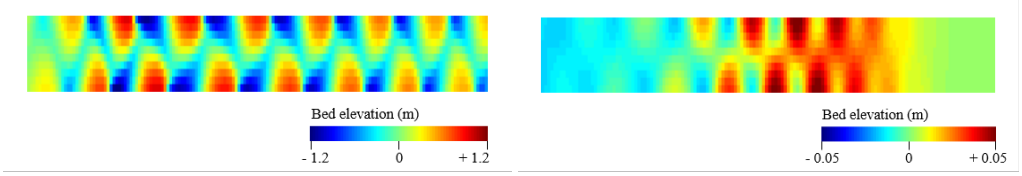

FIGURE 4.8: Bed level change, showing the migrating bars in low- (Q200, left) and high-flow (Q750, left) conditions.

4.3 Conclusion

The following bar regimes are determined based on theoretical analyses, ordered in increasing discharge magnitudes, i.e. decreasing half-width-to-depth ratio.

TABLE 4.1: Regimes of the riverbed - Numerical results.

Regime	β	Characteristics from numerical simulations
Superresonant	...66.9 - 42.1	H - Amplitude grows in downstream direction. F - Only as initial response, migrating downstream.
Resonance	37 - 38	
Subresonant	36.3 - 22.9	H - Amplitude is damped in downstream direction. F - Migrating downstream. New bars develop at the leeside of the most downstream hybrid bar.
Transition *	20.3 - 11.0	H - Amplitude is damped in downstream direction. F - Migrating downstream. A group of bars develops with intervals from a flat bed.
Stable	9.1 - 7.8...	Absence of free and hybrid bars.

Note: H - Hybrid bars, F - Free bars. * See *critical half-width-to-depth ratio*.

In the numerical simulations, the different types of bar regimes are identified. The intersection of the bar regimes provides the following remarks, based on the simulations.

The *critical half-width-to-depth ratio* appears to be a more gradual transition than the table suggests. This transition between the absence and presence of migrating bars is governed by an initial development of a group of migrating bars, travelling through the domain, leaving a flat bed behind. The development of new group of migrating bars occurs in time intervals in the order of months. This transition is at half-width-to-depth ratios from 9 to 14.

The *resonance point* is clearly observed in the numerical simulation. The pattern of hybrid bars is either growing or damped in downstream direction for half-width-to-depth ratio just above or below the resonance point of the river. This is at a half-width-to-depth ratio of 37-38.

Free bars in subresonant conditions develop at the tail of the damped bar pattern, migrating downstream. Free bars in superresonant conditions develop, migrating downstream, until a pattern of hybrid bars has developed. Therefore, the numerical model does not comply with theoretical predicted characteristics, which are based on linear theory. It is therefore recommendable to investigate the contribution of the nonlinear effects, which could explain the downstream migration of free bars in superresonant conditions.

In the numerical analysis, both free and hybrid bars do develop. However, they do not coexist: free bars develop as initial response. The development of hybrid bars takes longer. When the hybrid bars have developed, they suppress the development of free bars.

An analysis of the bar characteristics shows that the damping lengths and wavelengths of the hybrid bars have a good fit with the theoretically obtained values from Struiksma et al. (1985).

What?
The results of the numerical model in constant-discharge conditions, varying in discharge magnitude, are compared to theoretically obtained values and show a good fit. In superresonant conditions, free bars migrate downstream which is in contradiction to the linear theory. This could be explained by nonlinear effects.

So what?
The numerical model is suitable for the analysis of the formation of alternate bars in constant-discharge conditions. No restriction is found in the ability to assess the alternate bars in varying discharge conditions.

What is next?
Continue with subquestion 1. Determine the timescales of development of the different types of bars.

Chapter 5

Time dependency of alternate bars

Objective

The objective of this chapter is to determine the timescales associated with the development of the different types of bars and to link this to (existing) morphological timescales. As such, this chapter provides a basis to answer the first subquestion of this research:

1. What are the timescales related to bar development with respect to natural discharge variability?

To compare the determined timescale with timescales regarding discharge variability, the effect of discharge variability on bar formation is assessed.

Chapter outline

The constant-discharge simulations are analysed. The focus of Chapter 4 was the final (quasi-steady) bed topography. This chapter will analyse the development over time of the bed topography, starting from a flat bed.

Section 5.1 starts with a general description of this development. A distinction is made between the timescale of development of free and hybrid bars, which are separately discussed. Section 5.2 compares the determined timescales with existing morphological timescales. Finally, the outcomes of this study are presented in Section 5.3.

5.1 Results

This section focuses on simulations Q50 - Q750, as no periodic bars develop in simulations Q1000 and Q1250.

The development of the bars shows a similar pattern in both super- and subresonant conditions. Figure 5.1 shows the development of the bed in Q150 and is provided here as an example. The development is charactererised by the following three phases. Firstly, the forced bar around the groyne develops (t = 0-4 days). Secondly, free bars develop (t = 1 month). And thirdly, a pattern of hybrid bars develops (t = 4-11 months). The development of the forced bar is shortly discussed below. The description above already implies the different timescales on which free bars and hybrid bars develop, and are discussed separately in the following subsections.

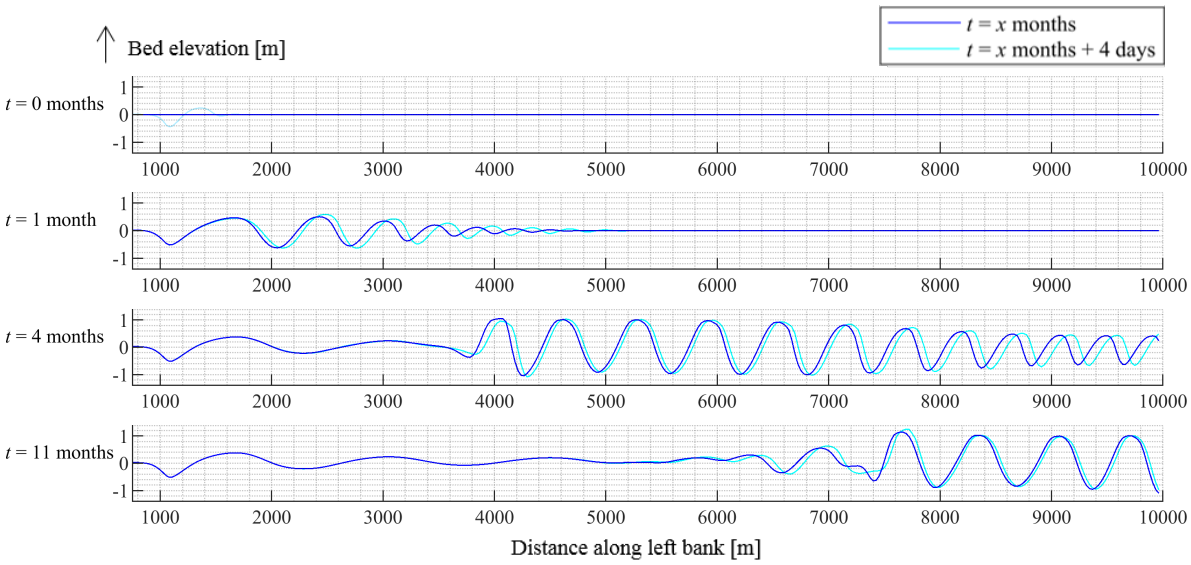

FIGURE 5.1: Development of forced, free and a pattern of hybrid bars for Q150.

The forced bar
The development of the forced bar shows an asymptotic behaviour towards the equilibrium depth, shown in Figure 5.2. After 4 days of simulation, the final depth is reached.

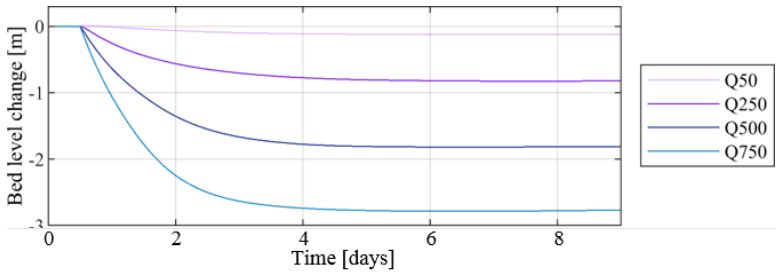

FIGURE 5.2: Development of the depth of the forced bar.

Development and timescale of free bars

The numerical simulations highlight the complexity of the free bars, due to the development over time. In the subsequent analysis of free bars, a distinction is made between the initial response and the final-amplitude state.

Initial response
Free, migrating bars develop in simulations Q50 - Q750. They are shown in Figure 5.3, after 1 month and 1 month and 4 days of simulation. It is observed that the initial amplitude decreases for increasing discharge, except simulations Q50 and Q100 where the amplitude is depth limited. The wavelength is nearly constant in the simulations. A slight increase in wavelength can be observed in simulations Q100/Q125/Q150.

Finite-amplitude state
The free bars have the following characteristics in the different bar regimes in their final state. In simulation Q50 and Q100 (superresonant conditions), a pattern of hybrid bars has developed; no free, migrating bars are in the domain anymore (see Figure 4.1). For simulations Q125 - Q200, the amplitude of migrating bars increases as they travel downstream. New migrating bars develop at the tail of the pattern of hybrid bars (see Figure B.6 - B.10). In simulations Q300 - Q750, the amplitude of the migrating bars shows a little increase as they travel downstream, but remains relatively small (see Figure B.14 - B.20).

Timescale of free bars
The following definition is assigned to the timescale of development of free bars:

> T_{free}: the timescale of free bars is the time until a group of 5 free, migrating bars have developed.

This definition marks a clear moment in the development, so it is easy to distinguish, and it is applicable in all the simulations. The definition emphasizes the time it takes to develop the bed instability which is associated to free bars, starting from a flat bed. This timescale is representative for the time a formative discharge for free bars has to hold to develop a group of free, migrating bars. The numbers of bars in this group consists of mainly 5 bars. As the bars develop from the fixed perturbation, 6 wave tops have to be identified, including the forced bars. The snapshots of this timescale are presented in Appendix C.

The analysis of the simulations (Q50 - Q750) shows that in all simulations T_{free} is around the 20 days. A possible explanation is that the degree of instability decreases with increasing discharge, due to the decreasing half-width-to-depth ratio. The adaptability of the bed increases with increasing discharge, due to the increase of transported sediments. The effect of these two processes appears to counterweight each other, which results in a constant timescale for the development of free bars for the different discharge simulations.

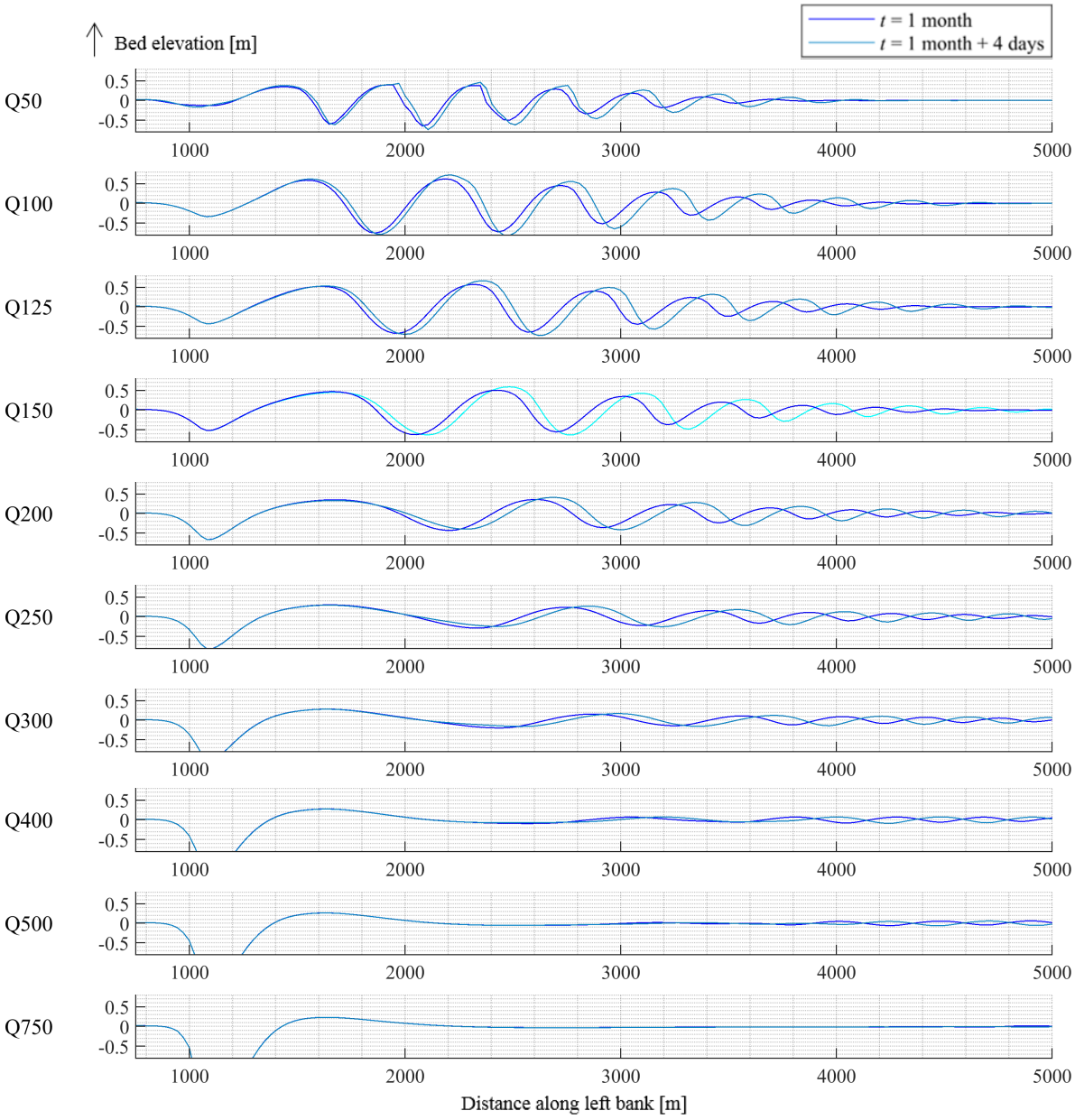

FIGURE 5.3: Development of free, migrating bars after 1 months of simulations.

Development and timescale of hybrid bars

Development of hybrid bars
The pattern of the hybrid bars develops in downstream direction, starting at the fixed perturbation.

Timescale of hybrid bars
To assign a timescale to the development of hybrid bars, the length of the reach which is developed is taken into account to determine the timescale. For the development of hybrid bars, two length scales are determined, being towards the development of the first bar and towards the development of the full pattern of hybrid bars. The snapshots of these timescales are again presented in Appendix C.

$T_{hybrid\ L_P}$: timescale of hybrid bars towards the development of the first bar.

$T_{hybrid\ L_D}$: timescale of hybrid bars towards a full pattern of hybrid bars has developed.

The timescales of development of the (free and) hybrid bars are plotted in Figure 5.4. The figure shows that both timescales of hybrid bars decrease for increasing discharge. Two effects play a role in the timescale for the first bar. The wavelength increases for increasing discharge (see Figure 4.6) which would result in an increasing timescale for increasing discharge. The transported sediment increases for increasing discharge which would result in an decreasing timescale for increasing discharge. From this it can be concluded that the effect of a longer wavelength is subsidiary as the timescale decreases for increasing discharge. The length of the pattern of hybrid bars decreases for increasing discharge, which intensifies the decreasing timescale for increasing discharge.

Concluding remarks

A clear difference in the timescales of development of the two bar types is determined. They are both shown in Figure 5.4. The timescale of hybrid bars is around 6 times greater than the timescale of free bars.

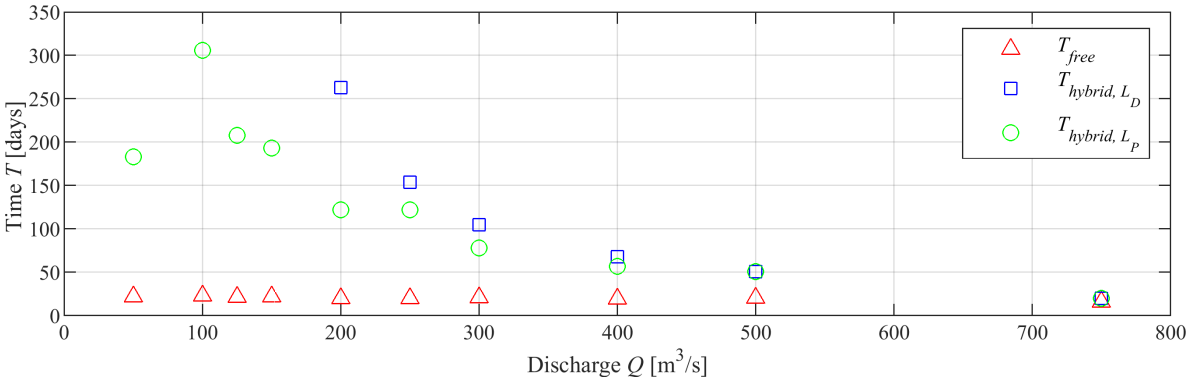

FIGURE 5.4: T_{free}, $T_{hybrid\ L_D}$ and $T_{hybrid\ L_P}$ from the simulations.

5.2 Predictive capacity of morphological timescales

The following two figures show the morphological timescales obtained from the literature study (T_{Taal}, T_{morph}, T_{Tubino}, T_{hybrid,L_P} and T_{hybrid,L_D}) applied to the river model together with the timescales obtained from the numerical analysis. In the figures, the theoretical values are solid lines; the symbols represent the numerical simulations. Figure 5.5 shows the new timescale for the development of hybrid bars T_{hybrid,L_P} and T_{hybrid,L_D} from Equation 2.9 and Equation 2.8 with the timescale of hybrid bars derived from the numerical simulations. Figure 5.6 shows the timescale of Taal (1989), Tubino (1991) and Schielen, Doelman, and Swart (1993) discussed in Section 2.2 together with the timescale of free bars derived from the numerical analysis. T_{Tubino} is determined per simulation. The steps to determine these values are presented in Appendix C.

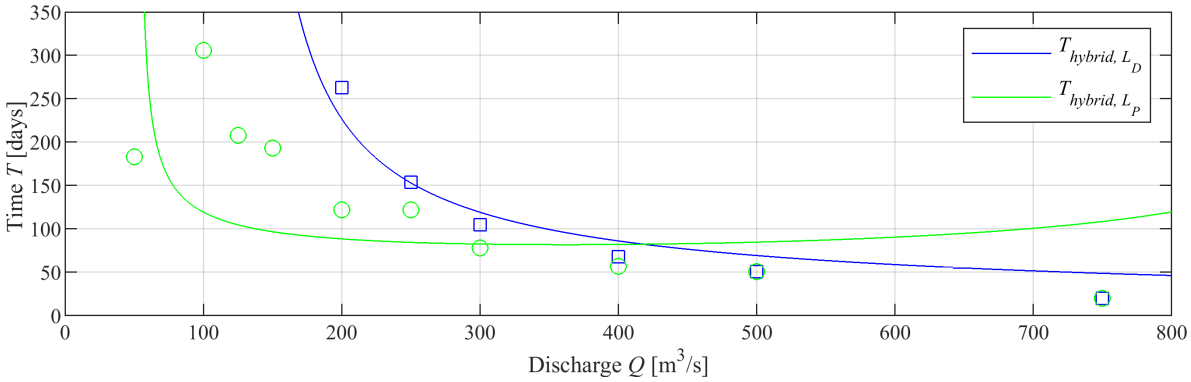

FIGURE 5.5: T_{hybrid} from the simulations Q50 - Q750, with morphological timescales.

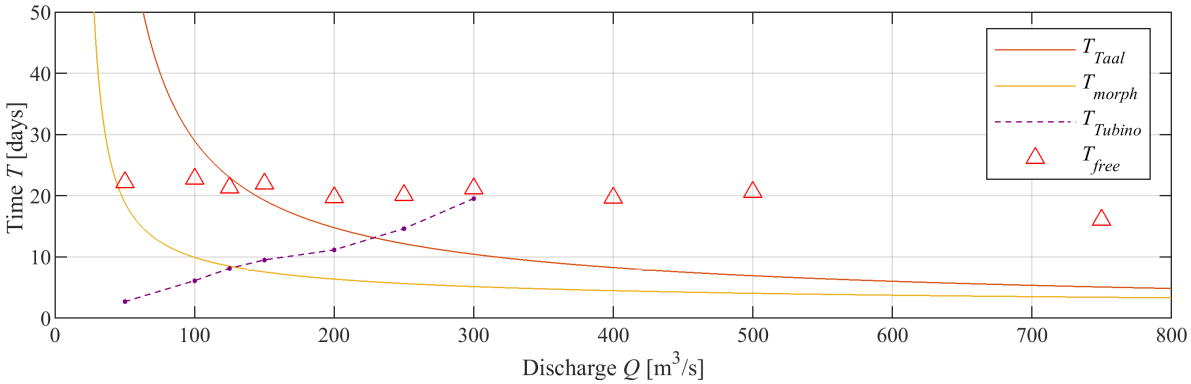

FIGURE 5.6: T_{free} from the simulations Q50 - Q750, with morphological timescales.

From this, the following statements can be concluded:

- The new timescale for the development of a pattern of hybrid bar T_{hybrid,L_D} shows a good fit for the timescale of hybrid bars obtained from the numerical analysis. The timescale is only valid in the subresonant regime, as L_{hybrid} goes to infinity in the superresonant regime.
- The other morphological timescales (T_{Taal}, T_{morph}, T_{Tubino} and T_{hybrid,L_D}) appear to be an underestimate of the timescales related to bar development from the numerical simulations, both for free bars as the development of the first bar in the pattern of hybrid bars.
- Especially the timescale of free bars is in same order of the timescale of seasonal discharge variability which is also in the order of days to months.

5.3 Conclusion

At the start of this chapter the question has been posed concerning the timescale related to bar development with respect to natural discharge variability. The results from this chapter substantiate the following conclusions.

The simulation results have shown that a difference in growth rate between hybrid and free bars exists. It was observed that the development of hybrid bars happens on a longer timescale compared to free bars, or equivalently that hybrid bars appear later in the bar formation process. Another difference that was observed is that hybrid bars develop in downstream direction whereas free bars initially develop from the fixed perturbation and as they travel through the domain, new bars spontaneously develop from the flat bed. This is in the mathematical derivations for describing the two types of bars, as they distinct between an initial response (free bars, Colombini, Seminara, and Tubino (1987)) and a final stable bed (hybrid bars, Struiksma et al. (1985)).

Three timescales have been determined of which two characterise the development of hybrid bars, and one characterises the development of free bars. The timescale of free bars shows little variation over the different simulations. An explanation is provided, as the degree of instability increases for lower discharges, but the sediment transport transport rate decreases. These two processes seem to counterweight each other. A new timescale for the development of hybrid bars, based on their damping length, shows a good fit to the timescale of the development of a full pattern of hybrid bars.

Based on a comparison of the timescales of the alternate bars and timescales of discharge variability, in line with the unsteadiness parameter $\hat{U}$ from Tubino (1991), it can be concluded that the timescale of free bars and seasonal discharge variability are in the same order of magnitude, which is in the order of weeks to months, and therefore, discharge variability affects free bars' development. The timescale of hybrid bars is one order of magnitude greater, and therefore hybrid bars are expected to respond to variations over years. The timescales of single floods, being in the order of days to weeks, are presumably too short to interfere with the development of free and hybrid bars.

What?
The timescales of development of the hybrid and free bars have been determined, showing a large difference. The timescale of free bars is in the same order as magnitude of the timescales associated to seasonal discharge variability.

So what?
As the timescale of free bars is in the same order of the timescale of seasonal variations in river discharge, the evolution of free bars should be largely influenced by natural discharge variability. Therefore, it is interesting to assess alternate bars in varying discharge conditions. The difference in timescales of free and hybrid bars suggests a different response of the bars to varying discharge conditions.

What is next?
Based on the bar regimes and the timescale derived, the set-up for the varying discharge simulations is valid, so the research continues with answering subquestions 2 and 3: Assess the alternate bars in varying discharge conditions.

Chapter 6

Alternate bars in varying discharge conditions

Objective

The objective of this chapter is to understand the response of alternate bars to varying discharge conditions. As such, this chapter provides a basis to answer the last two subquestions of this research:

2. How is the transition from super- to subresonant conditions, and vice versa, due to a varying discharge?
3. How do alternate bars respond to a temporal in- or decreased discharge?

Chapter outline

The results of the varying discharge simulations are given in Section **??**. The transition between super- and subresonant conditions is assessed based on the in- or decreasing-discharge simulations. The response of the alternate bars is assessed based on the temporal in- or decreased-discharge simulations. The transition and response show a type of hysteresis, which is further elaborated on in the end of this section. Reflection on the subquestions is given in Section 6.4.

6.1 The transition between super- and subresonant conditions

Introduction
To study the transition of the riverbed from super- to subresonant, and vice versa, the numerical model from Chapter 5 and Chapter 4 was used but now with a steadily increasing or steadily decreasing discharge. The simulation ID is based on Slowly, Medium and Fast varying discharge. The overview of the simulations is presented in Table 3.3.

The imposed discharges of the six simulations are plotted in Figure 6.1. The horizontal lines correspond to half-width-to-depth ratios between 35 to 41, which capture the resonance point of the river. The intersections of the dashed lines and the imposed discharge correspond to the moments in time for which the bed levels are provided in Figure 6.2. The same colours in this figure correspond to the same half-width-to-depth ratio along the dashed lines from Figure 6.1.

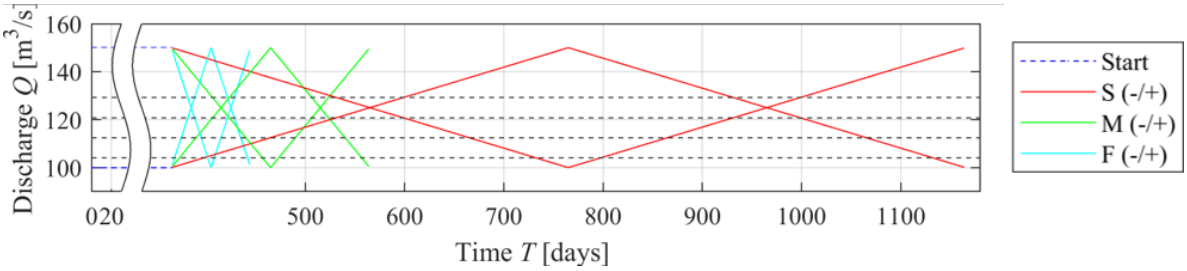

FIGURE 6.1: Input in- or decreasing-discharge simulations, with intersection of output plots (see Figure 6.2).

Results
Simulation S+ shows the transition of the bed from superresonant towards subresonant conditions. The amplitude of the hybrid bars decreases towards a constant amplitude in downstream direction, while at the same time the bars are slowly migrating. During the migration of the hybrid bars, we see the bars become more skewed in downstream direction. Starting from the fixed perturbation, a new pattern of hybrid bars with a damped character develops: see the bed elevation at t_4. The bars migrate faster than the development of hybrid bars starting from the perturbation. Furthermore, we see that the transition is accelerated as the discharge increases.

Simulation S- shows the response of the hybrid bars to a decreasing discharge, corresponding to a transition from subresonant towards superresonant conditions. At the location of the most downstream located hybrid bars, free bars develop. This bed instability slowly moves upstream. The pattern of hybrid bars becomes steeper with shorter wavelengths.

When the timeinterval is decreased, the difference in timescale of development of the hybrid and free bars can be observed. Based on simulations M-, we see that the steady, hybrid bars in the upstream part of the domain show little adaptation to the changing discharge. However, free bars located between 3500 m and 5000 m have developed over the domain. This suggests that the development of free bars is faster compared to hybrid bars, which is in agreement with the observations of Chapter 5. Simulations F+ and F- show little adaptation of the hybrid bars to the changing discharge. Also, no free bars develop in simulation F-, as the time to adapt to the new discharge conditions is too short.

Conclusion
From the results, we can conclude that the transition towards the new bar regimes is governed by a

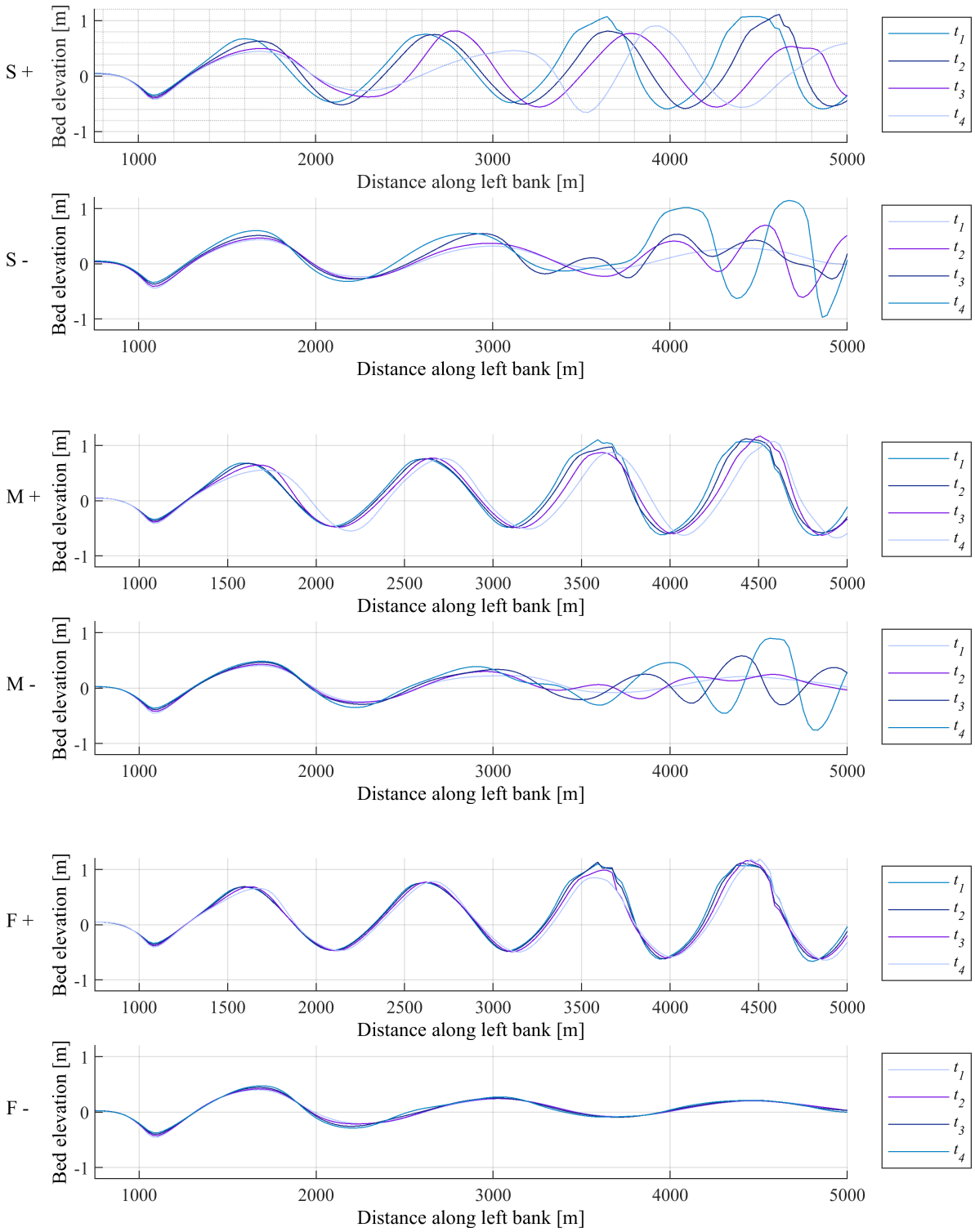

FIGURE 6.2: Results of in- or decreasing-discharge simulations.

migration of the alternate bars. For an increasing discharge, this is due to the downstream migration of the hybrid bars. For a decreasing discharge, the transition is captured by the development of free bars. But, the free bars only develop where the hybrid bars are damped strong enough. This suggests a stabilizing effect of the hybrid bars on the bed, suppressing the formation of free bars.

6.2 The response of the riverbed to a temporal in- or decreased discharge

Introduction

To study the response of the riverbed to a temporal in- or decreased discharge, the first set of simulations is extended, bringing the discharge conditions back to its initial condition. The imposed discharges of the six simulations are plotted in Figure 6.3. The bed levels just before the changing discharge are compared with the bed levels just after the changing discharge. For the temporal increased discharge, this corresponds to the squares in Figure 6.2; for the temporal decreased discharge, this corresponds to the circles in Figure 6.2.

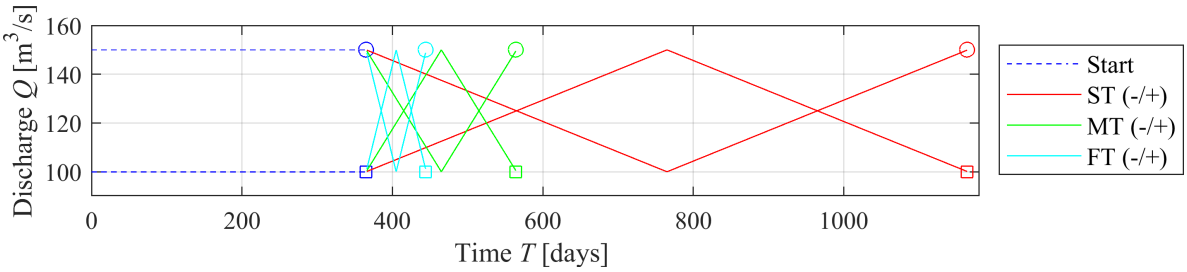

FIGURE 6.3: Input variable discharge, with intersection of output plots (see Figure 6.2).

Results

Figure 6.4 shows the bed levels of the three simulations after a temporal increased discharge. We see that for all simulations, the wavelength of the hybrid bar is larger after the temporal increased discharge. The pattern for the Medium variation (green) shows the presence of higher harmonics which have developed during subresonant conditions. The Fastly variation (cyan) only shows a downstream migration of the pattern of hybrid bars.

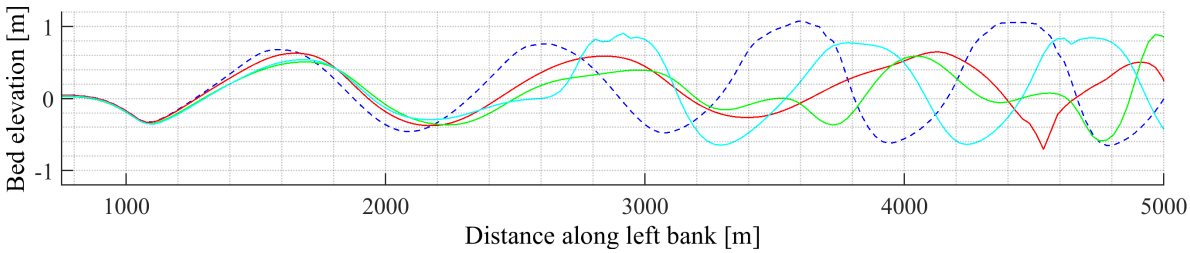

FIGURE 6.4: Results of temporal increased discharge simulations. The colours correspond to the simulations indicated in Figure 6.3.

Figure 6.5 shows the results after a temporal decreased discharge. For all the simulations, the bed has become unstable in the transition towards superresonant conditions, and the free bars are still in the domain. The pattern of hybrid bars at the end of the Slowly variation (red) nearly resembles the initial conditions, except for the free bars between 4000 and 5000 m. For the Medium and Fastly variation, free bars are still in the domain.

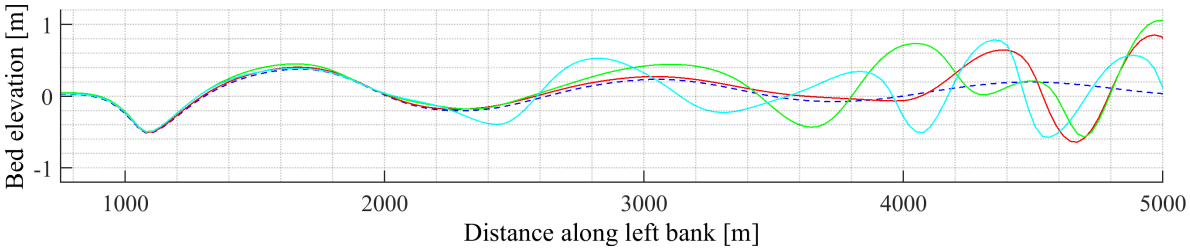

FIGURE 6.5: Results of temporal decreased discharge simulations. The colours correspond to the simulations indicated in Figure 6.3.

Conclusion
So for the simulations, we see that the bed levels after a temporal in- or decreased discharge are not the same as the initial bed level. Two factors play a role. Firstly, the bed needs time to adapt to the new flow conditions. Especially, if the final state is in superresonant conditions, the bed needs a longer time to adapt to the final flow conditions. This results in a shorter wavelengths of the hybrid bars. This is in line with the analysis of Hall (2004), which expects shorter bars for increasing discharge variability. Secondly, the appearance and disappearance of free bars happens in a different manner. Free bars develop from a bed instability, growing in vertical direction. They leave the domain by a downstream migration, which takes longer time than the development. This finding is based on the temporal decreased discharge conditions, as the free bars have developed fastly during the temporal superresonant conditinos, but are still in the domain when the bed returns to subresonant conditions.

6.3 Hysteresis

From the previous two sections, the following two observations can been done:

- The transition around resonant conditions differs for rising and falling discharge stage.
- The bed levels after a temporal discharge variation is different than the bed levels before the discharge variation.

Those two conclusions are captured in a hysteresis loop, visualized in Figure 6.6. The figure is applicable at the location of the first hybrid bars. This is for the numerical model between x = 2000 and 5000 m. Two essential factors play a role in the hysteresis loop, being the difference in timescales and development of free and hybrid bars.

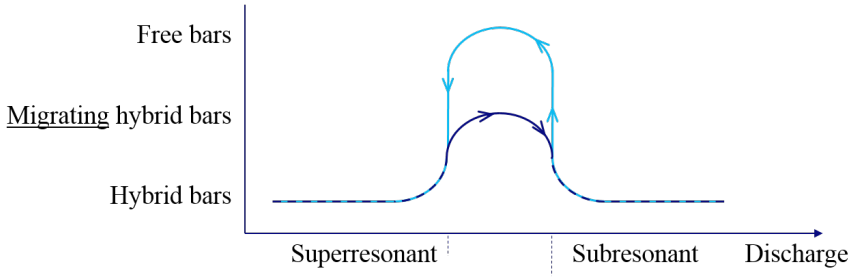

FIGURE 6.6: Hysteresis in the transition between sub- and superresonant conditions. The transition from superresonant to subresonant conditions (blue line) is characterized by the donwstream migration of the pattern of hybrid bars. The transition from subresonant to superresonant conditions (cyan line) is characterized by the development of free bars.

The distance between 'Superresonant' and 'Subresonant' conditions refers to the time lag to which the bed needs to adapt to the new flow conditions. The transition from super- to subresonant conditions is characterized by an acceleration, due to the decreased timescales in subresonant condition. A deceleration is applicable for the reversed direction.

6.4 Conclusion

At the start of this chapter two questions have been posed, regarding the transition from super- to subresonant conditions, and vice versa, due to a varying discharge and the response of alternate bars to a temporal in- or decreased discharge. They both substantiate a type of hysteresis and the following conclusions.

The response of the bars to the discharge variation rate is governed by a downstream migration of the alternate bars. Free bars only develop at locations where the bed is flat enough. The presence of hybrid bars suppresses the development of free bars. The new hybrid bar configuration develops in downstream direction, starting at the fixed perturbation.

Based on the response and transition around resonant conditions, a type of hysteresis could be observed during rising and falling stages of varying flow. Hysteresis in the transition around the resonance point of the river is detected, due to an increased stability of the bed when a steady bar pattern has developed. This bed stability suppresses the formation of free bars in the simulations with an increasing discharge (the transition from superresonant to subresonant conditions).

Chapter 7

Discussion

The previous chapters have provided answers to the research questions to achieve the research goal of this thesis. However, some relevant problems and topics are not yet dealt with and are essential to provide a constructive conclusion. This discussion is partly due to undealt topics, and due to limitations to this research. An overall conclusion and recommendations for further research are provided in Chapter 8.

Effect of groyne length on timescales of development
Duró, Crosato, and Tassi (2015) described that the length of the groyne (the intensity of forcing) influences the speed of morphological changes; the rate increases with increasing groyne length. Quantitative values are not provided. However, it means that the timescales of the bars' development should thus be a function of the amount of forcing. Additional simulations have been carried out with an increased groyne length. The results are shown in Figure 7.1. These results contradict the findings of Duró, Crosato, and Tassi (2015), as the simulations showed little to zero variation in the rate of development. Why and how much the amount of forcing affects the timescales of bar formation is still questionable.

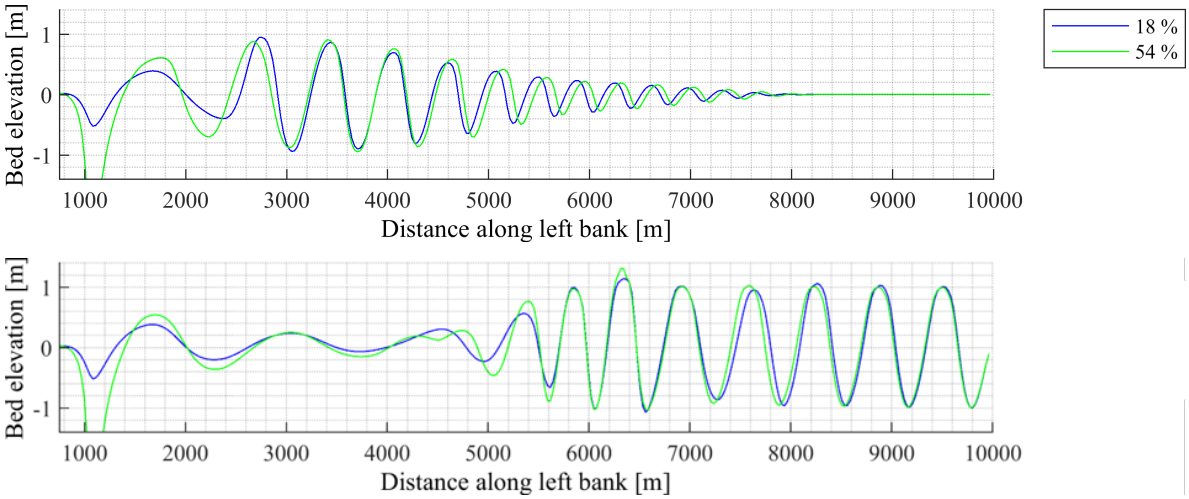

FIGURE 7.1: Bed level along left bank for simulation Q125 with 18% channel obstruction and 54% channel obstruction, after 2 (top) and 8 (bottom) months of simulation.

Effect of transverse bed slopes
The effect of the transverse bed slope on the direction of sediment transport is assessed in the numerical analysis and the theories in a different way. The numerical analysis in Delft3D make use of the empirical relation derived by Talmon, Struiksma, and Mierlo (1995) (Equation 3.2), which is an adaptation of the formula of Koch and Flokstra (1980), which is used in the work of Struiksma et al. (1985). The theory of Colombini, Seminara, and Tubino (1987) and Tubino (1991) makes use of the empirical parameter r (Engelund 1981; Ikeda 1982), ranging between 0.3 and 0.6. Verbruggen (2012)

showed with a numerical study that the strength of the gravitational pull on the transverse bed slope has strong consequences on the bar amplitude. Despite a large number of studies on the transverse bed slope effect, it has still large uncertainties. As the effect of the transverse bed slopes on the sediment transport rates also affects the rate of the development of the bars, the settings of the transverse bed slope may influence the timescales derived in Chapter 5.

The following simplifications has been done in this research, with respect to natural rivers. To apply the findings of this research to real rivers, the following limitations should be taken into account. They are separately discussed on how they will influence the results if their complexity would be taken into account.

River geometry
First of all, the river geometry is strongly simplified, neglecting 1) temporal and longitudinal variations in river width (due to bank erosion), 2) curvature, and 3) varying width over depth. 1) and 2) are a type of forcing to the river bars, which limits the migration of bars, as they can get stuck to local perturbations. 3) has strong implications to the half-width-to-depth ratio of the river. The half-width-to-depth ratio is not proportional to the water depth anymore. The inundation of flood plains during high discharges (see Figure 7.2) results in a sudden increase of the half-width-to-depth ratio. This could lead to the development of alternate bars, even in higher discharge regimes. Furthermore, the varying width over depth has strong implications on the transverse bed slope.

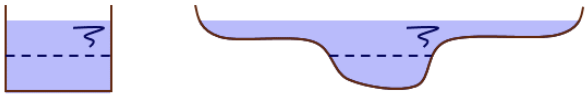

FIGURE 7.2: Simplified river cross-section used in this research and a 'natural' cross-section with floodplains.

Sediment sizes and transport relation
For this research, a small, uniform sediment size is used. However, the Grensmaas and other natural rivers with higher bar modes are typical sand-gravel rivers and show large sediment heterogeneity (see Table A.1). Sediment sorting on free alternate bars has shown to provide small sediments in the pools and coarse sediments on the bar tops (Lanzoni 2000; Cordier et al. 2019). A numerical study by Singh et al. (2017) showed that the degree of heterogeneity and mobility has effect on the bar geometry (bar height and lengths, even bar mode). Especially the case of partial mobility has effect on the outcomes of this research, as relatively small sediment transport rates result in delayed bed adaptations.

The sediment transport relation in this research only takes bed-load into account. Fredsøe (1978) elaborates the effect of suspended and bed-load transport on the formation of dunes and antidunes. Bed-load dominated rivers are linked to the formation of dunes. Within the analogy of dunes with river bars, the formation of river bars would be limited in suspended-dominated rivers, as their inertial time lag is very long. To verify this, additional simulations can be done using different sediment transport relations.

Small-scale bed forms
The formation of small-scale bedforms (ripples, dunes and antidunes) are neglected in this analysis, even though they affect the hydraulic roughness. A field study by Rodrigues et al. (2015) analysed the superimposed dunes on the river bars during flood events and found that the hysteresis of the steepness of the dunes affects the flow resistance of the dunes as well as the celerity of the migrating bars. Furthermore, the dune height is a function of water depth and flow velocity and therefore shows variations

over the bars. Linking this to a variable hydraulic roughness over the bars, it can be argued that the formation of small-scale bedforms can alter the bar geometry significantly.

From a numerical model to real rivers
The final, inevitable limitation of using a numerical model is the numerical model itself. The Delft3D scheme is rather diffusive. Verbruggen (2012) analysed the effect of numerical diffusion on alternate bars. Hybrid bars seems to be hardly influenced by the morphological scheme introducing numerical diffusion. However, numerical diffusion causes free bars to be damped, increasing their wavelengths.

Chapter 8

Conclusion

This thesis aims to create a better understanding of the development of alternate bars in varying discharge conditions. Therefore, insight into the timescales of alternate bar development and the response of alternate bars to (natural) discharge variability is studied by means of a numerical model. A list of new findings is provided in this chapter, finishing with a reflection on the research objective.

Possibility to asses free and hybrid bars in one numerical model

This thesis shows the applicability of linear theories for both free and hybrid bars in one numerical model. As the model domain is straight, long and a fixed perturbation is applied, both free and hybrid bars developed in the domain. Most of the studies on alternate bars focus on one type of alternate bars. However, this study shows that it is also possible to assess both types of alternate bars.

Difference in the development of free and hybrid bars and their associated timescales

The numerical study has shown that free bars need less time to develop to their final amplitude than hybrid bars. The development of hybrid bars is in downstream direction, starting at a fixed perturbation. Free bars can develop over the full domain when the bed becomes unstable. The timescale of the development of free bars appears to be in the same order as the timescales of seasonal variations. A single flood has a too short timescale and would show little variation to the development of the bars.

Hysteresis in the transition around resonant conditions

Concerning the transition around resonant conditions, it is observed that free bars only develop where the bed is initially relatively flat during the decreasing discharge simulations. The pattern of hybrid bars provides a stable configuration, suppressing the development of free bars. The transition from a pattern of hybrid bars with an amplitude growing in downstream direction towards a subresonant condition with an amplitude damped in downstream direction starts from the fixed perturbation, developing in downstream direction. The transition is governed by a downstream migration of the pattern of hybrid bars. This difference in the development and associated timescale for free and hybrid bars has led to a type of hysteresis.

Reflection on the research objective

The longer timescales for lower discharges suggest subresonant conditions to be more determinative for the final bed topography than superresonant conditions. The development of free bars, originating from a bed instability, takes less time than the development of hybrid bars. But this thesis also shows the increased stability of the bed due to the formation of hybrid bars. Therefore, the bed configuration is not solely related to discharge conditions in subresonant conditions, but the bed topography from earlier discharge conditions should be taken into account too. Based on the findings, the following recommendations have been made.

Practical recommendations

As the development of (alternate) bars are important for creating suitable habitats for aquatic fauna and riparian vegetation in river restoration project, some insight relevant for river restoration projects is provided. Therefore, the complexity of alternate bars in varying discharge conditions should be reduced to applicable design criteria. It was already clear that river widening simulates the development of river bars Duró, Crosato, and Tassi (2015).

The project locations along the Grensmaas are mostly located in the area of bends. Bends are known for their complex flow structure (helical flow) and the development of point bars, which indeed would stimulate the formation of a point bar. This thesis emphasises the presence of a straight part for the development of free bars. Therefore, it is recommended to widen relatively straight parts for the development of free bars.

River restoration projects span multiple years. During construction, bed instabilities could lead to the formation of free bars. The final configuration would be dominated by the formation of hybrid bars, as natural rivers are not perfectly straight. Therefore, it is recommended to base the spatial scales of projects on the wavelength of hybrid bars.

To take the discharge variation into account, a first analysis of the bar regimes should be done. The theory for hybrid bars Struiksma et al. (1985) shows to be suitable to determine the bar regime. Based on an analysis of the timescales of discharge variability and the timescale for hybrid and free bars, the effect of the discharge variability can be assessed. A decreased wavelength of the hybrid bars can be expected when intervals in superresonant conditions occur during subresonant conditions.

Practical recommendations - Grensmaas

To apply the findings of this research to the Grensmaas, the theory of Struiksma et al. (1985) which is applied to the river model is adapted to the sediment size of the Grensmaas ($D_{50} \approx 15$ mm, from Duizendstra (1999)) presented in Figure 8.1. Resonance occurs at a discharge of 470 m^3/s which corresponds to a wavelength of the hybrid bars of 835 m. The critical discharge for the formation of bars is at 685 m^3/s. A number of relatively new, steady bars in the Grensmaas are shown in Figure 8.3. In

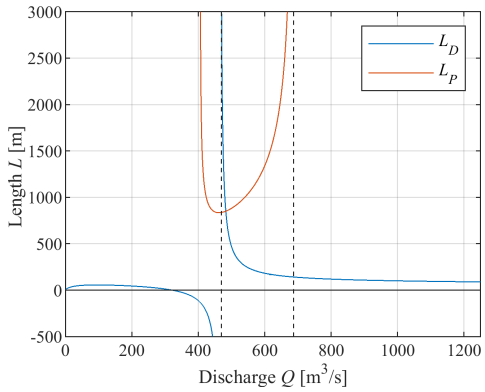

FIGURE 8.1: Damping length and wavelengths of hybrid bars, applied to the Grensmaas, with D_{50} = 15 mm.

the figure caption, the forming mechanism is presented. Bar 2 shows the only alternate pattern, with an amplitude damped in downstream direction, which has a wavelength of 600 m. This is shorter than the expected wavelengths in the subresonant regime. However, one of the limitations of this research is

strongly applicable to the Grensmaas, as the sediment sizes in the Grensmaas is strongly non-uniform. The study of Singh et al. (2017) shows that sediment heterogeneity reduces the bars length, which is in agreement with this outcome.

Migrating bars are not present in the Grensmaas, which was assigned to the limited sediment supply to the river system[1]. However, the insights provided by this research emphasise the necessity of a flat bed for the development of free, migrating bars. Therefore the absence of free, migrating bars should be related to the non-uniform geometry of the Grensmaas and the presence of steady (hybrid) bars, suppressing the development of free, migrating bars. The 'most straight reach' is also sinusoidal (Figure 8.2).

FIGURE 8.2: Meandering of the Grensmaas.

(a) Bar 1. Local widening.

(b) Bar 2. Alternate bars.

(c) Bar 3. Point bars.

(d) Bar 4. Local widening.

FIGURE 8.3: Bars along the Grensmaas.

Recommendations for further research

As explained in the discussion on the limitations, additional research is still possible to take the next steps to real river systems.

- First of all, an easy next step is to *increase the complexity of the river geometry*. Interesting results can be obtained using a triangular river cross-section, as the initial bed is not flat anymore, having a transverse bed slope. Furthermore, the outcomes of this research are based on one base case, with a constant slope, bed roughness, sediment size etc. The interplay between the timescales determined and other morphological parameters can be further explored.
- For this analysis, the response of alternate bars to a single flood wave and seasonal variations of one year has been discussed, based on the timescale of adaptation of alternate bars. Further research would be geared towards analysing the response of river bars to (for instance) *series of river floods*, or *long-term discharge variation*, due to climate change. The work of Carlin,

[1]Personal communication with Ron Agtersloot, hydraulic advisor of Consortium Grensmaas

Redolfi, and Tubino (2020) could be a good starting point, as they analysed the response of free bars to multiple floods by means of a weakly nonlinear model.

- This thesis assess the transitions around resonance conditions, as this marked a clear transition for the hybrid bars. An extension of this research can be made towards *the transition around critical conditions*.
- For continued research with a numerical model, it is recommended to *validate the numerical model* with a real river where free or hybrid bars have developed or with (long-term) laboratory experiments (for instance from Crosato et al. (2011)).

References

Adami, L., W. Bertoldi, and G. Zolezzi (2014). "Morphodynamics of alternate bars in the Alpine Rhine River: Methods for the applicability of mathematical models using fields observations". In: *Proceedings of the International Conference on Fluvial Hydraulics - River Flow 2014*, pp. 1213–1218.

Bai, Y. and Z. Wang (2014). "Theory and application of nonlinear river dynamics". In: *International Journal of Sediment Research* 29.3, pp. 285–303.

Blondeaux, P. and G. Seminara (1985). "A unified bar-bend theory of river meanders". In: *Journal of Fluid Mechanics* 157, pp. 449–470.

Buijse, A.D., H. Coops, M. Staras, L.H. Jans, G.J. van Geest, R.E. Grift, B.W. Ibelings, W. Oosterberg, and F.C.J.M. Roozen (2002). "Restoration strategies for river floodplains along large lowland rivers in Europe". In: *Freshwater Biology* 47.4.

Carlin, M., M. Redolfi, and M. Tubino (2020). "Effect of flow unsteadiness on the long-term evolution of alternate bars". In: *Proceedings of the International Conference on Fluvial Hydraulics - River Flow 2020*.

Colombini, M., G. Seminara, and M. Tubino (1987). "Finite-amplitude alternate bars". In: *Journal of Fluid Mechanics* 181, pp. 213–232.

Cordier, F., P. Tassi, N. Claude, A. Crosato, S. Rodrigues, and D. pham van bang (2019). "Numerical Study of Alternate Bars in Alluvial Channels With Nonuniform Sediment". In: *Water Resources Research*.

Crosato, A. and F.B. Desta (2009). "Intrinsic steady alternate bars in alluvial channels. Part 1: experimental observations and numerical tests." In: *Proc. of the 6th Symp. on River Coastal and Estuarine Morphodynamics (RCEM 2009), 21-25 Sept. 2009, Santa Fe, Argentina, RCEM 2009, Vol. 2, pp. 759-765.*

Crosato, A., Desta F.B, Le U, Getaneh A.A., and W. Uijttewaal (2010). "Long-duration laboratory experiment of slow development of steady alternate bars". In: *Proceedings of the International Conference on Fluvial Hydraulics - River Flow 2010*.

Crosato, A. and E. Mosselman (2009). "Simple physics-based predictor for the number of river bars and the transition between meandering and braiding". In: *Water Resources Research* 45.

Crosato, A., E. Mosselman, F. Beidmariam Desta, and W. S. J. Uijttewaal (2011). "Experimental and numerical evidence for intrinsic nonmigrating bars in alluvial channels". In: *Water Resources Research* 47.3.

Dongen, B. van and D. Meijer (2008). *Zomerbedveranderingen van de maas (1889-2007)*. Tech. rep. Meander Advies en Onderzoek. By order of Rijkswaterstaat Dienst Limburg.

Duizendstra, H.D. (1999). *Sedimenttransport in de Grensmaas. Transportcapaciteit en aanbod van sediment*. Tech. rep. Ministerie van Verkeer en Waterstaat Directoraal-Generaal Rijkswaterstaat RIZA Rijksinstituut voor Integraal Zoetwaterbeheer en Afvalwaterbehandeling.

Duró, G., A. Crosato, and P. Tassi (2015). "Numerical study on river bar response to spatial variations of channel width". In: *Advances in Water Resources* 93, pp. 21–38.

Engelund, F. (1981). "The motion of sediment particles on an inclined bed". In: *Tech. Univ. Denmark ISVA Prog* 53, pp. 15–20.

Engelund, F. and O. Skovgaard (1973). "On the origin of meandering and braiding in alluvial streams". In: *Journal of Fluid Mechanics* 57, pp. 289–302.

Fredsøe, J. (1978). “Meandering and braiding of rivers”. In: *Journal of Fluid Mechanics* 84, pp. 609–624.

Fujita, Y. and Y. Muramoto (1985). “Studies on the Process of Development of Alternate Bars”. In: *Bulletin of the Disaster Prevention Research Institute* 35, pp. 55–86.

Fukuoka, S. (1989). “Finite Amplitude Development of Alternate Bars”. In: *River Meandering*. Ed. by S. Ikeda and G. Parker, pp. 237–265.

Hall, P. (2004). “Alternating bar instabilities in unsteady channel flows over erodible beds”. In: *Journal of Fluid Mechanics* 499, pp. 49–73.

Ikeda, A. (1982). “Lateral bedload transport on side slopes”. In: *Journal of the Hydraulics Division* 108.11, pp. 1369–1373.

Koch, F.G. and C. Flokstra (1980). “Bed level computations for curved alluvial channels”. In: *Proceedings of the XIXth congress of the International Association for Hydraulic Research, 2-7 Feb. 1981, New Delhi, India,* 2, pp. 357–364.

Lanzoni, S. (2000). “Experiments on bar formation in a straight flume: 2. Graded sediment”. In: *Water Resources Research* 36.11, pp. 3351–3363.

Lesser, G.R., J.A. Roelvink, J.A.T.M. van Kester, and G.S. Stelling (2004). “Development and validation of a three-dimensional morphological model”. In: *Coastal Engineering* 51.8. Coastal Morphodynamic Modeling, pp. 883 –915.

Meer, C. van der, E. Mosselman, K. Sloff, B. Jagers, G. Zolezzi, and M. Tubino (2011). “Numerical simulations of upstream and downstream overdeepening”. In: *Proc. of the 7th Symp. on River Coastal and Estuarine Morphodynamics (RCEM 201), 6-9 Sept. 2011, Tsinghua University, Beijing, China, RCEM 2011, pp. 1721-1729.*

Meyer-Peter, E. and R. Müller (1948). “Formulas for bed-load transport”. In: *Proceedings of the 2nd IAHR World Congress, 6–9 June, Stockholm, Sweden,* pp. 39–64.

Mosselman, E., M. Tubino, and G. Zolezzi (2006). “The overdeepening theory in river morphodynamics: Two decades of shifting interpretations”. In: *Proceedings of the International Conference on Fluvial Hydraulics - River Flow 2006* 1–2, pp. 1175–1181.

Murillo-Muñoz, R. and G. Klaassen (2006). “Downstream fining of sediments in the Meuse River”. In: *Proceedings of the International Conference on Fluvial Hydraulics - River Flow 2006* 1, pp. 895–905.

Nelson, J. M. (1990). “The initial instability and finite-amplitude stability of alternate bars in straight channels”. In: *Earth-Science Reviews* 29.1, pp. 97–115.

Parker, G. (1976). “On the cause and characteristic scales of meandering and braiding in rivers”. In: *Journal of Fluid Mechanics* 76, pp. 457–480.

Parker, G. and H. Johannesson (1989). “Observations on Several Recent Theories of Resonance and Overdeepening in Meandering Channels”. In: *River Meandering*. American Geophysical Union (AGU). Chap. 12.

Redolfi, M., M. Welber, M. Carlin, M. Tubino, and W. Bertoldi (2020). “Morphometric properties of alternate bars and water discharge: a laboratory investigation”. In: *Earth Surf. Dynam. Discuss.* 2020, pp. 1–31.

Rijkswaterstaat (2019). *Statistisch overzicht afvoeren en waterstanden Watersysteem Maas en Kanalen 1991-2015*. Tech. rep. Ministerie van Infrastructuur en Waterstaat, Rijkswaterstaat (RWS).

Rodrigues, S., E. Mosselman, N. Claude, C.L. Wintenberger, and P. Juge (2015). “Alternate bars in a sandy gravel bed river: generation, migration and interactions with superimposed dunes”. In: *Earth Surface Processes and Landforms* 40.5, pp. 610–628.

Schielen, R., A. Doelman, and H. E. de Swart (1993). “On the nonlinear dynamics of free bars in straight channels”. In: *Journal of Fluid Mechanics* 252, pp. 325–356.

Seminara, G. and M. Tubino (1992). “Weakly nonlinear theory of regular meanders”. In: *Journal of Fluid Mechanics* 244, 257–288.

Sharef, B.I. (2006). *Numerical Modelling with Graded Sediments for 2D Morphological changes for Pilot Project Meers (Common Meuse)*. (MSc Thesis). UNESCO-IHE Institute for Water Education.

Shimizu, Y., S. Giri, S. Yamaguchi, and J. Nelson (2009). "Numerical simulation of dune–flat bed transition and stage-discharge relationship with hysteresis effect". In: *Water Resources Research* 45.4.

Singh, U., A. Crosato, S. Giri, and M. Hicks (2017). "Sediment heterogenity and mobility in the morphodynamic modelling of gravel-bed braided rivers". In: *Advances in Water Resources* 104, pp. 127–144.

Struiksma, N. and G.J. Klaassen (1988). "On the threshold between meandering and braiding". In: *Proc. Int. Conf. River Regime, 1988, Wallingford.*

Struiksma, N., K. Olesen, C. Flokstra, and H. de Vriend (1985). "Bed deformation in curved alluvial channels". In: *Journal of Hydraulic Research* 23, pp. 57–79.

Surian, Nicola, Luca Mao, Matteo Giacomin, and Luca Ziliani (2009). "Morphological effects of different channel-forming discharges in a gravel-bed river". In: *Earth Surface Processes and Landforms* 34, pp. 1093 –1107.

Taal, M.C. (1989). *Time-dependent near-bank beddeformation in meandering rivers*. (MSc Thesis). Delft University of Technology.

Talmon, A.M., N. Struiksma, and M.C.L.M. van Mierlo (1995). "Laboratory measurements of the direction of sediment transport on transverse alluvial-bed slopes". In: *Journal of Hydraulic Research* 33.4, pp. 495–517.

Tubino, M. (1991). "Growth of alternate bars in unsteady flow". In: *Water Resources Research* 27.1, pp. 37–52.

Verbruggen, W. (2012). *Numerical nonlinear analysis of alternate-bar formation under super-resonant conditions*. (MSc Thesis). Delft University of Technology.

Villada Arroyave, J. (2008). *Influence of vegetation on the long term morphological processes in the Common Meuse River*. (MSc Thesis). UNESCO-IHE Institute for Water Education.

Visconti, F., C. Camporeale, and L. Ridolfi (2010). "Role of discharge variability on pseudomeandering channel morphodynamics: Results from laboratory experiments". In: *Journal of Geophysical Research: Earth Surface* 115.F4.

Vriend, H.J. de, H. Havinga, B.C. van Prooijen, P.J. Visser, and Z.B. Wang (2011). *CIE4345 River Engineering*. Delft University of Technology.

Wilkens, D.H. and J.J.P. Lambeek (1997). *Bodemtransportmetingen Grensmaas*. Tech. rep. Delft Hydraulics.

Zolezzi, G., M. Guala, T. Donatella, and G. Seminara (2005). "Experimental observation of upstream overdeepening". In: *Journal of Fluid Mechanics* 531, pp. 191 –219.

Zolezzi, G. and G. Seminara (2001). "Upstream influence in erodible beds". In: *Physics and Chemistry of the Earth, Part B: Hydrology, Oceans and Atmosphere* 26.1, pp. 65 –70.

Appendix A

Grensmaas

This thesis is inspired by the challenges faced by the Grensmaas.

General Grensmaas

A part of the river Meuse between Maastricht and Maasbracht is called the Grensmaas, a reach of 54 kilometers (Wilkens and Lambeek 1997). The Meuse originates in France (Pouilly-en-Bassigny) and flows through Belgium and the Netherlands through Hollands Diep and Haringvliet in the North Sea. The Grensmaas has (for being a Dutch river) a strong gradient of almost 0.45 m/km. Parallel to the Grensmaas is the Julianakanaal, which is open for navigation. So without navigation restrictions, the Grensmaas is very suitable for nature development.

Consortium Grensmaas

Consortium Grensmaas is an association of gravel extractors, contractors and "Natuurmonumenten": an organisation that buys, protects and manages nature reserves in the Netherlands. Driven by the flood in 1993 and 1995, flood safety and nature development are key drivers for the project along the Grensmaas, financed by the selling of the extracted gravel. The activities are taking place along a reach of 43 kilometers along the Grensmaas. Most of the project locations consist of river widening in combination with gravel extraction and the excavation of a side channel to increase the discharge capacity and for nature development. The project will take place until 2027. More information can be found at https://www.grensmaas.nl/.

Sediment and bed material

Measurements of the sediment transport and the bed material, conducted in the Grensmaas from 1959 untill 1997, analysed by Delft Hydraulics, are presented in the report of Wilkens and Lambeek (1997). The measurements show that the bedmaterial is strongly graded, and along the reach, the bedmaterial gets finer (see figure A.1). The challenges faced by the researchers consist of the formation of armouring layers. The measurements focused on the transport of bed material (instead of suspended material). This would be justified by the assumptions that in gravel rivers like the Grensmaas, bed transport would dominate over suspended transport. Research by Murillo-Muñoz and Klaassen (2006) focused on the fining of sediments along the Meuse, and explained this by selective transport and the abrasion of sediment particles. A report published by the Ministry of Transport, Public Works and Water Management of the Netherlands by Duizendstra (1999), investigated the sediment transport (transport capacity and supply of sediment) in the Grensmaas. The report highlights the complexity of the transport of the Grensmaas due to geological condition of the bed, the tectonic dynamics of areas in the Meuse valley, the large sediment size, and the process of armouring of the bedmaterial. The sediment transport is not only a function of transport capacity (flow velocity), but also a function of the supply of sediment (Duizendstra 1999).

The Grensmaas is prone to bed degradation. Dongen and Meijer (2008) explained this (1) due to gravel extraction of the main channel, (2) seeing it for freeflowing river as an autonomous process, (3) due to gravel extraction upstream, and (4) due to land subsidence due to mining activities. The main channel has also been narrowed by groynes that are now buried in the floodplain.

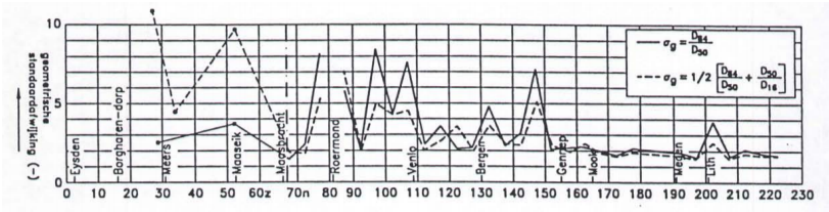

FIGURE A.1: Sediment distribution Grensmaas (Wilkens and Lambeek 1997).

Hydrological characteristics

The Meuse is a typical 'rainriver', which means an irregular discharge regime (Wilkens and Lambeek 1997). The short reaction time is due to the stretched shape of the drainage basin and the limited storage into the groundwater basin.

Kenmerk	datum	afvoer
overschrijdingsfrequentie werklijn TMR2017 Maas		
1 x per 1000 jaar	n.v.t.	3862
1 x per 300 jaar	n.v.t.	3573
1 x per 100 jaar	n.v.t.	3224
1 x per 30 jaar	n.v.t.	2776
1 x per 10 jaar	n.v.t.	2302
Kenmerkende waarden		
hoogste	22/12/1993 7:00	3039
gemiddelde	n.v.t.	222
zomer gemiddelde	n.v.t.	92
laagste	n.v.t.	10

FIGURE A.2: Characteristics of discharge at Borgharen (Grensmaas) (Rijkswaterstaat 2019).

Numerical modelling on Grensmaas

Pilotproject Meers is the first project where the renaturalization measures have been implemented, started around 2001 (Sharef 2006). In the period 2002-2003, some major floods lead to substantial deposits of gravel in the main channel at the beginning of the excavated area, some erosion along the outer (Belgium bank) side of the river, and some finer particles had deposited on the floodplain away from the main channel. Sharef (2006) used the model package Delft3D with the graded-sediment option to simulate the observed phenomena. He concluded that "probably the implemented Pilot Project Meers is the major cause of the observed phenomena" (Sharef 2006). Villada Arroyave (2008) modelled the effect of vegetation on the morphological processes in the Grensmaas, also using the Delft3D software package.

TABLE A.1: Characteristics and values of comparable rivers to the Grensmaas.

	Grensmaas	Allier	Tagliamento
Width	70 m	50 m	40 m
Slope	0.0005	0.0007	0.001
Discharge (average)	230 m^3/s	140 m^3/s	70 m^3/s
Sediment	Gravel	Sand and gravel	Fine gravel

FIGURE A.3:
Allier River
(from maps.google.com).

FIGURE A.4:
Tagliamento River
(from maps.google.com).

Comparable rivers to the Grensmaas

Field research on bar characteristics has been done in the Allier River (France) (Figure A.3) and the Tagliamento River (Italy) (Figure A.4) (Surian et al. 2009). Some characteristics have been summed up in Table A.1.

Appendix B

Model results

Overview of the simulations:

TABLE B.1: Overview simulations - Constant discharge.

#	$Q\ [\mathrm{m^3\,s^{-1}}]$	$d_e\ [\mathrm{m}]$	$u\ [\mathrm{m\,s^{-1}}]$	β	Page
Q50	50	0.67	0.83	66.9	70
Q100	100	1.07	1.04	42.1	72
Q125	125	1.24	1.12	36.3	74
Q150	150	1.40	1.19	32.1	76
Q200	200	1.70	1.31	26.5	78
Q250	250	1.97	1.41	22.9	80
Q300	300	2.22	1.50	20.3	81
Q400	400	2.69	1.65	16.7	82
Q500	500	3.12	1.78	14.4	83
Q750	750	4.09	2.04	11.0	84
Q1000	1000	4.96	2.24	9.1	85
Q1250	1250	5.75	2.41	7.8	86

TABLE B.2: Overview simulations - Constant discharge: Output.

		Theoretical conditions						Output		
					Hybrid bars			Hybrid bars		
#	Q [$\mathrm{m^3\,s^{-1}}$]	d_e [m]	u [$\mathrm{m\,s^{-1}}$]	β	L_P [10^3 m]	L_D [10^3 m]	Regime	L_P [10^3 m]	L_D [$+/-$]	Regime
Q50	50	0.67	0.83	66.9	-	- 0.13	Superresonant	0.95	-	Superresonant
Q100	100	1.07	1.04	42.1	1.08	- 1.14	Superresonant	1.0	-	Superresonant
Q125	125	1.24	1.12	36.3	1.11	10.6	Subresonant	1.4	+	Subresonant
Q150	150	1.40	1.19	32.1	1.15	1.43	Subresonant	1.45	+	Subresonant
Q200	200	1.70	1.31	26.5	1.25	0.70	Subresonant	1.5	+	Subresonant
Q250	250	1.97	1.41	22.9	1.34	0.53	Subresonant	1.5	+	Subresonant
Q300	300	2.22	1.50	20.3	1.44	0.45	Subresonant	1.55	+	Transition
Q400	400	2.69	1.65	16.7	1.64	0.38	Subresonant	1.6	+	Transition
Q500	500	3.12	1.78	14.4	1.88	0.33	Subresonant			Transition
Q750	750	4.09	2.04	11.0	2.86	0.28	Subresonant			Transition
Q1000	1000	4.96	2.24	9.1	-	0.25	Stable			Stable
Q1250	1250	5.75	2.41	7.8	-	0.23	Stable			Stable

Simulation Q50

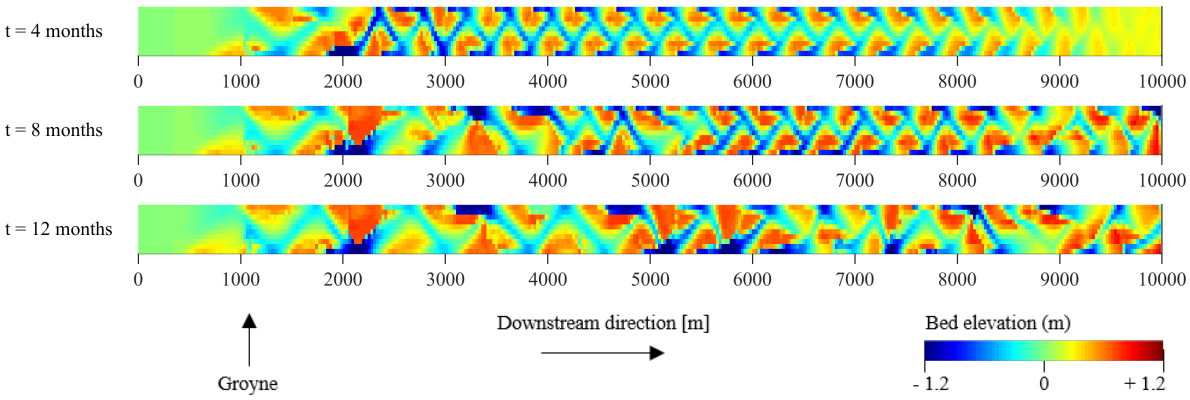

FIGURE B.1: Simulation Q50: Bed level change.

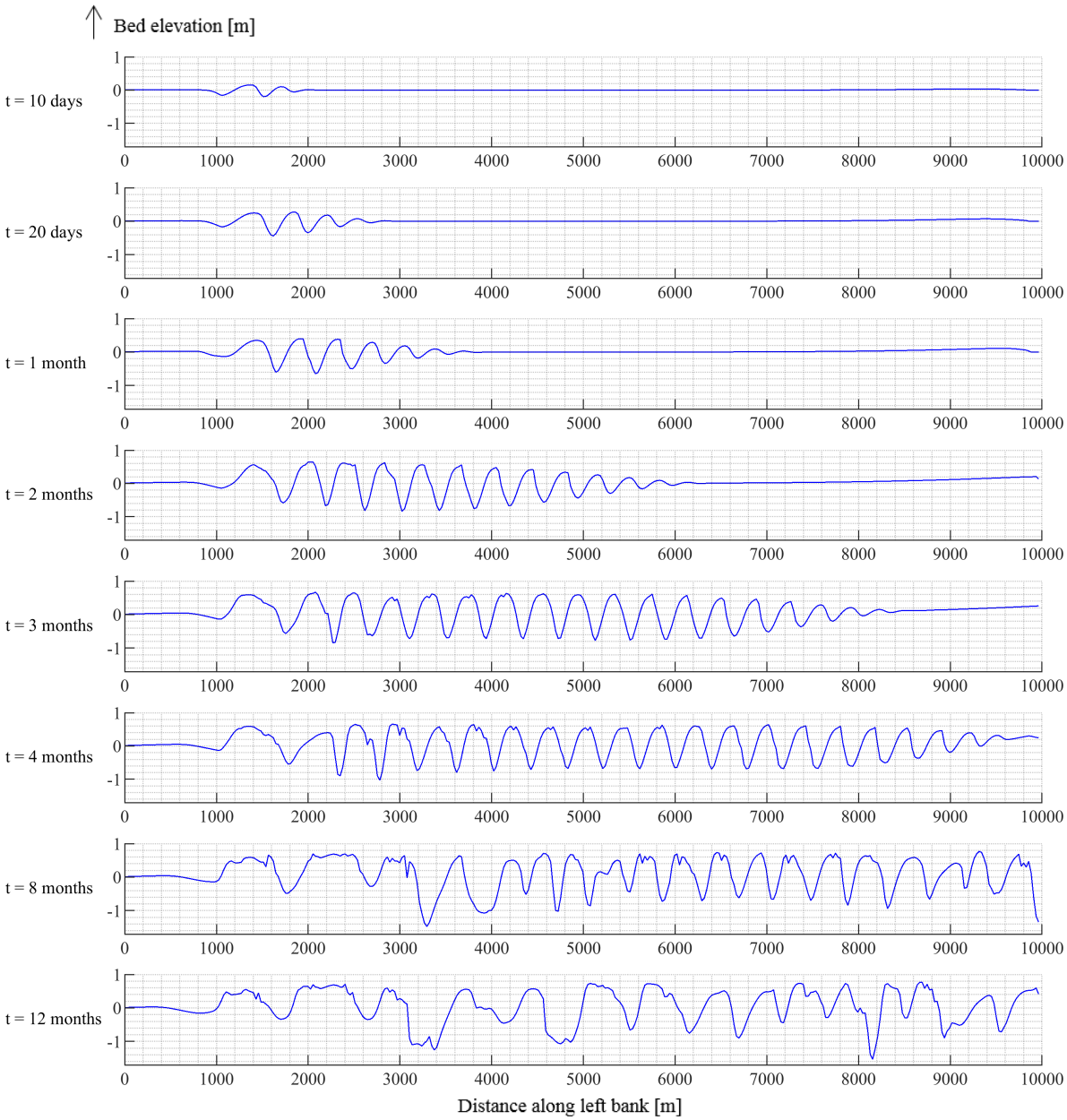

FIGURE B.2: Simulation Q50: Bed level change along left bank.

Simulation Q100

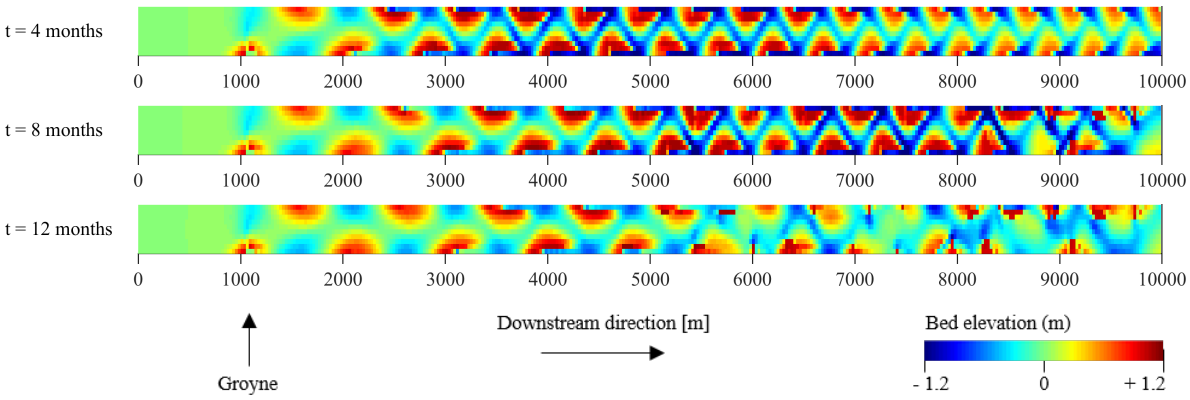

FIGURE B.3: Simulation Q100: Bed level change.

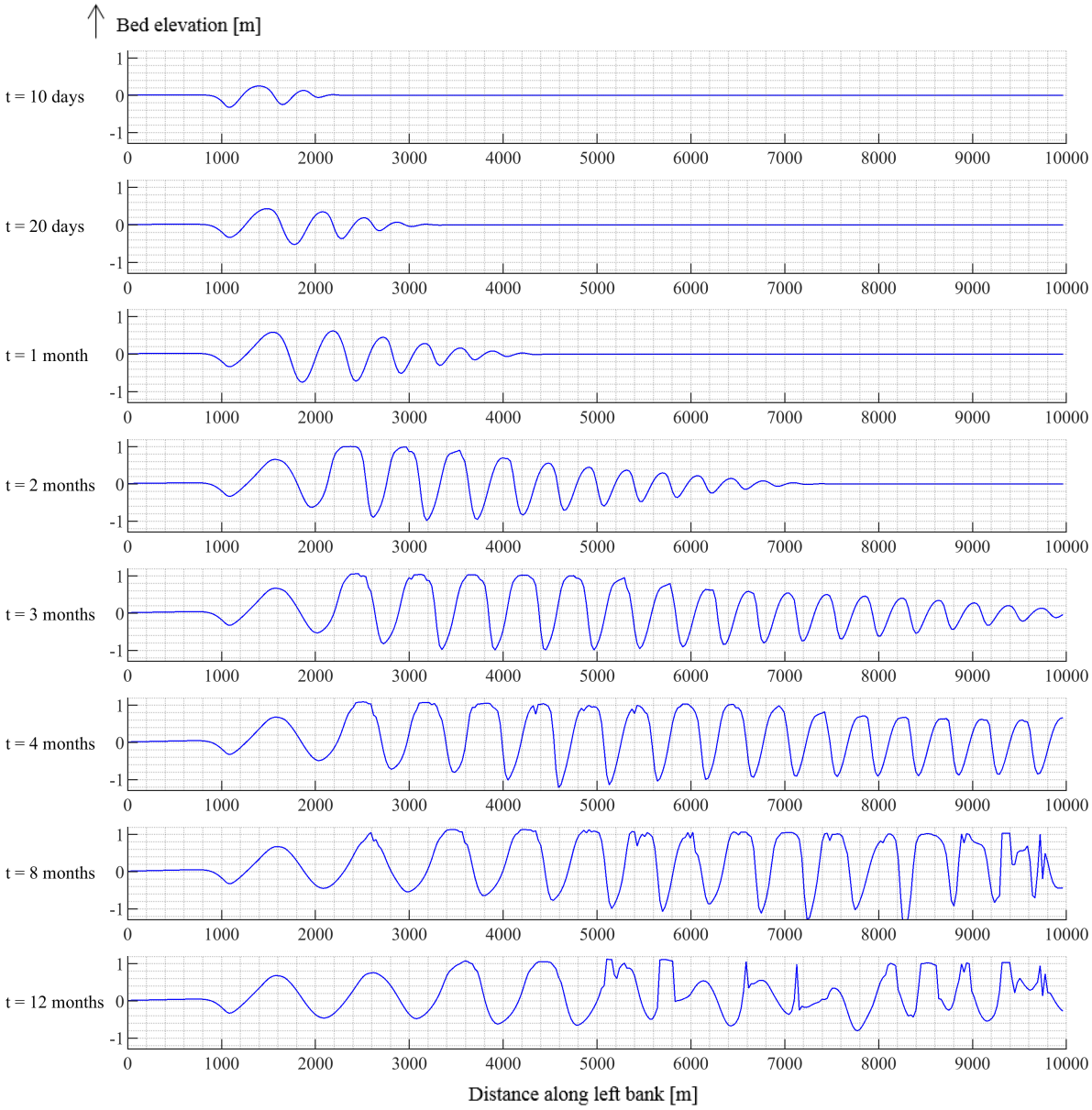

FIGURE B.4: Simulation Q100: Bed level change along left bank.

Simulation Q125

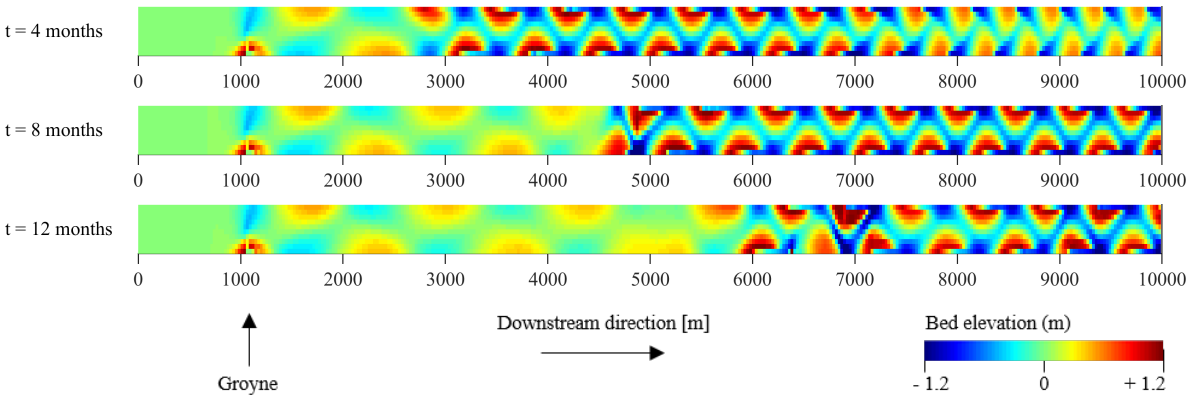

FIGURE B.5: Simulation Q125: Bed level change.

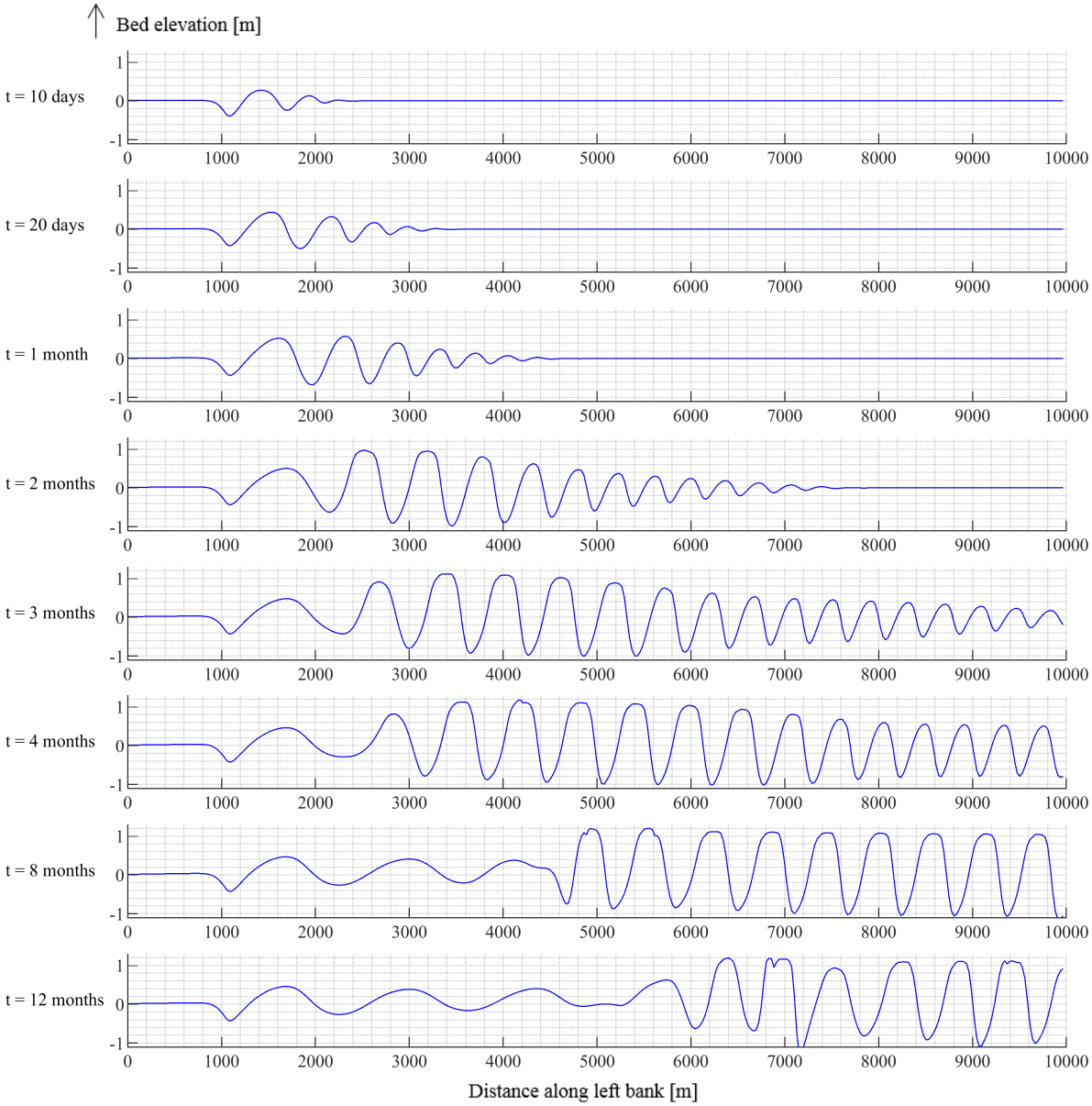

FIGURE B.6: Simulation Q125: Bed level change along left bank.

Simulation Q150

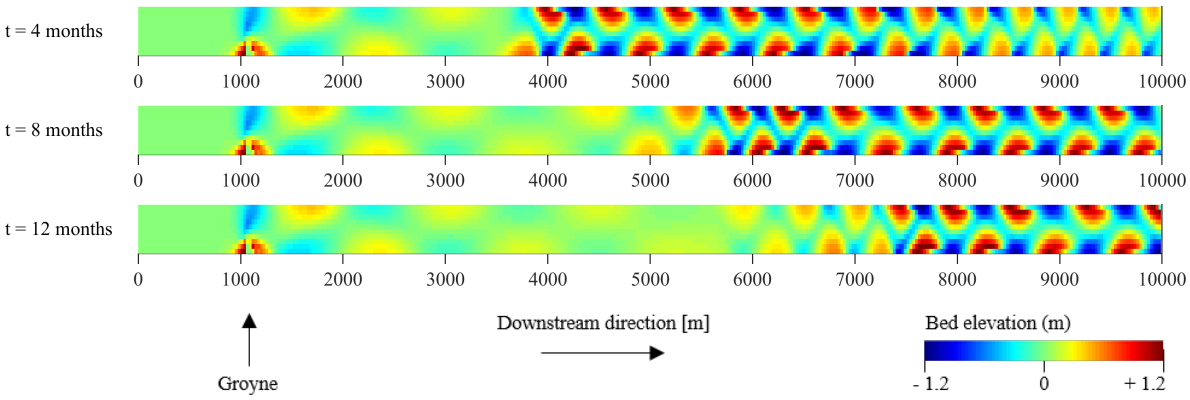

FIGURE B.7: Simulation Q150: Bed level change.

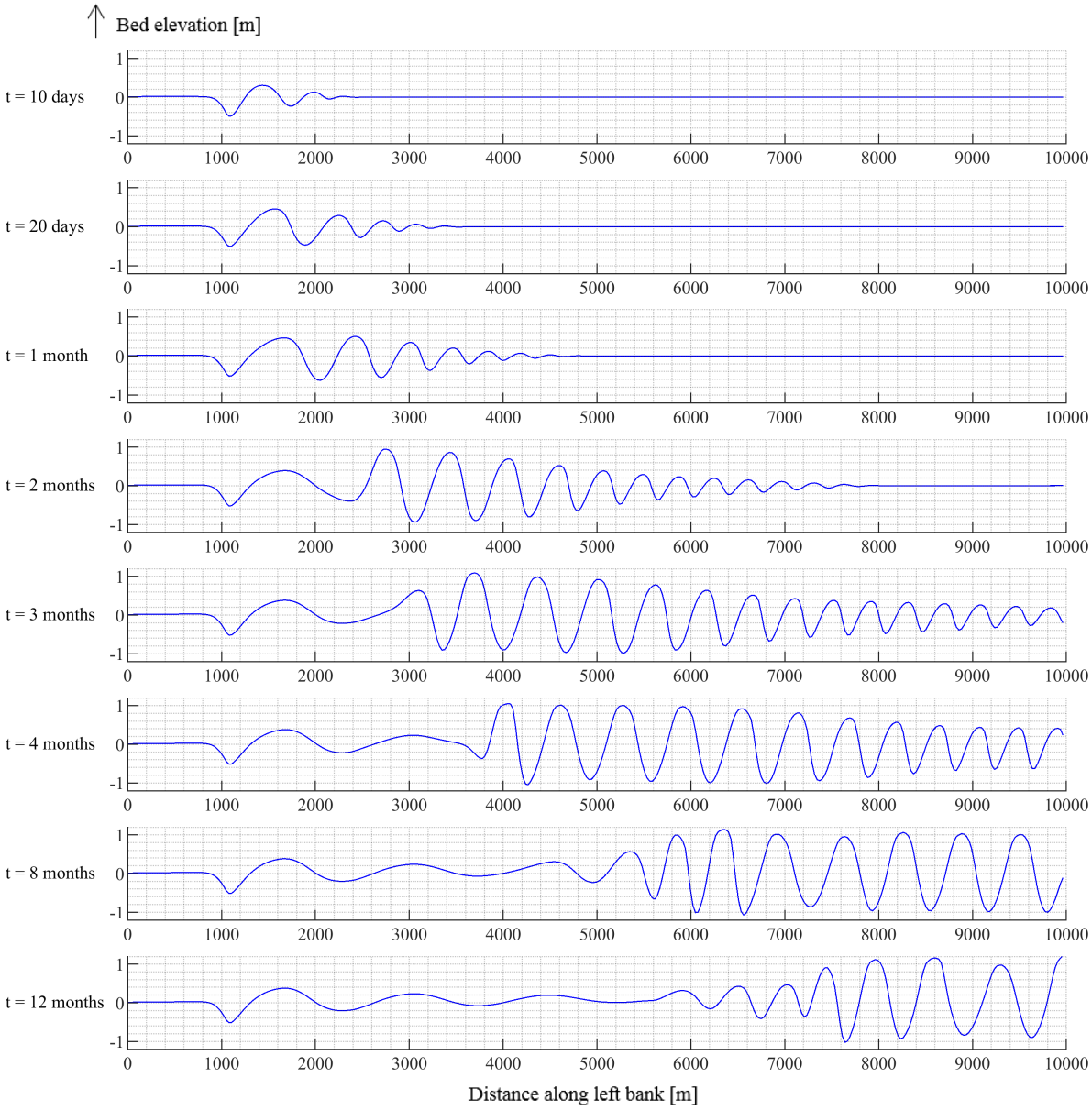

FIGURE B.8: Simulation Q150: Bed level change along left bank.

Simulation Q200

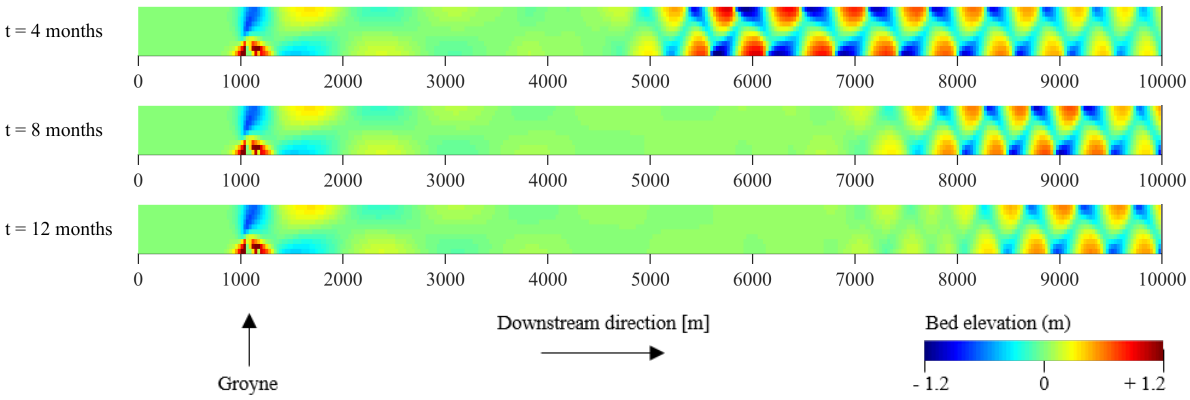

FIGURE B.9: Simulation Q200: Bed level change.

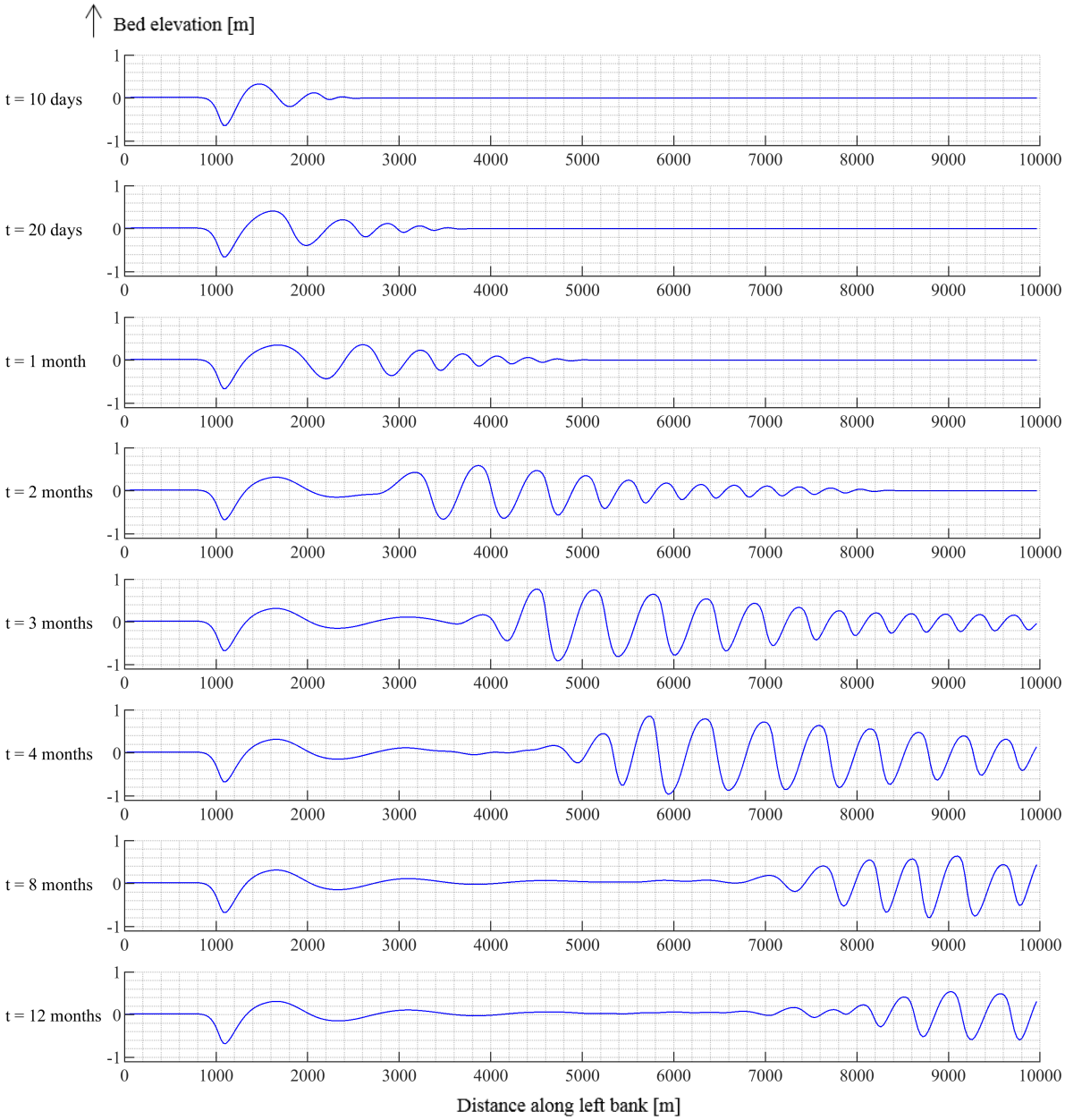

FIGURE B.10: Simulation Q200: Bed level change along left bank.

Simulation Q250

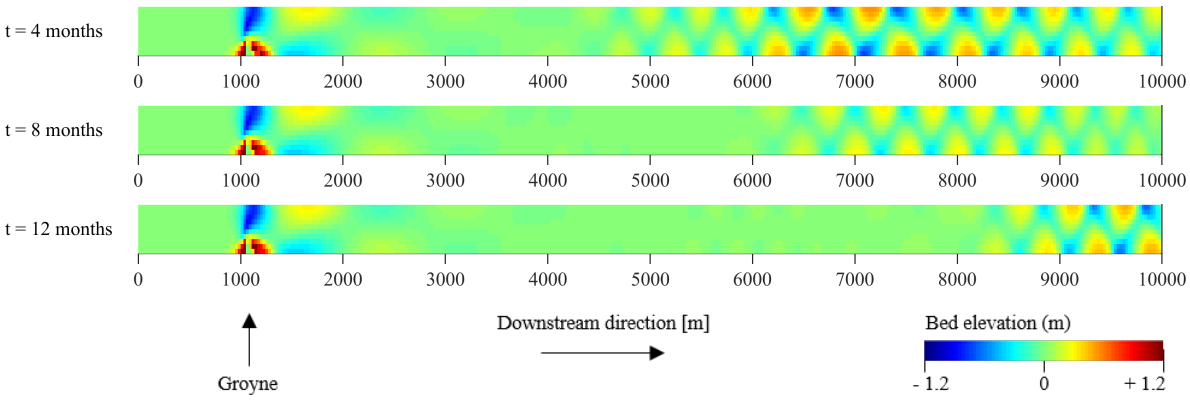

FIGURE B.11: Simulation Q250: Bed level change.

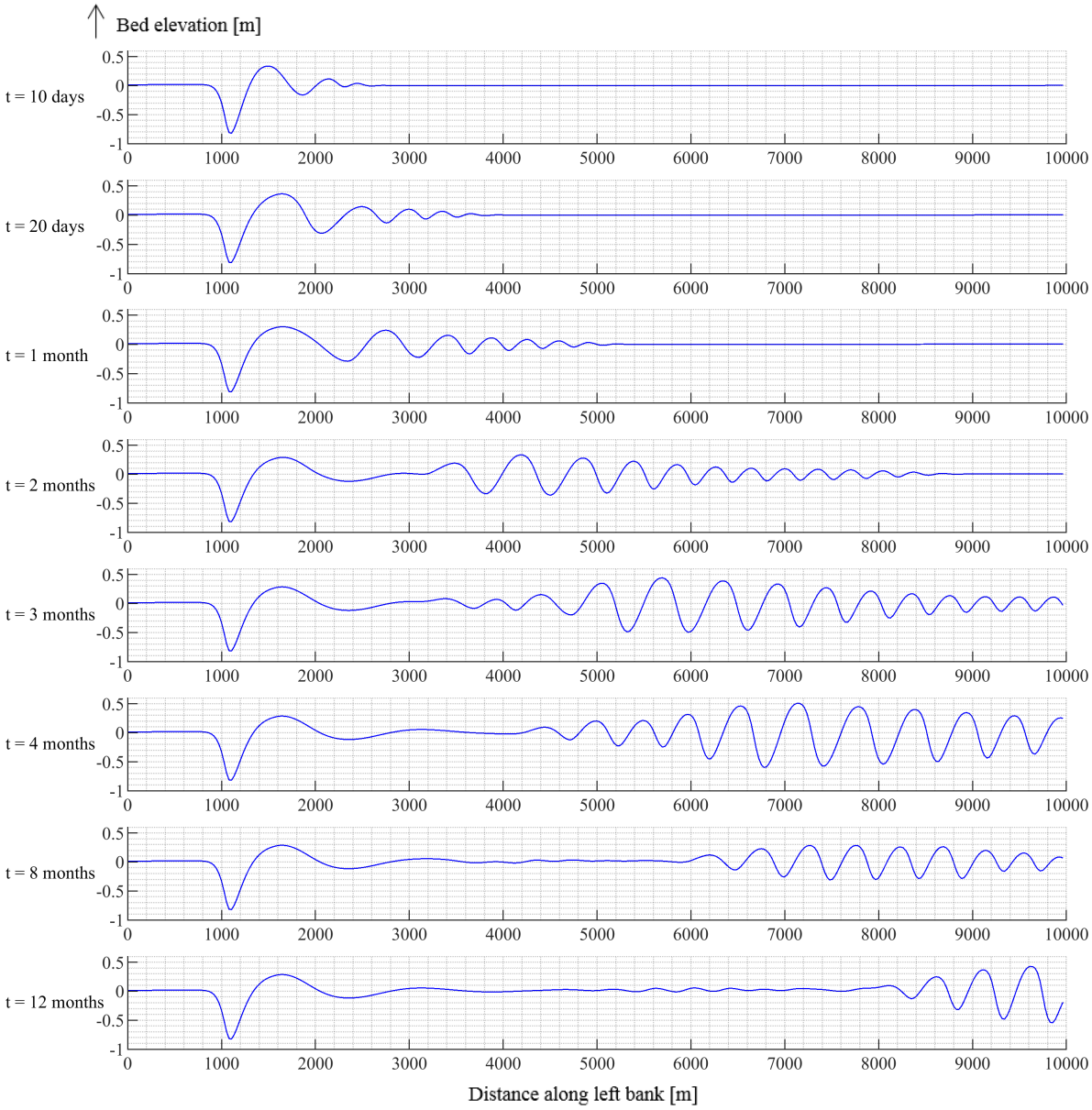

FIGURE B.12: Simulation Q250: Bed level change along left bank.

Simulation Q300

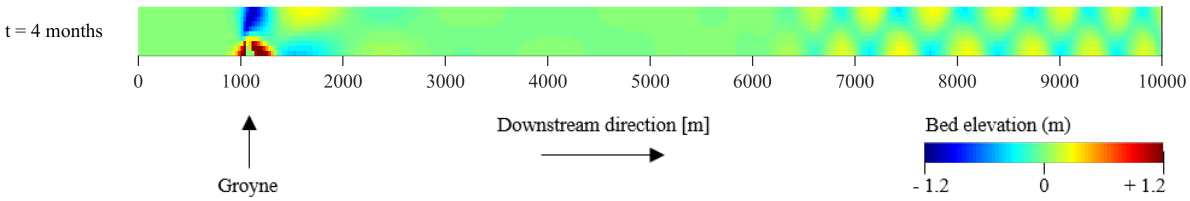

FIGURE B.13: Simulation Q300: Bed level change.

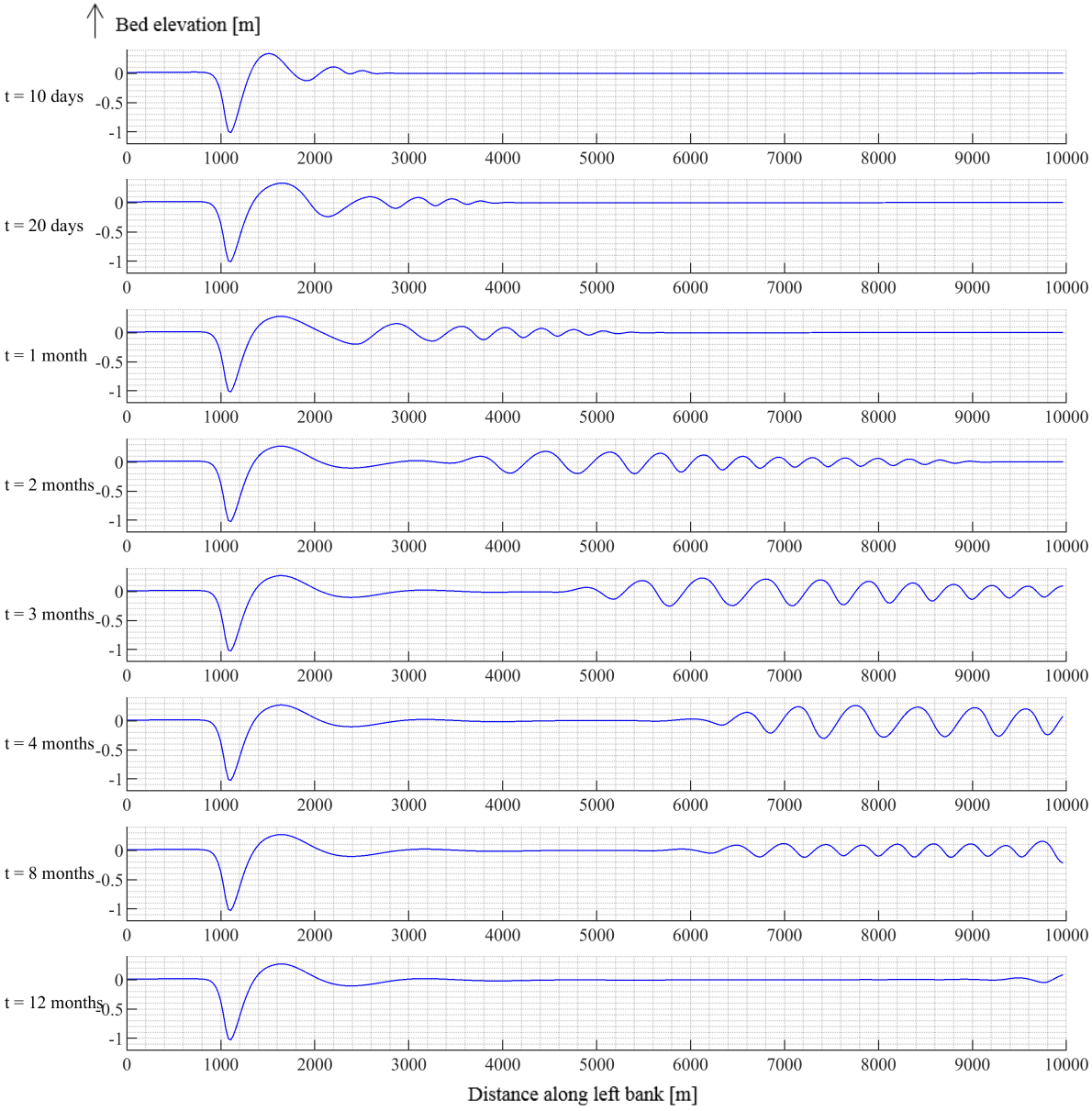

FIGURE B.14: Simulation Q300: Bed level change along left bank.

Simulation Q400

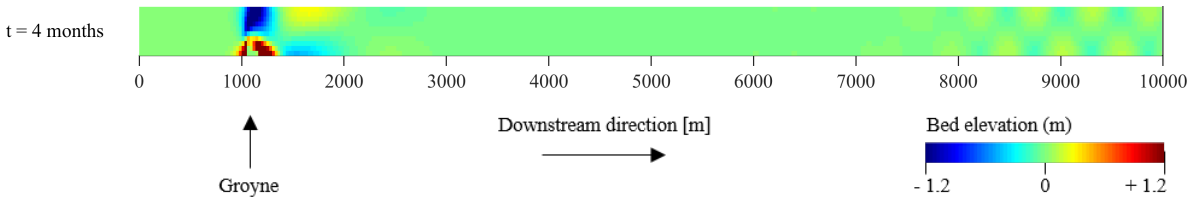

FIGURE B.15: Simulation Q400: Bed level change.

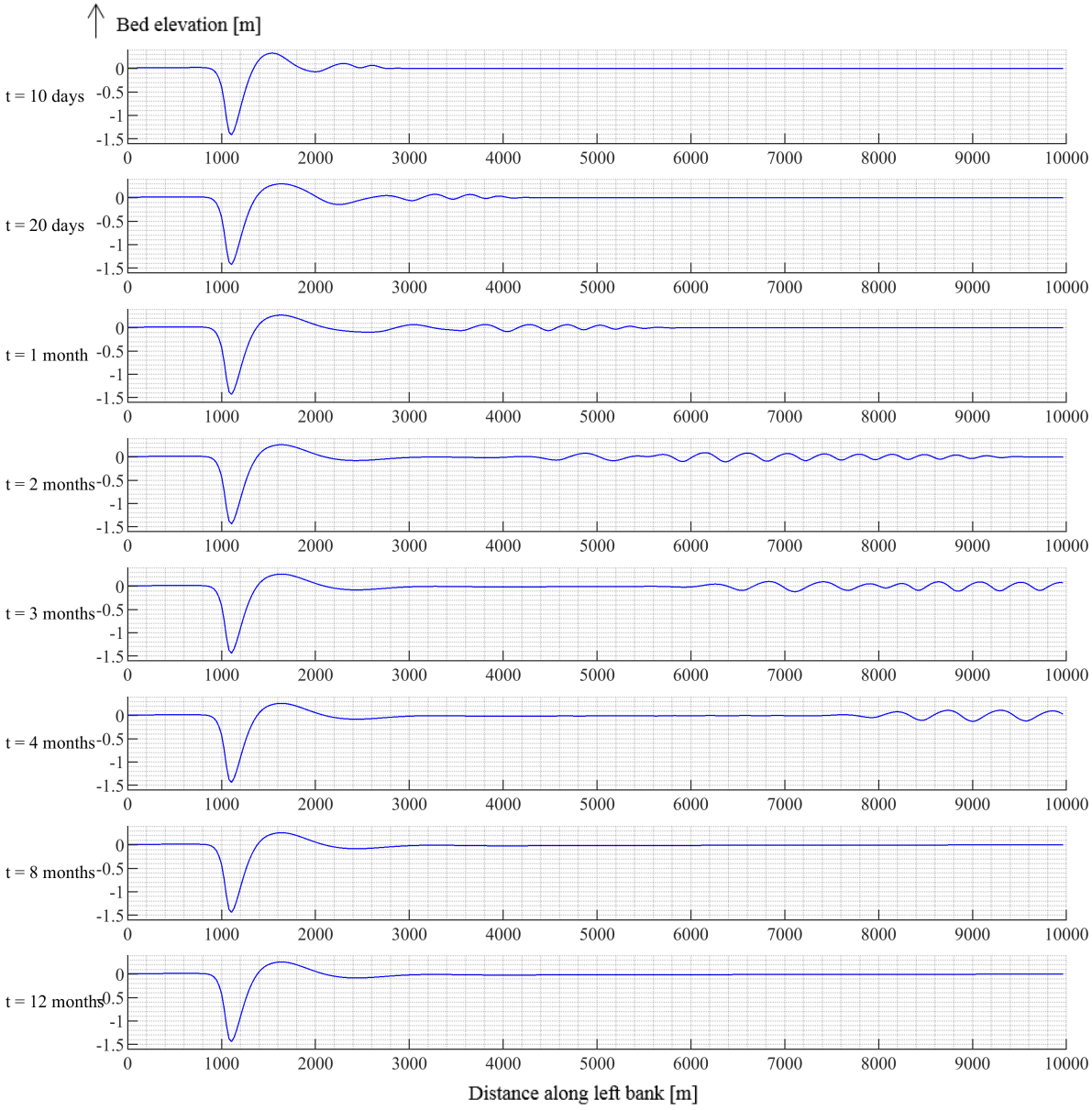

FIGURE B.16: Simulation Q400: Bed level change along left bank.

Simulation Q500

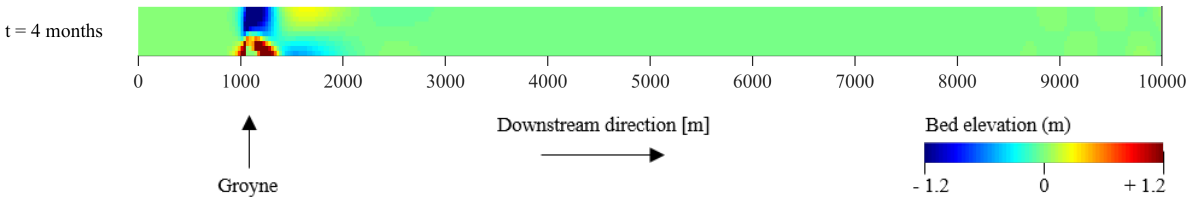

FIGURE B.17: Simulation Q500: Bed level change.

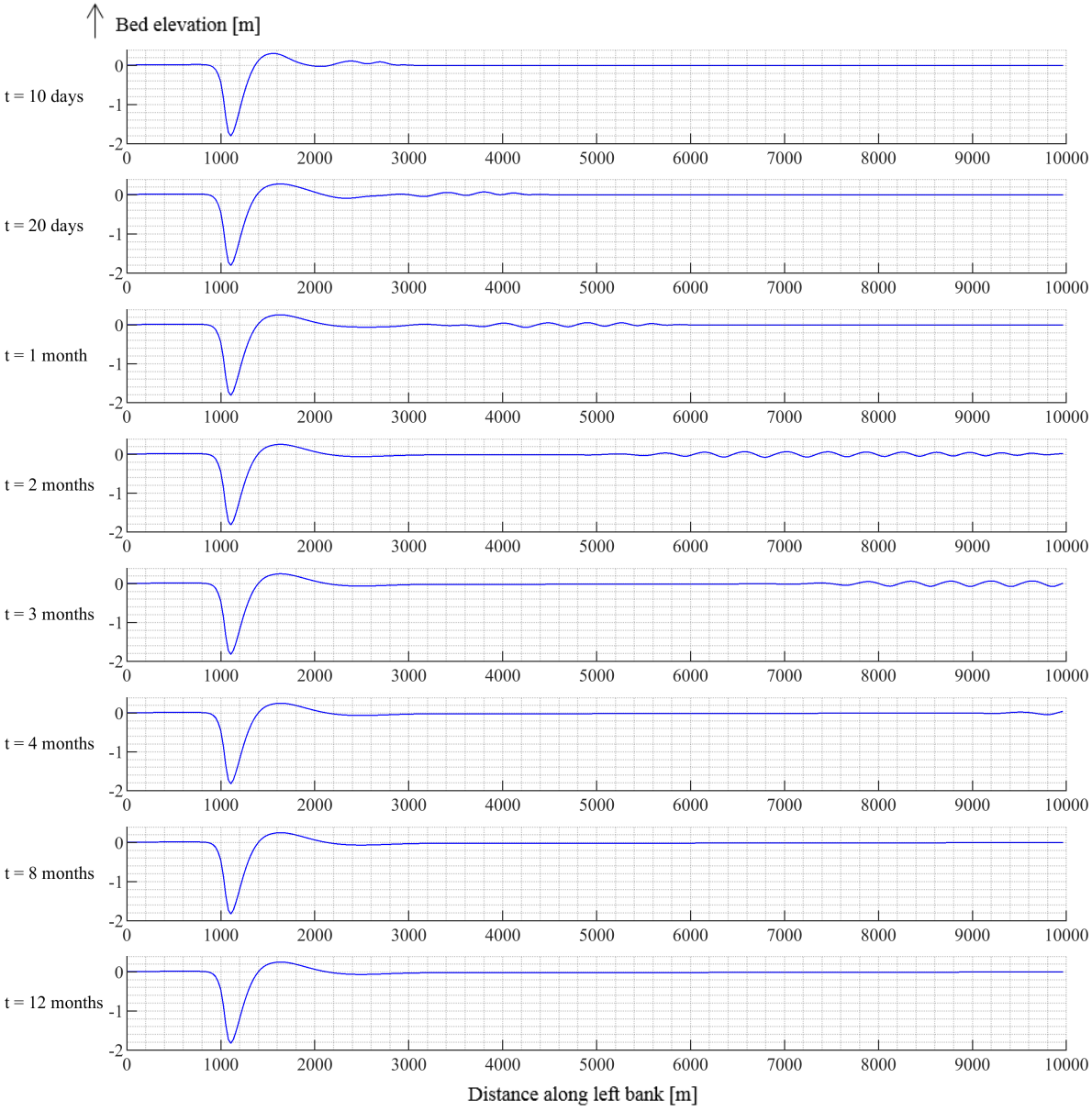

FIGURE B.18: Simulation Q500: Bed level change along left bank.

Simulation Q750

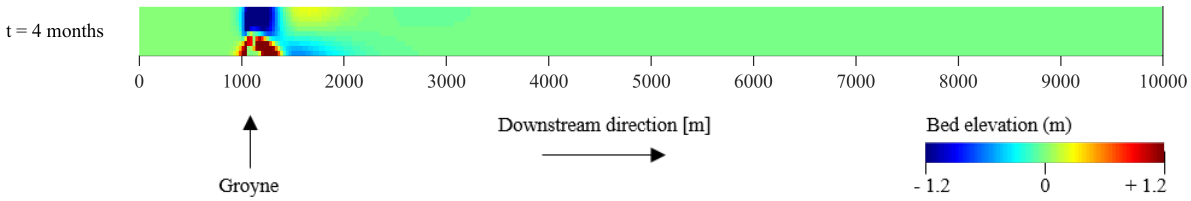

FIGURE B.19: Simulation Q750: Bed level change.

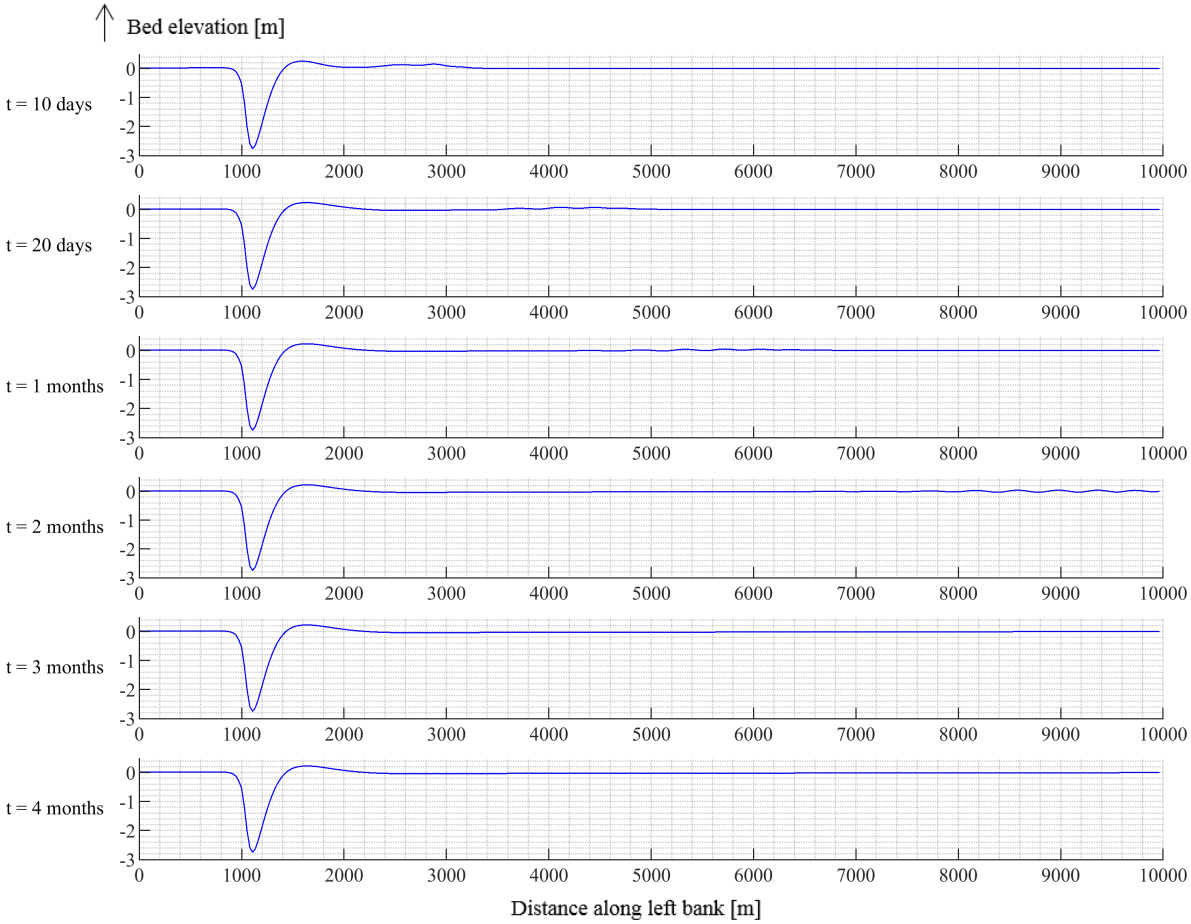

FIGURE B.20: Simulation Q750: Bed level change along left bank.

Simulation Q1000

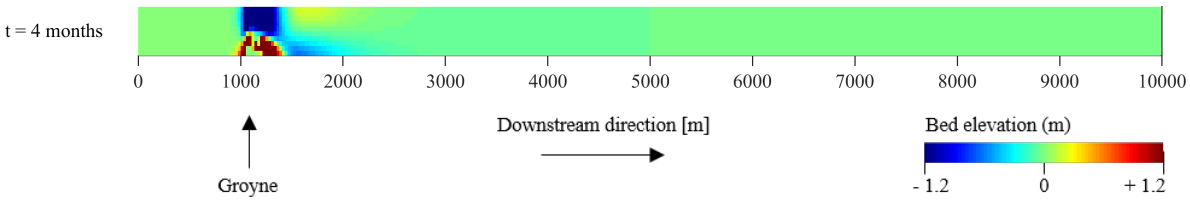

FIGURE B.21: Simulation Q1000: Bed level change.

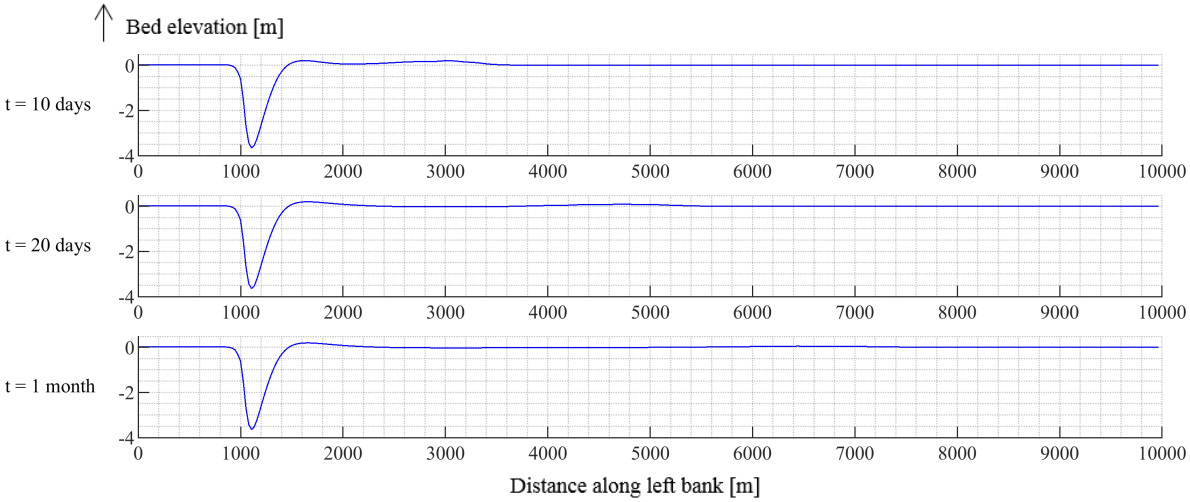

FIGURE B.22: Simulation Q1000: Bed level change along left bank.

Simulation Q1250

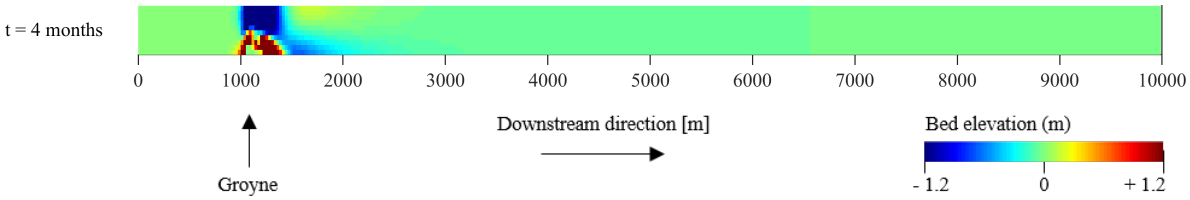

FIGURE B.23: Simulation Q1250: Bed level change.

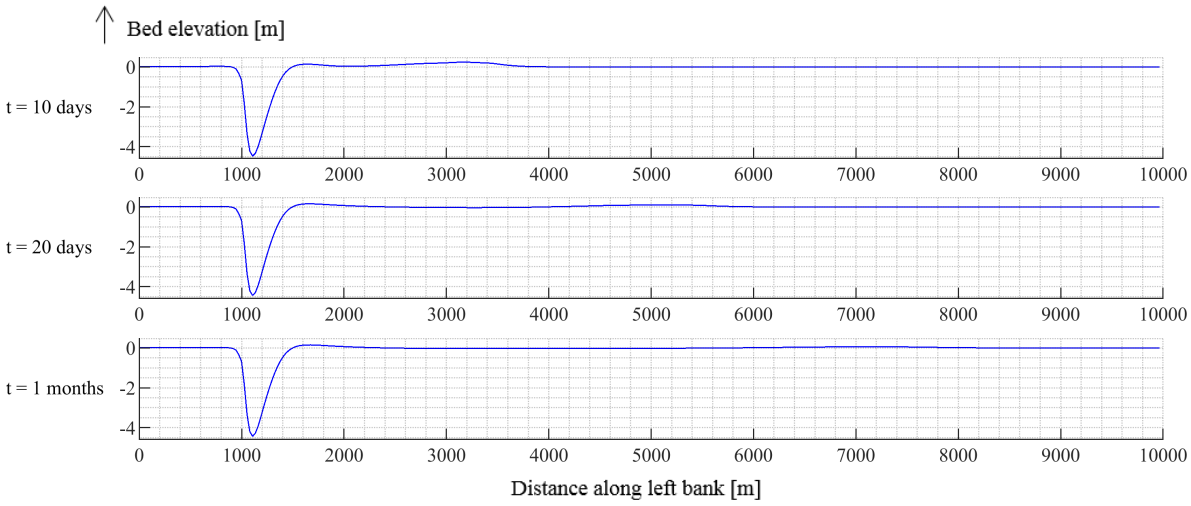

FIGURE B.24: Simulation Q1250: Bed level change along left bank.

Appendix C

Model analysis

In this research, a number of quantitative values are obtained from the numerical simulations. The determination of the values from the simulations is presented in the following section. Table C.1 of the values which are determined and provided in this Appendix. They are all based on the constant-discharge simulations.

The steps to determine T_{Tubino} per simulation is provided, which is not based on the output of the numerical simulations.

TABLE C.1: Overview values determined based on the numerical simulations.

Value		From Section	Page
L_P	Wavelength of hybrid bars	4.2	88
$T_{hybrid\ L_P}$ and $T_{hybrid\ L_D}$	Timescale of hybrid bars	5.1	89
T_{free}	Timescale of free bars	5.1	91
T_{Tubino}	Timescale of Tubino (1991)	5.2	92

Wavelength of hybrid bars

The wavelength of the hybrid bars L_P from the numerical simulations is determined in the following figures. The wavelength is determined between two wave throughs, which is the length between the two black dashed lines. The results are shown in Table B.2 (Output/Hybrid bars/L_P) and corresponds to the red dots in Figure 4.6.

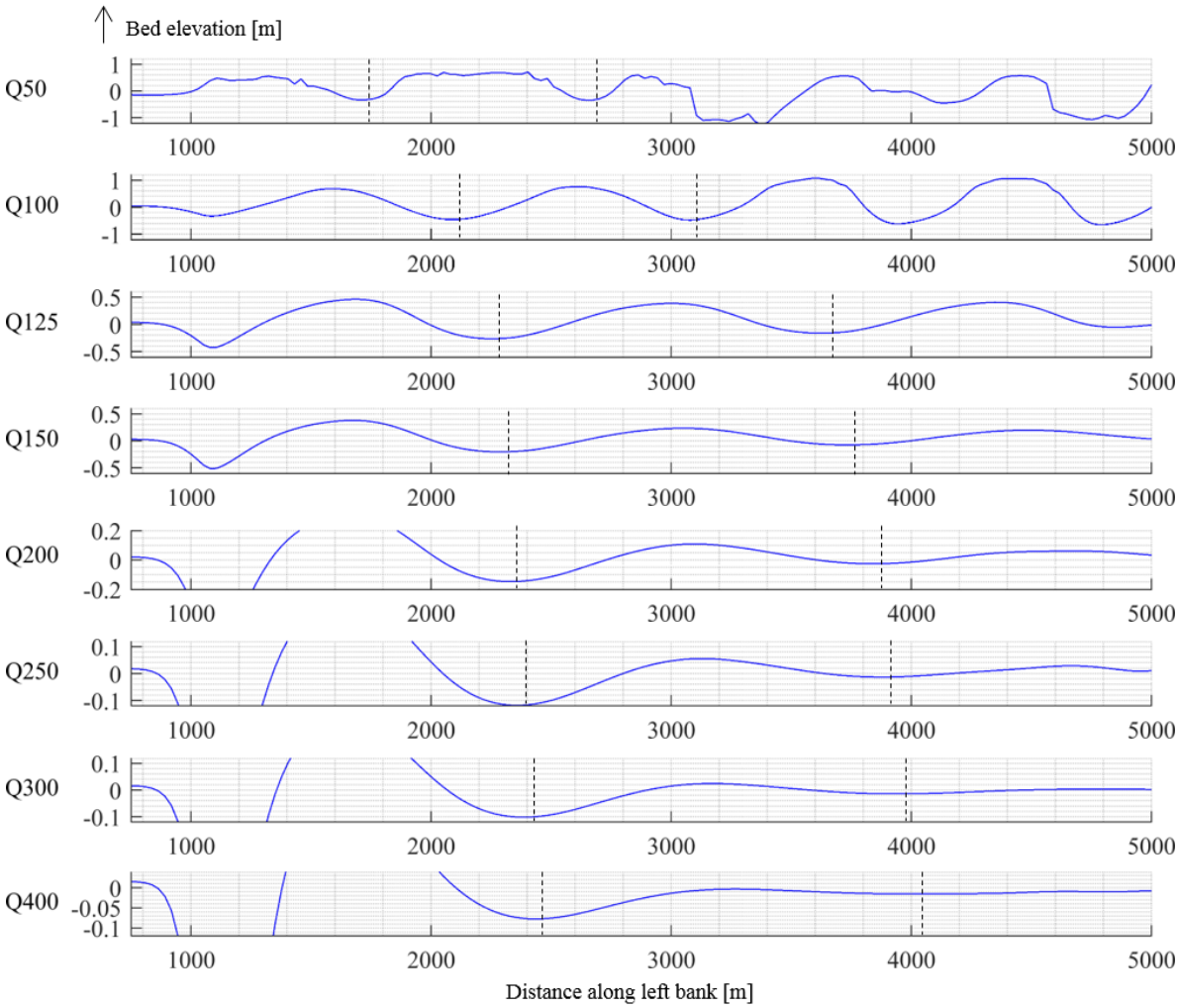

FIGURE C.1: Determine wavelength of hybrid bars (between black dashed lines). After 12 months of simulations.

Timescale of hybrid bars

In Section 5.1 the definitions of the timescale of development of the bars is provided. In the following figures, the snapshots of this moment in time is provided for the simulations. The results can be found in Figure 5.4.

$T_{hybrid\ L_P}$: timescale of hybrid bars towards the development of the first bar.

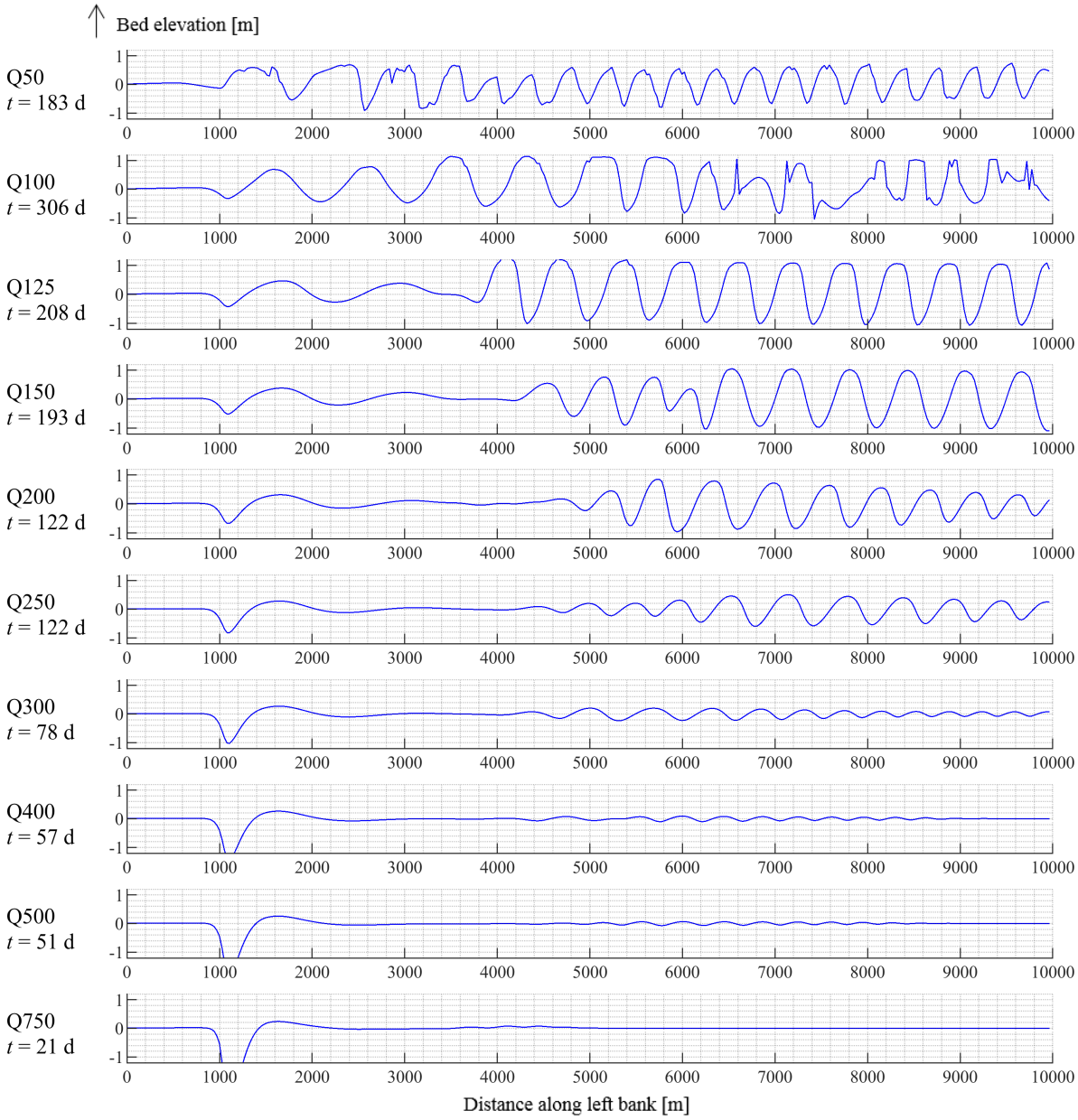

FIGURE C.2: $T_{hybrid\ L_P}$: Development of the first hybrid bar.

$T_{hybrid\ L_D}$: timescale of hybrid bars towards a full pattern of hybrid bars has developed.

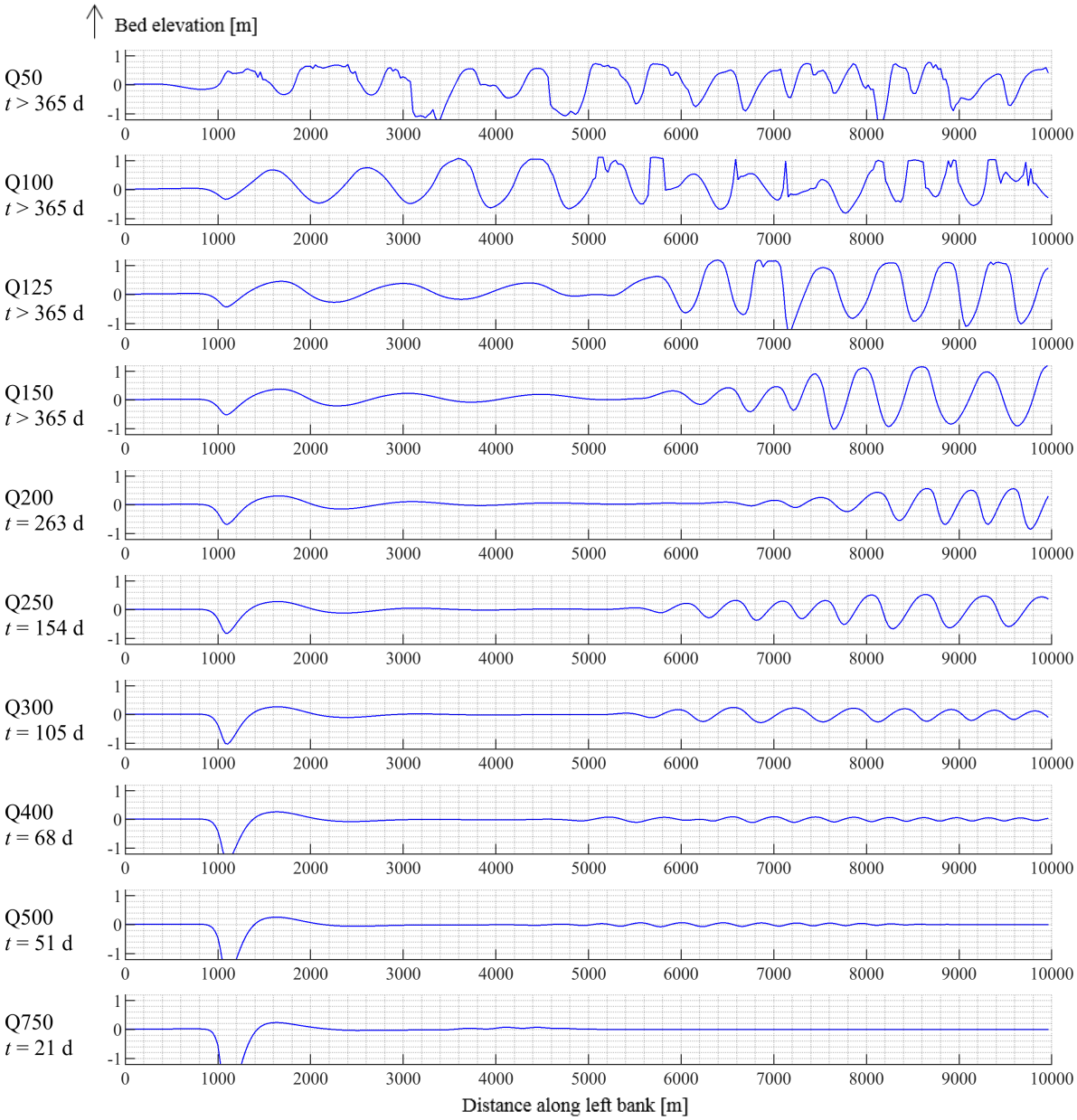

FIGURE C.3: $T_{hybrid\ L_D}$: Development of a full pattern of hybrid bars.

Timescale of free bars

T_{free}: the timescale of free bars is until a group of 5 free bars have developed.

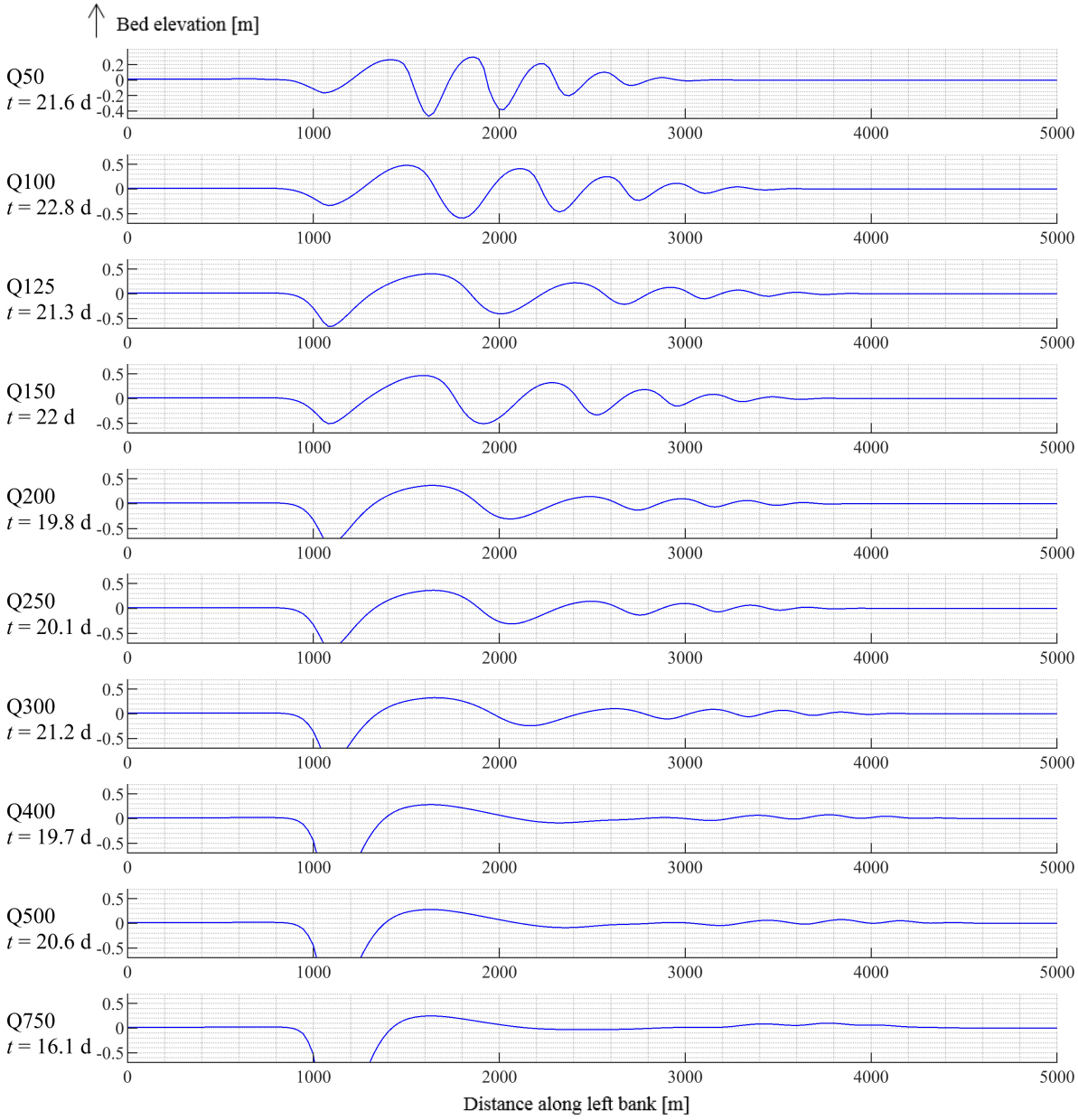

FIGURE C.4: T_{free}: Development of the free bars.

Timescale of Tubino (1991)

The steps towards T_{Tubino} are shown on this page. The validity of the timescale is restricted to simulation Q50 - Q300, as the roughness parameter $\overline{d_s}$ drops below 0.001.

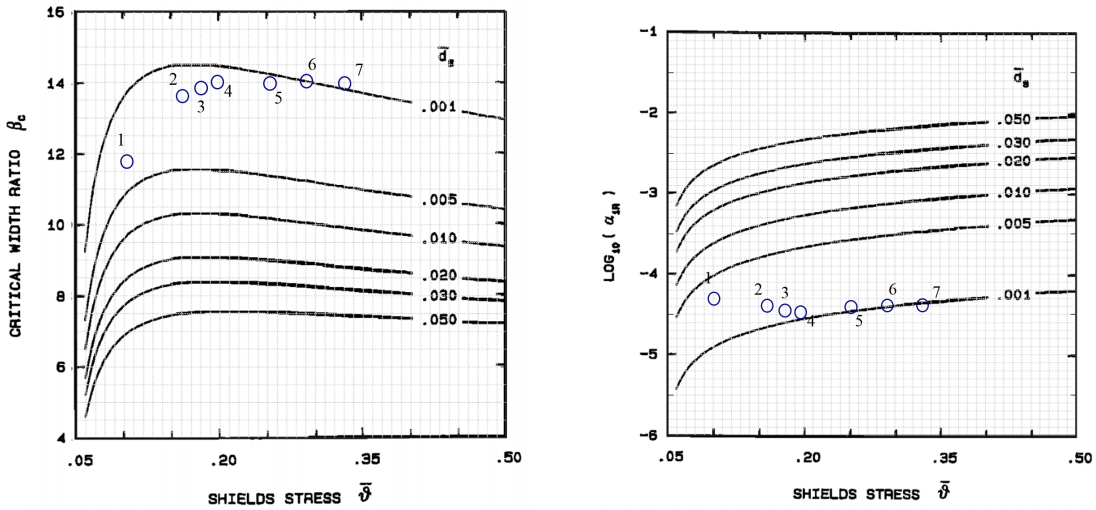

FIGURE C.5: Determine timescale of Tubino (1991)

TABLE C.2: Determine timescale of Tubino (1991)

Simulation		Q50	Q100	Q125	Q150	Q200	Q250	Q300
Reference number		1	2	3	4	5	6	7
Q	$[\mathrm{m^2\,s^{-1}}]$	50	100	125	150	200	250	300
θ	$[-]$	0.102	0.1619	0.1878	0.2121	0.257	0.2982	0.3367
$\overline{d_s}$	$[-]$	0.003	0.0019	0.0016	0.0014	0.0012	0.001	0.0009
β	$[-]$	66.9	42.1	36.3	32.1	26.5	22.9	20.3
u	$[\mathrm{m\,s^{-1}}]$	0.83	1.04	1.12	1.19	1.31	1.41	1.50
β_c	$[-]$	11.8	13.8	13.9	14	14	14	14
$log(\alpha_{R1})$	$[-]$	-4.3	-4.4	-4.45	-4.45	-4.4	-4.4	-4.4
T_{Tubino}	[days]	2.7	6.1	8.1	9.5	11.2	14.6	19.5